Experimental and numerical study of confined masonry walls under in-plane loads : case : guerrero State (Mexico)

Sulpicio Sánchez Tizapa

UNIVERSITÉ PARIS-EST

ÉCOLE DOCTORALE "MATERIAUX – OUVRAGES – DURABILITÉ – ENVIRONNEMENT - STRUCTURES"

THÈSE

Pour obtenir le grade de

DOCTEUR DE L'UNIVERSITÉ PARIS-EST

Discipline: Génie Civil

Présentée par

Sulpicio SÁNCHEZ TIZAPA

Titre:

Étude expérimental et numérique des murs en maçonnerie confinée chargés dans leur plane. Cas: État de Guerrero (Mexique)

Thèse dirigée par M. Ahmed MEBARKI

Soutenue le 10 décembre 2009

JURY

M. Michel LORRAIN	*Rapporteur*
M. Djillali BENOUAR	*Rapporteur*

Le conventionnel Je veux dire que l'homme a un tyran, l'ignorance. J'ai voté la fin de ce tyran-là. Ce tyran-là a engendré la royauté qui est l'autorité prise dans le faux, tandis, que la science est l'autorité prise dans le vrai. L'homme ne doit être gouverné que par la science.

L'évêque Et la conscience

Le conventionnel C'est la même chose. La conscience, c'est la quantité de science innée que nous avons en nous.

Les Misérables. Victor Hugo

Dedico este trabajo a mi amada esposa Elvia y a mis queridos hijos Tonatiuh y Jesús porque el tiempo utilizado en este trabajo es el mismo que les falté,
A mi paciente papá Martín y a mis estimados hermanos Sotero y Marciano de quienes he aprendido tantas cosas,
A mi mamá Lucía (q.e.p.d.) y a mi hermana La Guera (q.e.p.d.) quienes me dieron la vida y continúan a mi lado.

Acknowledgements

I would like to thank all those who have contributed to this research work, especially to the thesis director and members of jury: Professors Mr. MEBARKI, Mr. LORRAIN, and Mr. BEONUAR for their important commentaries, as well as to the actual and anterior director of the Academic Unity of Engineering (Autonomous University of Guerrero, Mexico) Apolonio BAHENA and Andres GAMA.

Special thanks are due to the technical staff of the Laboratories: Raziel BARRAGAN, Alfredo CUEVAS, and Daniel DELGADO who together with Ivan PASTRANA and Victor MUÑOZ developed the most of experimental tests. I owe a great deal of gratitude to Anselmo SOTO, Roberto ARROYO and Francisco CASTRO for the moral and technical support provided.

I am also thankful to Victor FLORES for its help to develop some tests of the Laboratory of National Center of Disasters Prevention (CENAPRED). Finally, I thank to the Program for the Academic Improvement (PROMEP, Mexico) for the scholarship provided during my doctoral research.

Summary in English

This research work proposes methods to rises the resistance and to evaluate the behavior of confined masonry walls built from clay solid bricks. These elements are widely used in Guerrero State (México) to build masonry structures, which should resist high lateral loads because of the serious seismic hazard.

Therefore, a large experimental program to evaluate the mechanical properties of bricks and masonry currently required in the design process and masonry analysis was developed. To rises the masonry resistance and to counteract the influence of the compressive strength of the pieces on the masonry behavior, a high compressive strength mortar and a metallic reinforcement inside the joints were used. With respect to referenced values of the mechanical properties, some were similar and others were twice bigger. In this country zone, the first three tests under lateral load on full-scale confined masonry walls built from clay solid bricks were carried out in order to evaluate its behavior. A reinforcement composed by metallic hexagonal mesh-mortar coat was placed on the faces of two walls to rise or to restore the resistance. The walls showed good behavior and the reinforcement had adequate structural efficiency.

Numerical models of panels and walls built by using the experimental data evaluated the envelope resistance, the failure mode and showed the influence of the mechanical properties of the pieces and joints on the global behavior. Two models had metallic reinforcement inside the joints. In addition, a constitutive law of the masonry defined from experimental results allowed to elaborate a simple model, which results were concordant with respect to the experimental results and similar to those calculated by complex models.

Finally, two simplified models to evaluate the resistance of confined masonry walls by considering the failure plane on the wall diagonal were developed. One supposes the masonry failure by shear effect and the other supposes the masonry failure by induced tension. The ratio theoretical resistance vs. experimental resistance was adequate for walls built from different materials and tested under different loads, which had ratio Height/Length ranging from 0.74 to 1.26.

Summary in French

Cette recherche propose des méthodes d'amélioration de résistance et d'évaluation du comportement de murs en maçonnerie confinée construits en briques solides d'argile cuite. Ces éléments sont largement utilisés dans la construction des bâtiments à l'État du Guerrero (Mexique) lesquels doivent résister charges séismiques importantes.

Ainsi, un programme expérimental a été développé pour évaluer les propriétés mécaniques des briques et de la maçonnerie, qui sont nécessaires dans la conception et analyse des constructions. Pour augmenter la résistance de la maçonnerie et compenser la variabilité de la résistance à la compression des briques, un mortier à haute résistance et un renfort métallique dans les joints ont été utilisés. Certaines propriétés mécaniques sont égales à celles communément citées, cependant, les autres ont des valeurs deux fois plus grandes. Dans cette région du pays, les trois premiers tests de murs à échelle réelle construits en briques solides d'argile cuite ont été réalisés sous charge latérale alternée afin d'évaluer son comportement. Un renfort métallique et une couche du mortier ont été placés dans les surfaces de deux murs. Ceux-ci ont présenté un bon comportement et le renfort a eu un comportement structural adéquat.

Avec les données expérimentales, plusieurs modèles numériques de panneaux et de murs ont été mis au point afin de reproduire l'enveloppe de résistance et le mode de défaillance. Ces modèles ont également évalué l'influence des propriétés mécaniques des briques et des joints sur le comportement global des spécimens. Aussi, un renfort métallique a été placé à l'intérieure des joints dans deux modèles. D'un autre côté, à partir de résultats expérimentaux obtenus et cités, une loi de comportement de la maçonnerie a été définie pour construire un modèle simple qui donne des résultats concordants à la fois avec les résultats expérimentaux et ceux obtenus par la méthode des éléments finis.

Finalement, deux modèles simplifiés ont été proposés afin d'évaluer la résistance de murs en maçonnerie en supposant que le plan de rupture est suivant la diagonale du mur. L'un suppose la rupture de la maçonnerie par effet de cisaillement tandis que l'autre suppose la rupture par effet de tension induite. Le ratio entre résistance théorique et résistance expérimentale a été acceptable pour 27 murs faits de matériaux différents et testés sous différents types de chargement où le ratio hauteur sur longueur varie entre 0,7 et 1,2.

Summary in Spanish

Este trabajo propone métodos para aumentar la resistencia y evaluar el comportamiento en muros de mampostería confinada elaborados con tabique rojo recocido. Dichos elementos son ampliamente utilizados en el Estado de Guerrero (México), donde las fuerzas sísmicas de diseño son elevadas.

Así, un programa experimental fue desarrollado para evaluar las propiedades mecánicas de piezas y mampostería requeridas en el diseño y análisis de la mampostería confinada. Para aumentar la resistencia y contrarrestar la variabilidad de la resistencia a compresión de las piezas fue utilizado un mortero de alta resistencia a la compresión y un refuerzo metálico en las juntas. Algunas valores de las propiedades mecánicas fueron iguales a los comúnmente referenciados, sin embargo, otros registraron valores dos veces mayores. Adicionalmente, en esta región del país fueron realizadas las primeras pruebas bajo carga lateral alternada de tres muros a escala real construidos con tabique rojo recocido con el objeto de evaluar su comportamiento. Un refuerzo constituido por malla tipo gallinero y mortero fue colocado en las caras de dos muros. Éstos presentaron un buen comportamiento y el refuerzo tuvo una adecuada eficiencia estructural.

Con los datos experimentales fueron elaborados varios modelos numéricos de paneles y muros para reproducir la envolvente de resistencia y el modo de falla. Dichos modelos también evaluaron la influencia de las propiedades mecánicas de las piezas y de las juntas en el comportamiento global de los especimenes. En dos modelos fue colocado refuerzo metálico en las juntas. Por otro lado, a partir de resultados experimentales obtenidos y referenciados fue definida una ley de comportamiento de la mampostería para construir un modelo simple de un muro, que proporciona resultados adecuados y tiene aproximación similar a la obtenida en modelos elaborados mediante elementos finitos.

Adicionalmente fueron propuestos dos modelos simplificados para evaluar la resistencia de muros de mampostería considerando el plano de falla en la diagonal del muro. Uno supone la mampostería falla por efecto cortante mientras el otro supone la falla por tensión inducida. La relación resistencia teórica entre resistencia experimental fue satisfactoria para 27 muros elaborados con distintos materiales y probados ante distintos tipos de carga cuya relación Altura/ Longitud varió entre 0.7 y 1.2.

Table of Contents

List of Tables

List of Illustrations

CHAPTER 1

Introduction

1.1 Justification

Since ancient times, masonry has been used to build all types of structures providing excellent resistance in presence of different natural phenomena. Nowadays, around the world a large variety of masonry units can be adopted for many structural and architectonic forms in an extensive variety of construction such as buildings, bridges, dams, walls, etc [106].

This project analyses the confined masonry, which has been extensively practiced in the last 30 to 35 years in regions of high seismic hazard such as the Mediterranean Europe (Italy, Slovenia, and Serbia), Latin America (Mexico, Chile, Peru, Venezuela, Argentina, and other countries), south Asia (Indonesia), and the Far East (China) [92]. For instance, it represents 40% of the total housing stock in Slovenia, whereas in Mexico, it could reach up to 70% [49] [92]. The first report about confined masonry construction concerns the reconstruction of buildings damaged by the 1908 Messina, Italy earthquake. In Chile, its use started in 1930 after the 1928 Talca earthquake [19].

Confined masonry construction was introduced in Mexico City, Mexico in the 1940's to control the wall cracking caused by large differential settlements under the soft soil conditions. The system became popular in other areas of highest seismic hazard in Mexico due to its excellent earthquake performance [63]. The use of confined masonry in Colombia started in the 1930's and it is currently used for housing construction: single-storey dwellings up to five storey buildings [40]. The limitation to five-storey building height given by the seismic design [86] usually coincides with most construction codes' height restrictions for buildings without elevators [47].

Concerning to the seismic contact in Mexico, the movement of four tectonic plates generates high seismic hazard. Figure 1.1 shows this configuration, where the arrows present direction and mean velocity among plates. Then main earthquakes in Mexico have been caused by two kinds of movement:

a) By subduction phenomenon along the Pacific coast from Jalisco to Chiapas: the Rivera plate and the Cocos plate move beneath the North American plate,

b) By lateral displacement between the Pacific plate and the North American plate in Baja California State continues until California State (USA).

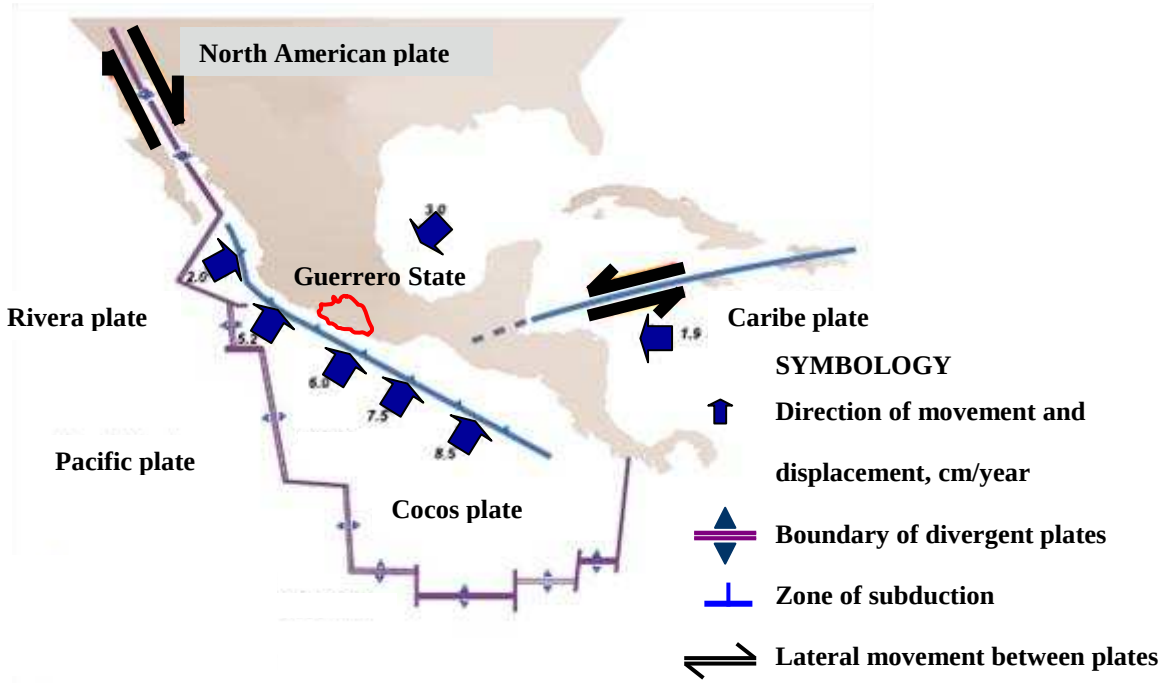

Figure 1.1: Movement of tectonic plates in the Pacific Mexican coast [23]

Figure 1.2 shows the epicenters of strong earthquakes larger than 7 occurred during the 20th century. Approximately, 77% of these events have their hypocenter within the zone from Jalisco to Chiapas, with less than 40 km deep [23]. In addition, this figure presents a concentration of epicenters in Guerrero State, where is located the Guerrero seismic gap, Figure 1.3. According to research, this zone has the highest potential seismicity in Mexico because registered major earthquakes in 1899, 1907, 1909, and 1911. After this period, only have occurred moderate earthquakes in 1957, 1962, and 1989, Figure 1.3. Thus, it is expected the occurrence of two earthquakes with magnitude larger than 8 [23].

To face the high seismic hazard in the Pacific Mexican coast, the seismic behavior of masonry constructions must be accurately evaluated in order to propose reinforcement or confinement aiming high resistance of the masonry buildings. Analysis of behavior under seismic loads is done through the numerical models, which complexity levels vary. Some models evaluate the behavior of the whole elements (masonry units, joints, concrete elements), others evaluate the

global behavior of the masonry, and the others focus only on the masonry resistance. Another way to evaluate the behavior of confined masonry is by means of full-scale walls tests.

Figure 1.2: Epicenters of earthquakes M ≥ 7 during the 20th century and geographical position of Guerrero State [23]

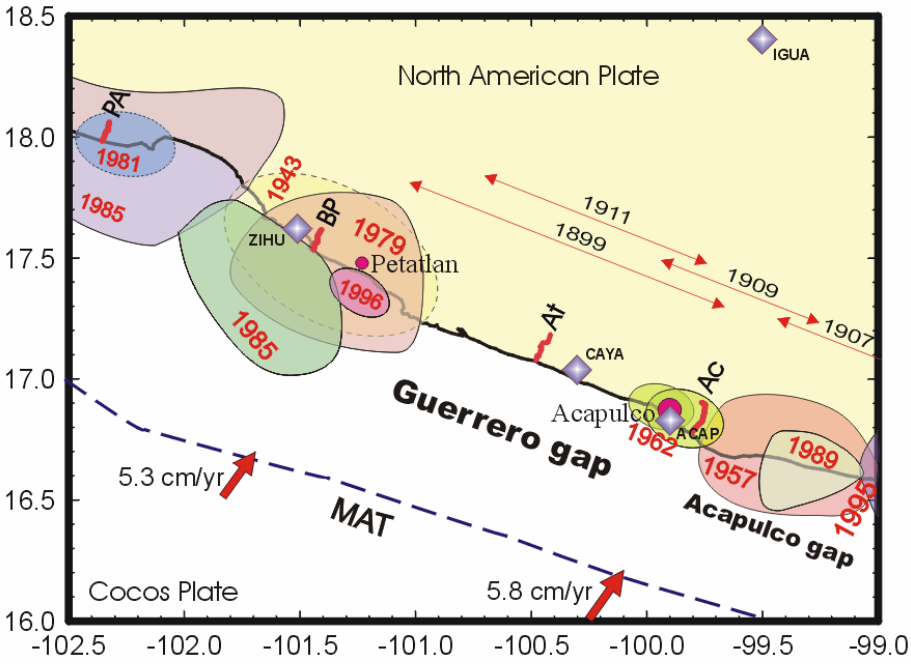

Figure 1.3: Seismic history of Guerrero gap [54]

This project, devoted to the particular case of Guerrero State (Mexico), considers the following factors:

a) High seismic forces for the masonry structures design [23],

b) Use of confined masonry walls in 70% of houses and buildings [49],

c) Large variation of the masonry units' mechanical properties [64] [65],

d) Lack of data for some masonry mechanical properties.

1.2 Main objective and goals

This project is divided into three parts: the first part contains the development and results of tests on solid clay bricks, mortar specimens, masonry specimens, and confined masonry walls subject to lateral load. The second part shows the results of numerical models of panels and walls elaborated with the mechanical properties obtained previously. Finally, the third part contains two simplified models developed in order to evaluate the resistance of confined masonry walls.

The main objective of this research is to evaluate the mechanical properties of units and masonry specimens, study the influence of the metallic reinforcement on the masonry shear strength, and to evaluate the experimental and numerical behavior of confined masonry walls under lateral loads. The materials and quality control in this project are similar to those used for the construction of masonry structures in Guerrero State (Mexico).

The experimental program aims to:

a) Asses the mechanical properties of solid clay bricks and masonry specimens (expected values and/or equations to behavior modeling),

b) Measure the resistance increment in panels with metallic reinforcement inside the joints and evaluate the change of the failure patterns,

c) Evaluate the resistance, failure mode, stiffness degradation, and hysteretic cycles of confined masonry walls with or without reinforcement.

The numerical part aims to:

a) Reproduce the behavior of one tested masonry wall through a micro-model built with the experimental data of units and joints previously obtained,

b) Obtain the load-displacement response of tested masonry walls by means of a macro-model with the experimental data of masonry panels,

d) Measure the influence of the reinforcement inside the joints on the walls and panels behavior,

c) Propose simplified models to assess the resistance of confined masonry walls under lateral and vertical loads.

1.3 Study contents

This document contains seven chapters. The first chapter presents the justification of the research. The second chapter shows the characteristics and components of the confined masonry walls, their behavior, and the failure mode. Experimental programs developed in Mexico, as well as the characteristics of the building local code, and the existent proposals of masonry reinforcement are described.

The third chapter describes the types of numerical modeling currently used to evaluate the masonry behavior. First part contains the micro-models, where all elements are modeled. The second part shows the macro-models built with homogenized properties and the simplified methods focused to obtain the ultimate load.

The fourth chapter contains the results of the experimental program on individual specimens, masonry specimens and three full-scale walls. The experimental envelope, dissipated energy, stiffness degradation, damping, and failure mode are evaluated in the full-scale walls tests, the mean values of the mechanical properties and mean curve of stress vs. strain are obtained for remaining tests.

The fifth chapter contains the numerical models implemented by means of the finite element method. The application to panels and full-scale walls, as well as the comparison with respect to the experimental results are provided. One macro-model developed from experimental data of masonry panels is also presented.

The sixth chapter describes two simplified methods in order to evaluate the ultimate lateral resistance regardless the deformation by considering the failure plane on the wall diagonal. Finally, the chapter seven shows the general conclusions and research perspectives.

CHAPTER 2

Masonry review

2.1 Introduction

This chapter shows important aspects of the confined masonry and its situation in Mexico: the components, the materials, the making processes, and mean values of the more important mechanical properties. Most experimental programs developed, their location, validation, and the failure modes of the masonry walls are presented. The review continues with the description of the seismic risk and the characteristics of the local building code in Guerrero State.

Furthermore, common methods of rehabilitation and retrofit of masonry structures to improve its resistance by means of low cost, easy placement and structural efficiency are described.

2.2 Confined masonry

"Confined masonry is a construction system, where masonry structural walls are confined on all four sides with reinforced concrete elements or reinforced masonry vertical and horizontal confining elements, which are not intended to carry either vertical or horizontal loads, and are consequently not designed to perform as moment-resisting frame" (Tomazevic, 2000).

Construction of confined masonry wall is different from masonry infilled reinforced concrete frame. In fact, the structural masonry walls are constructed in the first steps. Afterwards, the vertical confining elements, and finally the floors with horizontal bond-beams elements are put in place [19]. Figure 2.1 shows a confined masonry wall.

As the experimental investigations and the experiences obtained after earthquakes have shown [106], confining the masonry walls with bond-beams and tie-columns results in:

- Improvement in the connection between structural walls
- Improvement in the stability of slender structural walls
- Improvement in the strength and ductility of masonry panels

- Reduction of the risk of masonry panels destruction by earthquakes

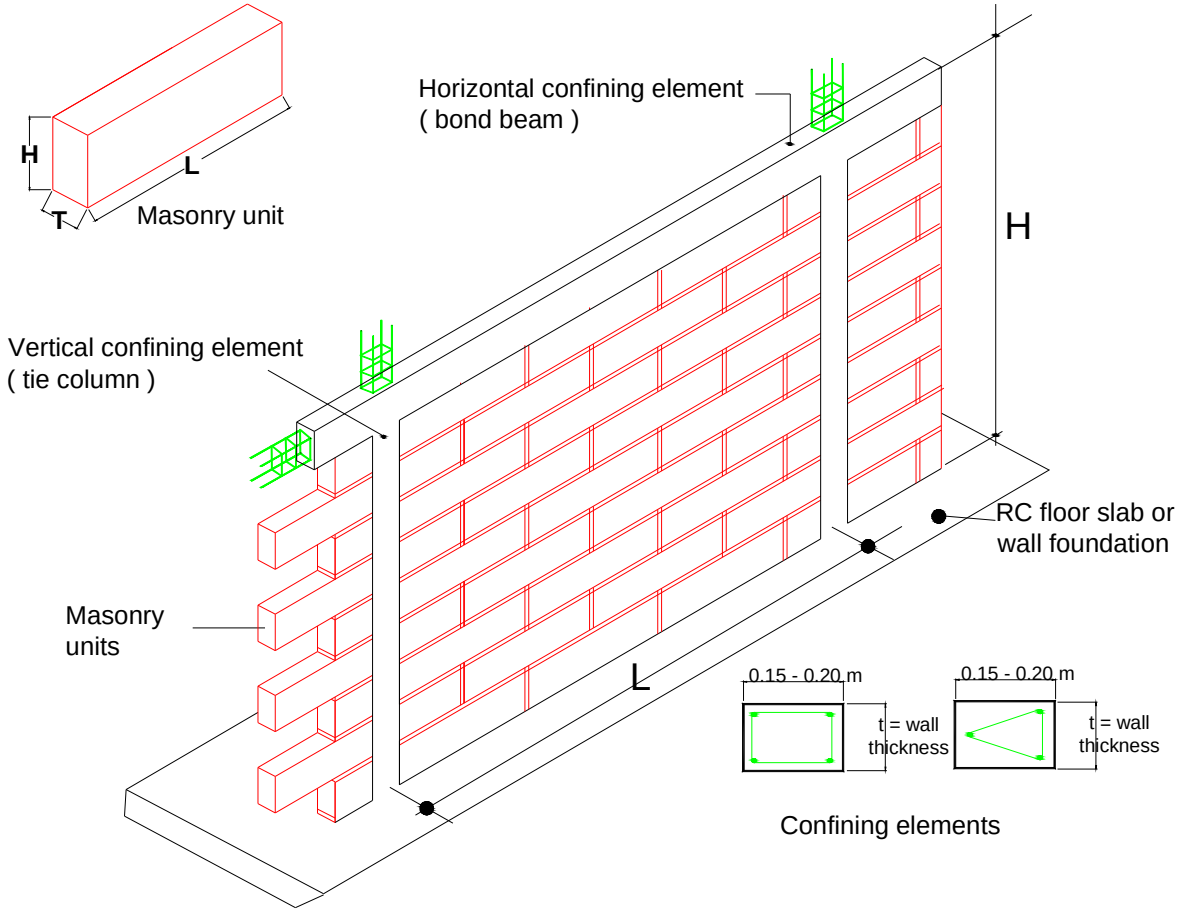

Figure 2.1: Confined masonry wall characteristics [42] [106]

2.2.1 Masonry units

Masonry units solid or hollow are made with different materials: sand-cement, lime-cement, concrete, or clay. The current size of the units are 0.06 m X 0.24 m X 0.125 m (*Height x Length x Thickness*) for clay solid brick, from 0.1 m X 0.4 m X 0.20 m to 0.30 m X 0.40 m X 0.3 m for hollow concrete blocks, Figure 2.1. Concrete blocks size must have at least 0.06 m X 0.24 m x 0.10 m [71]. Figure 2.2 presents the common masonry units used in Mexico. The mechanical properties governing the behavior are the compressive strength and the initial rate of absorption (IRA). The first must be greater than or equal to 0.6 MPa and the second must be smaller than 21% for clay solid bricks and 15% for concrete blocks [42] [71].

In Mexico, well as in other parts of the world, the masonry units may be obtained by means of three processes: manual, semi-industrialized, and industrialized. Usually, concrete and cement units are produced by the last two processes whereas clay units are elaborated by either manual or industrial ways, Figure 2.3. The manual process used to produce 85% of units in Guerrero State [5] has neither quality control in the selection and dose of materials nor

adequate process of preparing and firing. Therefore, the compressive strength and IRA have large scatterness. For these variables, results obtained by Meli and Hernandez (1971) of various lots of clay brick show coefficients of variation ranging from 20% to 36% for solid units and from 8% to 16% for hollow bricks. This causes a large uncertainty of the masonry constructions' reliability designed according to the local building codes.

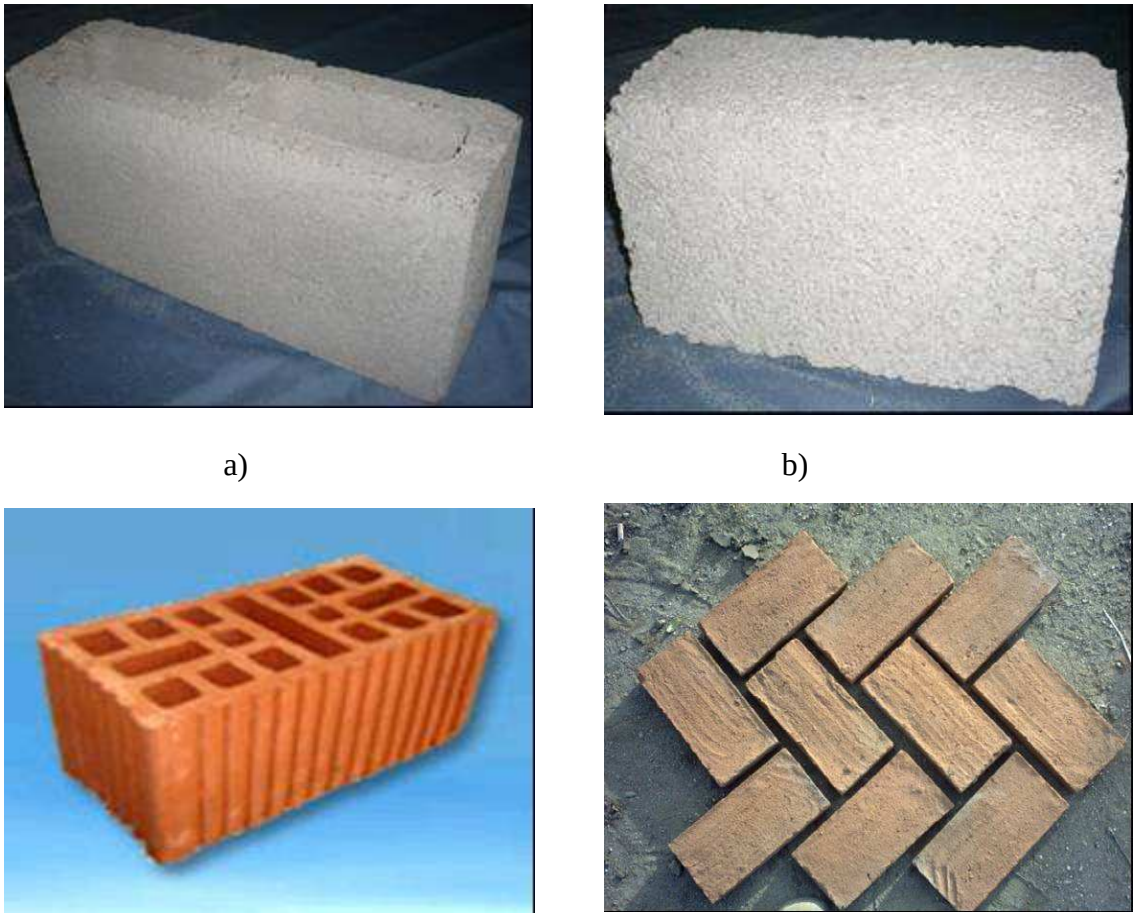

a) b)

c) d)

Figure 2.2: Common masonry units used in Mexico, a) Hollow concrete block, b) Solid concrete block, d) Hollow clay block, and d) Solid clay brick

2.2.2 Mortars

Mortars are mixtures plastic binder resulting from the combination of sand and water with cementing material that may be cement, lime, or a mixture of both materials. Their main properties are the compressive-tensile strength, elasticity, and ability to avoid the water absorption [110]. The indicative parameter to classify them (type I, II and III) is the compressive strength (12.5 MPa, 7.5 MPa or 4.0 MPa [42]), which varies according to cementing used and ratio sand vs. Cementing. The structural mortars elaborated with cement have compressive strength from 0.6 MPa to 28.0 MPa and modulus of elasticity from 1000 MPa to 5000 MPa [110]. In addition, premixed mortars called masonry cements containing

cement, lime and additives are used. To ensure adequate resistance, good adhesion, and low shrinkage, volumetric ratio sand vs. cementing from 2.25 to 3 is recommended [42].

Figure 2.3: Manual process to obtain solid clay bricks

Unlike the masonry units, the selection of raw materials and production of mortars have good quality control. However, the dosage by volume and the non-control of the water amount are important points, which cause a coefficient of variation equal to 20% [110].

2.2.3 Confining elements of reinforced concrete

Masonry is a brittle material that resists small deformations. Then concrete elements with thickness equal to the wall thickness and width ranging from 0.15 m to 0.20 m are in general added to improve its behavior. The compressive strength of these elements must be greater or equal than 15.0 MPa and the percentage of the longitudinal steel ratio must be greater (or equal) than $0.2f'_c/f_y$, where f'_c is the concrete compressive strength and f_y is the steel yield strength [42].

In Mexico, concrete elements commonly used have four longitudinal bars 9.5 mm diameter yield stress equal to 42 MPa and stirrups 6.5 mm diameter yield stress equal to 23 MPa [48] [107]. Besides, in the market there are prefabricated rebar formed by three or four longitudinal smooth or rough wire and stirrups of the same material with steel yield stress greater than 50 MPa [33]. Figure 2.1 shows the components of confined masonry walls, which tie-columns should be located at maximum distance of 3.0 m or 1.5H. For any wall opening with length greater than one quart of wall length confining elements should be used [42].

2.3 Failure modes of confined masonry walls

From damage observed after earthquakes and tests' results of confined masonry walls have been identified several mechanisms of failure under in-plane lateral loads. Among many other variables, the resistance of masonry (combination of masonry units and joints), the resistance of the concrete columns, the quality of workmanship and steel reinforcement ratio define the failure pattern [66] [85] [106]. The following paragraphs describe four main failure modes.

1. Flexion failure. This failure mode appears on slender walls, where the tension is high and causes the yield of the longitudinal steel and the compression failure on the wall's corners [20], Figure 2.4a.

2. Sliding shear failure. Sliding of a portion of the wall along to the horizontal joint occurs when the shear stress is greater than the shear strength. Sliding produces the short column effect on the concrete elements that generates plastic hinges [106], Figure 2.4b.

3. Diagonal tension failure. This failure mode occurs because the stress along the wall diagonal exceeds the masonry tensile strength causing diagonal cracking. [106][107], Figure 2.4c.

4. Splitting failure by diagonal compression. It happens when there is separation between masonry and concrete columns on discharged corners. A compression strut is then formed. This generates compression at the loaded corners and causes crushing of the masonry units [106], Figure 2.4d.

In two last failures modes, masonry may fail for a combination of the units cracking and joints sliding. In general, the failure occurs in the units when they are weaker than the joints. Indeed, the failure appears in the vertical or horizontal joints, Figure 2.5.

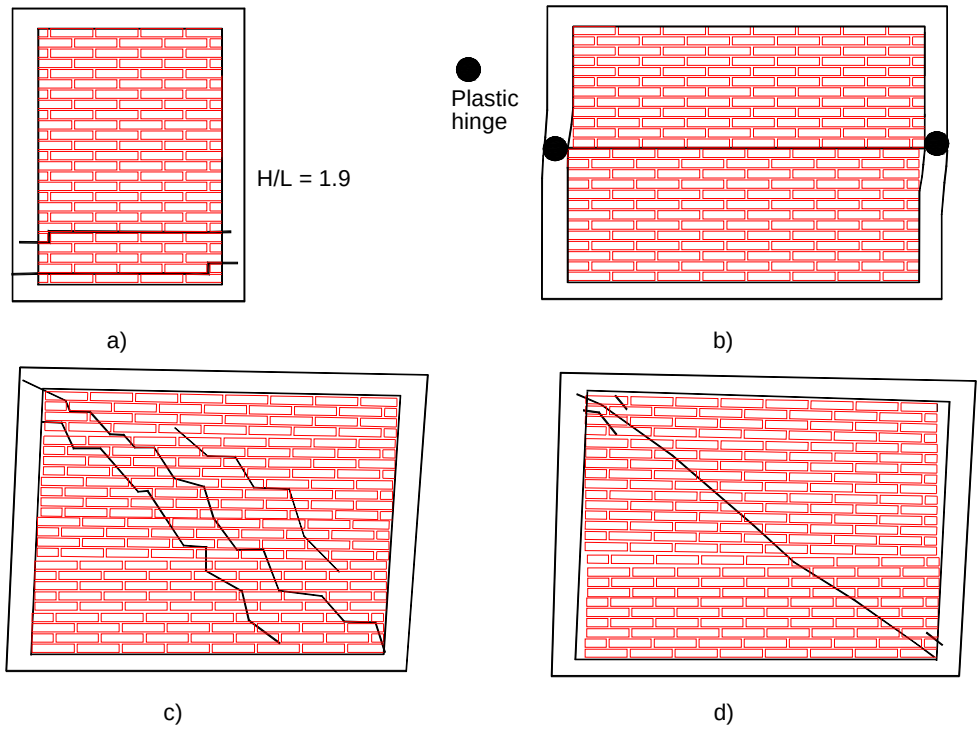

Figure 2.4: Failure modes of confined masonry walls: a) Flexion failure [20], b) Sliding shear [106], c) Diagonal tension failure [106] [107], d) Splitting failure and opening of interface at the unloaded corners [106]

Figure 2.5: Masonry panel failure caused by units cracking and joint sliding

2.4 Experimental research in Mexico

Seismic hazard map, Table 2.1 and Figure 2.6, elaborated according to Mexican seismic history [23] shows the highest seismic hazard for Mexico City and for one segment of the Pacific coast. The three Mexican States with the lowest economic level (Guerrero, Oaxaca, Chiapas) [49] are located in the last zone, where the masonry units are obtained by manual or semi-industrialized processes with slight or no quality control. Then the reliability of masonry buildings is difficult to assess.

Table 2.1 Seismic hazard and sites with confined masonry walls tests [23]

Zone	Seismic hazard level	Site
A	Low	Monterrey, Nuevo Leon
B	Moderate	
C	High	Guadalajara, Jalisco and Chilpancingo, Guerrero (in this project)
D	Very High	
Special	Moderate and High	Mexico City

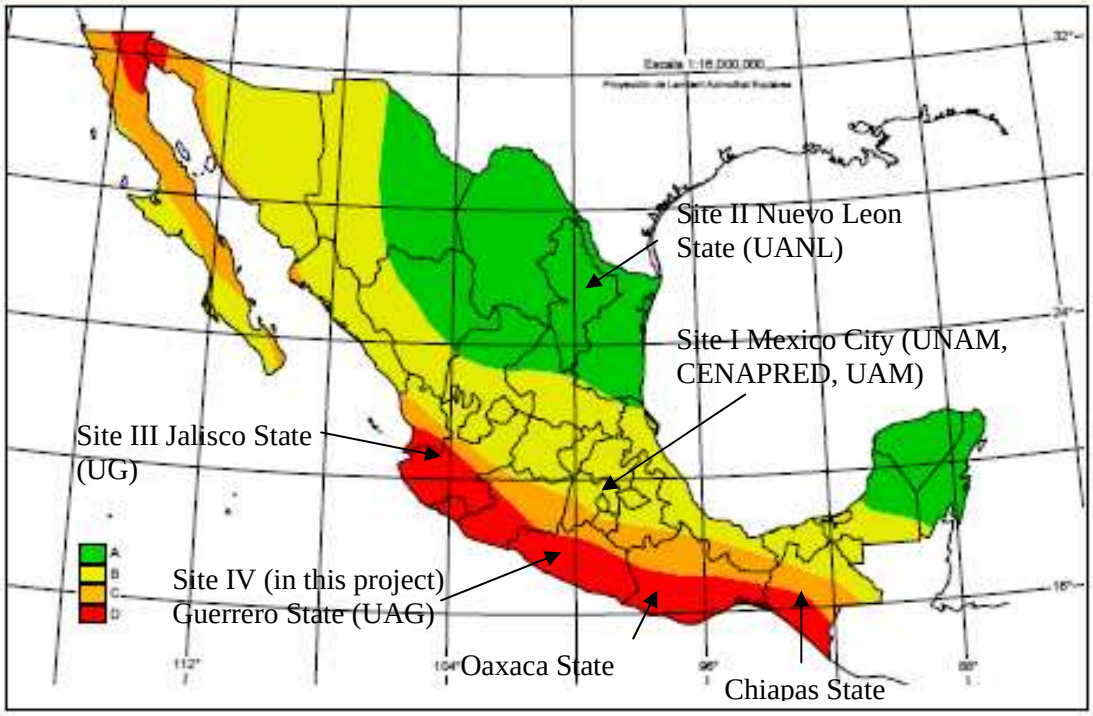

Figure 2.6: Seismic hazard map and sites with confined masonry walls tests [23]

In this context, it is important to define the state-of-the art of the experimental research guided to evaluate the behavior of masonry units and confined masonry walls. It is worth to notice that some experimental results were used to define the parameters required in the building codes. In addition, this information was useful to define the experimental program presented herein and to compare their results (chapter 4), in order to elaborate the numerical models (chapters 5 and 6). Figure 2.6 shows the different sites where have been developed full-scale masonry walls tests.

2.4.1 Experimental research in Mexico City

In Mexico City and its surroundings, where a quarter of the Mexican population lives, there are areas with records of large damage caused by earthquakes in 1957 and 1985. Then, the pioneering studies about the masonry walls behavior were carried out at the National Autonomous University of Mexico (UNAM). The more important experimental studies are:

- Meli and Salgado (1969) tested 34 confined masonry walls under monotonous and cyclic loading. They used the same mortar to glue hollow concrete blocks, hollow and solid bricks, whereas the reinforced concrete elements had different longitudinal reinforcement ratios. All walls were fixed to a bottom massive concrete beam and most of them had vertical and horizontal movement on top. The results showed the failure types, the load-deformation characteristics, the influence of the vertical load and established criteria to seismic design. The walls with low longitudinal reinforcement ratio showed horizontal cracks at the bottom concrete beam-masonry interface and at the top joints while the presence of vertical loads reduced by flexural cracks. At the end, cracks appeared along the wall diagonal.

- Meli and Hernandez (1971) and Meli and Reyes (1971) developed an extensive program on different pieces and mortars to evaluate the compressive strength and other statistical parameters. Besides, compression tests on prisms built from different units to measure the axial stress vs. strain relationship were carried out. Shear tests on three-piece prisms were also performed for assessing the joint cohesion under different confining stress. Diagonal tension test on masonry panels were also developed. Some results are still used by building local codes [42] [45].

- Alcocer, Muria and Peña (1999) tested in shaking table three models of reduced scale 1:3, two models ratio H/L = 1 (Height/Length) and other model ratio $H/$L = 1.5. These represented the ground floor of a four-level building, which were constituted by two parallel walls fixed by an upper reinforced concrete slab. From the results, it could be concluded that the shear deformations were more important for models H/L = 1, while the flexural deformations predominated for the model H/L = 1.5, Figure 2.7.

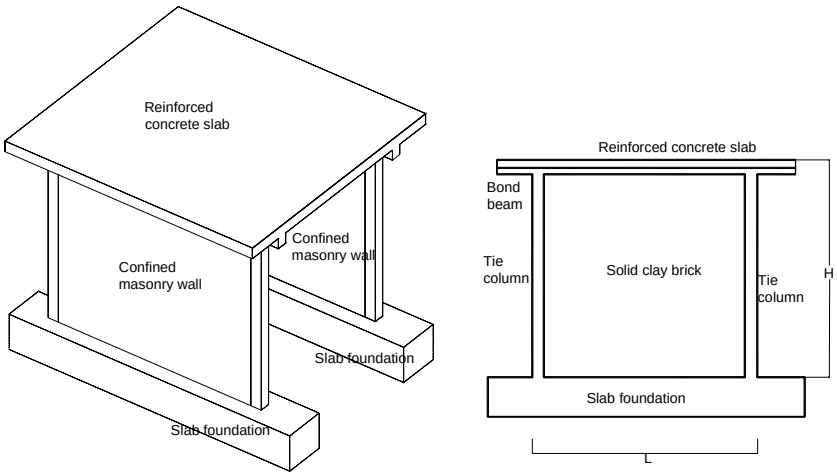

Figure 2.7: Reduced model of confined masonry buildings tested in shaking table by Alcocer, Muria and Peña (1999)

The National Center for Disaster Prevention (CENAPRED) has developed a large number of full-scale walls tests under cyclic loading. The following experiments are the more important:

- Alcocer, Flores and Sanchez (1993) tested three systems built from two confined masonry walls, 2.5 m height. An upper system beam-concrete slab cast in-situ linked the walls and created the space of a door, Figure 2.8. Different reinforcements in horizontal joints of two systems were placed and the third un-reinforced system was the control specimen. A compression stress equal to 0.50 MPa simulated the gravitational load and cyclic lateral loads were applied. All systems showed cracks in X. Besides, the edge wall above the diagonal wall displaced with respect to the inferior edge wall generating cracking at both ends of the tie-columns for the maximum load.

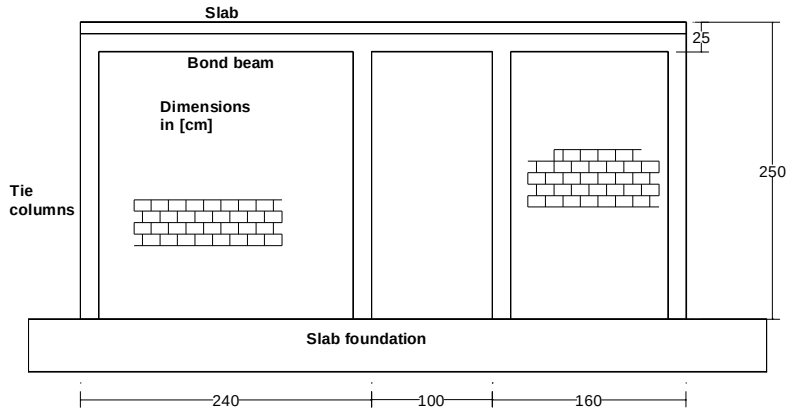

Figure 2.8: Structural system tested by Alcocer, Flores and Sanchez (1993)

- Sanchez, Alcocer and Flores (1996) developed the first full-scale test of a two-level building in Mexico. Two parallel systems of identical walls with perpendicular restriction

in order to eliminate torsion effects composed each level. The main conclusion were: a) the structure resistance was satisfactory with respect to that proposed by the local code, b) the shear deformation and diagonal tension cracking of the masonry dominated the building behavior, b) hysteretic cycles were symmetric and stables. In addition, it could be seen that the resistance of the three-dimensional structure can be extrapolated from the walls' individual resistance.

- Aguilar (1997) tested, under cyclic load, four masonry walls built with solid clay bricks, 2.5 m X 2.5 m. Three walls were reinforced with different percentages of steel ratio inside the horizontal joints. A fourth un-reinforced wall was the control specimen, which failed by diagonal cracking. The results showed resistance evolution, high deformation capacity of reinforced walls and identification of three behavior stages. The first stage is linear behavior and ends with the presence of the first cracks due to diagonal tension, the second stage finishes at the peak load, and the third stage shows resistance degradation and the distortion increment until the longitudinal steel failure, Figure 2.9. From wall instrumentation, it can be seen that the tie-columns resist 70% of the vertical load.

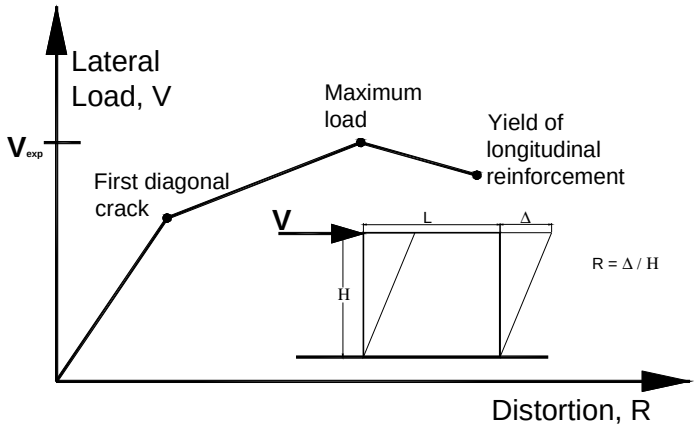

Figure 2.9: Experimental resistance envelope with tri-linear relationship (Aguilar, 1997)

2.4.2 Experimental research outside Mexico City

Additional to Mexico City, two sites have evidence of tests on confined masonry walls. The first site is the Structures Laboratory at the Autonomous University of Nuevo Leon (UANL) in the Northern, where there is not seismic hazard. The second site is the Structures Laboratory at the University of Guadalajara (UG) located in high seismic hazard zone, Figure 2.6. The following paragraphs describe these experimental programs.

- Trevino et. al (2004) tested eight confined masonry walls built with hollow concrete blocks, 2.5 m X 2.5 m, under cyclic loading. Four longitudinal bars 9 mm diameter linked

through stirrups reinforced the columns of four walls and prefabricated steel reinforcing frames were used on the columns of the remaining walls. The lateral load was applied in two series under constant vertical stress equal to that applied at the ground floor of a five-level building. Loading control for the first series and control displacement for the second series were applied. Symmetrical hysteretic, typical of the confined masonry were measured. In the same way, the tie-columns failure and the longitudinal reinforcement yield happened after the masonry units' failure. The authors found no significant behavioral differences between the two sets of walls, Figure 2.10.

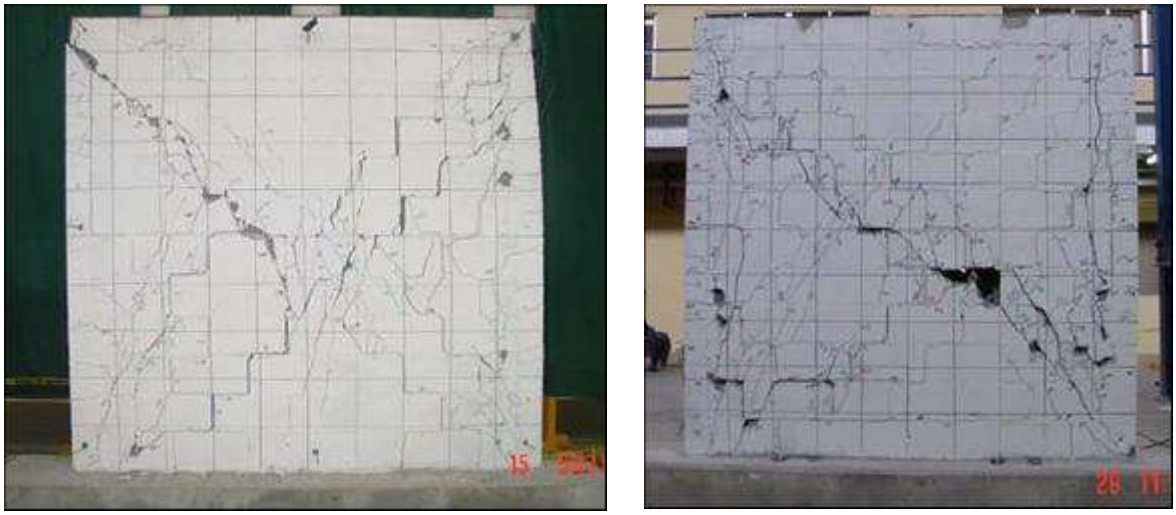

Figure 2.10: Failure modes of two walls tested by Treviño et. al (2004)

- Hernandez and Urzua (2002) built three masonry walls by using lightweight lime-cement blocks commonly used to construct residential buildings. Size of the walls, 2.50 m X 2.5 m, represented the dimension of a building wall with vertical loads similar to those applied at the ground floor of a two-level building. The concrete columns had four longitudinal bars 9 mm diameter. Tests on prisms and masonry panels were also carried out to evaluate the compressive strength, shear strength, and modulus of elasticity. Dynamic loads corresponding to displacement associated to El Centro accelerogram were applied. The main conclusions were: a) the walls have shear failure mode, b) the walls fail due to diagonal tension of masonry units, and c) the resistance of the three specimens was identical, Figure 2.11. They proposed an expression to evaluate the stiffness degradation in function of the walls rotation, R.

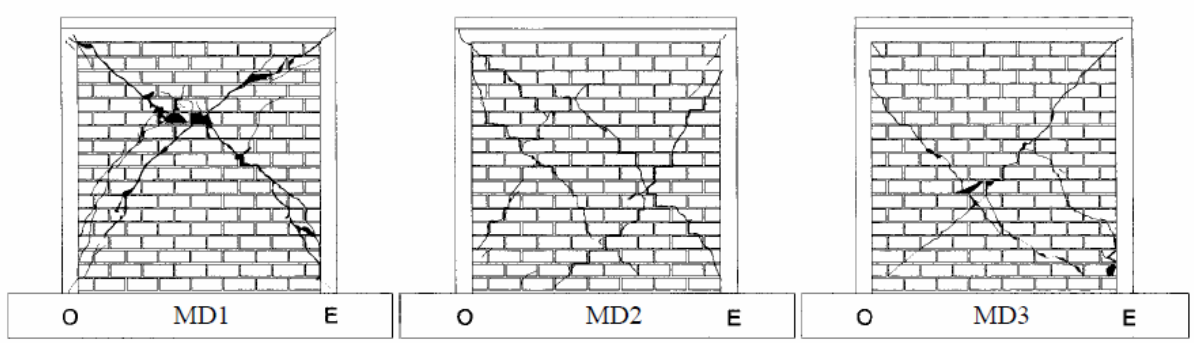

Figure 2.11: Failure modes of walls tested by Hernandez and Urzua (2002)

In other way, the influence area of this project is Guerrero State, where the experimental programs have focused on evaluation of the mechanical characteristics of masonry specimens and masonry units. For example, Salgado (2000) conducted a field study among the building workers for assessing the characteristics of mortars, masonry units, as well as the compressive strength of the concrete elements. Additionally, he tested eighteen panels of 0.80 m X 0.80 m reinforced with metallic reinforcement mesh and mortar.

A second study developed by Navez (2002) included tests on twenty-one panels of solid clay bricks, three panels of hollow concrete blocks, and three panels of solid concrete blocks. Mortars type I and II were used according to local code. The shear strength of solid clay bricks and hollow concrete blocks panels was slightly less than the specified value, while the shear strength of concrete block panels was adequate with respect to the normative value. In addition, tests on masonry prisms in order to evaluate the compressive strength were carried out with satisfactory results.

To determine the influence of the manual fabrication process on mechanical properties of solid clay bricks, Jorge (2005) conducted an experimental study to measure the physical properties of the raw material, the compressive strength of masonry units and the modulus of rupture. The two last parameters had mean values equal to 5.6 MPa and 1.2 MPa.

2.5 Retrofitting and rehabilitation of masonry

After an earthquake occurrence, an inspection to evaluate the residual safety of the buildings must be done. It has three possible outcomes: the building is safe, the construction should be repaired, and the building should be destroyed. For the second case, the reparation process called “retrofit” can apply in order to recover the original seismic resistance. A different situation occurs in those structures which resistance should be improved to achieve an

acceptable level of safety, as is the current case for historic structures. This process is called "rehabilitation" [105].

2.5.1 Types of reinforcement

There are two main forms to place the reinforcement, one placed on the wall faces, called herein external reinforcement, and another placed inside the joints[18] [87][106], Figure 2.12. Although other types of reinforcement exist, such as fiber reinforced polymer [37] [94] and plastics straps [91], next paragraphs describe the particular case of two experimental researches with similar reinforcements to those used herein. This information will be useful to compare the results in chapter 4.

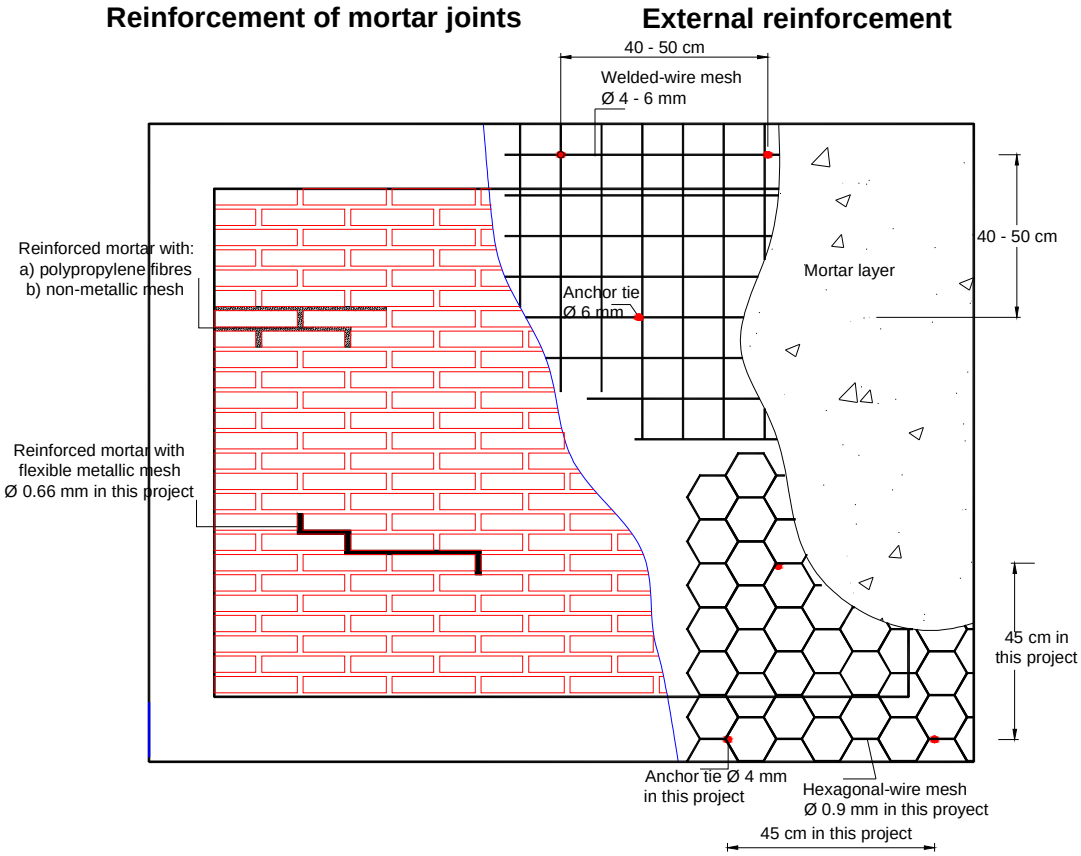

Figure 2.12: Types of reinforcement [18] [87] [106]

2.5.1.1 External reinforcement

Pineda (1996) tested three walls, 2.50 m X 2.50 m, with welded-wire reinforcement mesh fixed to wall faces by means of steel pins and coated by mortar 2.5 cm thickness. The percentage of reinforcement were ρ = 0.07%, ρ = 0.15%, and ρ = 0.21% according to local code. Cyclic load by using load control until the occurrence of the first crack was applied, and then displacement control was applied.

The first wall, ρ = 0.07%, showed some horizontal cracks on tie-columns and uniform inclined cracks on masonry caused by the beneficial effect of the reinforcement. The hysteretic cycles were symmetrical in linear range and relatively large with high-energy dissipation. Moreover, the yield of reinforcement wires over the diagonal crack caused the wall failure but the rest of the wall did not present damage. Finally, masonry failed at the top corners by compression-shear effect.

The second wall, ρ = 0.15%, was designed with partial safety factor equal to 1.5 in order to ensure the shear failure. The welded-wire fabric reinforcement was anchored to columns in order to prevent the masonry separation. At the central area next to columns and in the middle of the walls, the compression-shear effects caused crushing of the masonry units. At the end, neither the welded-wire reinforcement nor the columns have important damage.

Reinforcement of the third wall, ρ = 0.15%, was fixed to masonry and to right column with manufactured bolts. At the end, the lack of anchorage of the reinforcement generated the opening of the masonry-left column interface but an excellent performance of the bolts was observed. Figure 2.13 shows the resistance envelope of the three walls, where the distortion is the ratio between lateral displacement and wall height.

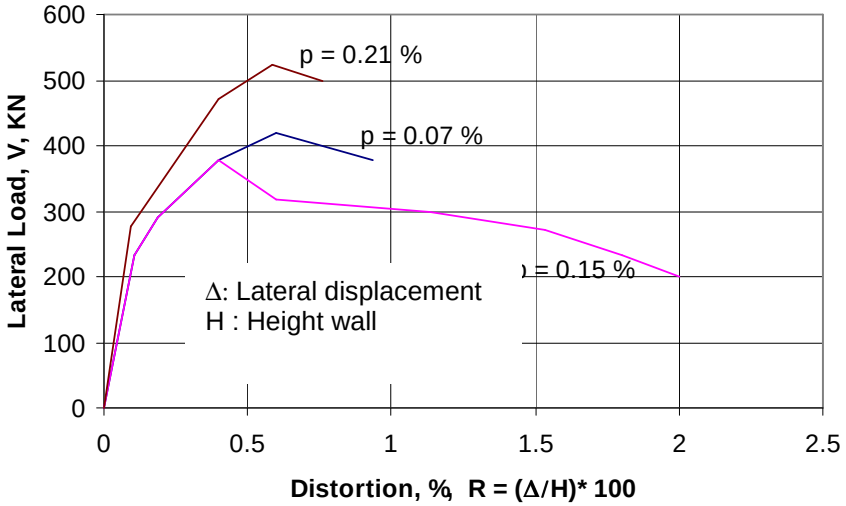

Figure 2.13: Experimental resistance envelope of walls tested by Pineda (1996)

2.5.1.1 Reinforcement of mortar joints

Bosiljkov (2005) developed an experimental program on three types of specimens (compression test, diagonal tension tests and shear tests) by placing two kinds of reinforcement inside the joints. The first type modified the normal mortar by adding polypropylene fibers (micro reinforcement). The second type (macro reinforcement) was a

non-metallic mesh placed inside the joints. Five types of mortar that represent different stages of the construction history were used to glue the masonry units. Thus, mortar “cement sand” has been used in modern construction. Mortar “cement lime sand” has been used in the latest five decades, and mortar “lime sand” has been used in historic structures. One additional type of mortar was reinforced with polypropylene fibers, and other was reinforced with non-metallic mesh, Figure 2.14.

The mesh-reinforced mortar panels showed a resistance slightly greater than the resistance registered with mortar “cement sand” panels. In the other way, the reinforced mortar panels had smaller elasticity modulus than the normal mortar panels.

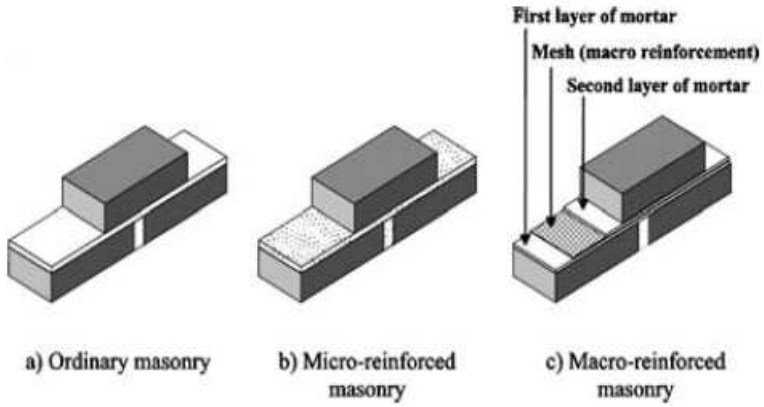

Figure 2.14: Ordinary, micro and macro-reinforced mortar [18]

For the diagonal tension tests, mesh-reinforced mortar panels showed the higher shear strength and an increase of ductility with respect to the reinforced mortar panels. The failures were combinations of joints sliding and masonry units cracking.

In the same way, Zhu and Chung (1997) developed a research in order to improve the bond resistance by adding carbon fibers to the mortar. They tested two types of specimens: one joint specimen subjected to tension, and other subjected to shear stress.

2.6 Design of masonry buildings in Guerrero State

Guerrero State located in zones C and D has high and very high seismic hazard according to seismic hazard map, Figure 2.6. This situation generates high values of the lateral loads to the masonry buildings design, Figure 2.15. Thus, a building placed on the same type of soil must resist a lateral load equal to 43% of its weight in Guerrero State [46], which decreases to 23% of its weight in Mexico City [43].

In addition, because of the limited experimental research conducted in Guerrero State about masonry or its components and due to absence of structures laboratories able to develop full-scale tests walls, the local code adopted identical parameters to those expressed in the Mexico City code. The compressive strength of units and masonry, the shear strength, and the modulus of elasticity and rigidity of masonry are the more important.

This generates high uncertainty about the behavior and reliability of masonry buildings because the raw materials and building processes of the masonry units are different to those used in México City. In this way, one goal of this project is to obtain representative values of the mechanical properties required for the design process or numerical analysis of masonry buildings.

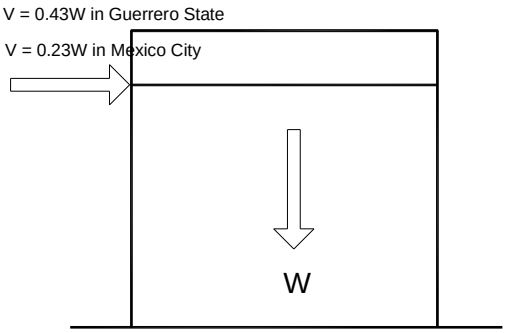

Figure 2.15: Lateral seismic load for two sites in Mexico [43] [46]

2.7 Conclusions

Confined masonry is the material most used for construction of buildings and houses in Guerrero State, where most masonry units are elaborated by means of manual process showing a large variation of their mechanical properties. In addition, the design seismic loads are high. Thus, the combination of both variables by using non-realistic normative parameters causes high seismic vulnerability for the masonry buildings.

To deal with this situation, a large experimental program (chapter 4) is proposed in order to: a) evaluate the mechanical properties of masonry units and masonry, b) determine the influence of reinforcement on masonry behavior, and c) evaluate the behavior of full-scale masonry walls. This experimental program requires the knowledge of the researches developed in the countrywide in order to evaluate its applicability Guerrero State or have comparative analysis of the results.

In addition, it is justified the development of either complex numerical models to simulate the masonry behavior or simplified models to evaluate only the masonry resistance (chapter 5 and 6). Besides, validation of the results requires the knowledge of the failure modes of the confined masonry walls.

CHAPTER 3

Masonry modeling review

3.1 Introduction

In addition to the analysis of the masonry behavior under lateral loads by means of experimental programs, the numerical modeling, mainly developed through the finite element method, is unavoidable for masonry research. Then the masonry behavior can be simulated without any need to develop expensive experimental tests of masonry walls or masonry buildings. Input vectors of these models can be modified to develop a large number of numerical simulations. Besides, one can be analyze several materials and different configurations, with or without opening, slender or short walls, and so on [1][9] [12] [29] [50].

This chapter shows the more common numerical model used to analyze the masonry. Its represents the basic hypothesis, the models characteristics, and the walls characteristics used to validate the results.

3.2 Types of masonry models

The numerical models can be classified into three groups: a) micro-models, b) macro-models, and c) simplified methods. The first group models the joints, masonry units, concrete frame, and the concrete frame-masonry interface. For each material, a behavior model based on plasticity theory, plasticity-damage theory or fracture theory is proposed, as well as the stress-strain relationship [1][38] [41][57], Figure 3.1b.

In this project, the second group is divided into two types. For “level-one” macro-models, masonry can have different behavior: homogeneous or inhomogeneous, isotropic or anisotropic. The mechanical properties are evaluated by means of either experimental tests on specimens or homogenization process. Usually, this kind of modeling evaluates the masonry behavior under monotonic load [12][50], Figure 3.1c. The second type of macro-models, called herein “level two”, evaluates the behavior of confined masonry walls tested under

cyclic loads by considering many simplifications. Most models consider the replacement of the masonry by strut elements [101] [114], Figure 3.1d.

The third group considers semi empirical or simplified models, which main purpose is to assess the ultimate resistance of masonry walls regardless to the displacement. Its application requires the tensile strength, the shear strength, or the compressive strength of the masonry and the vertical loads applied. Some models consider also the contribution of the external frame [42] [61][106].

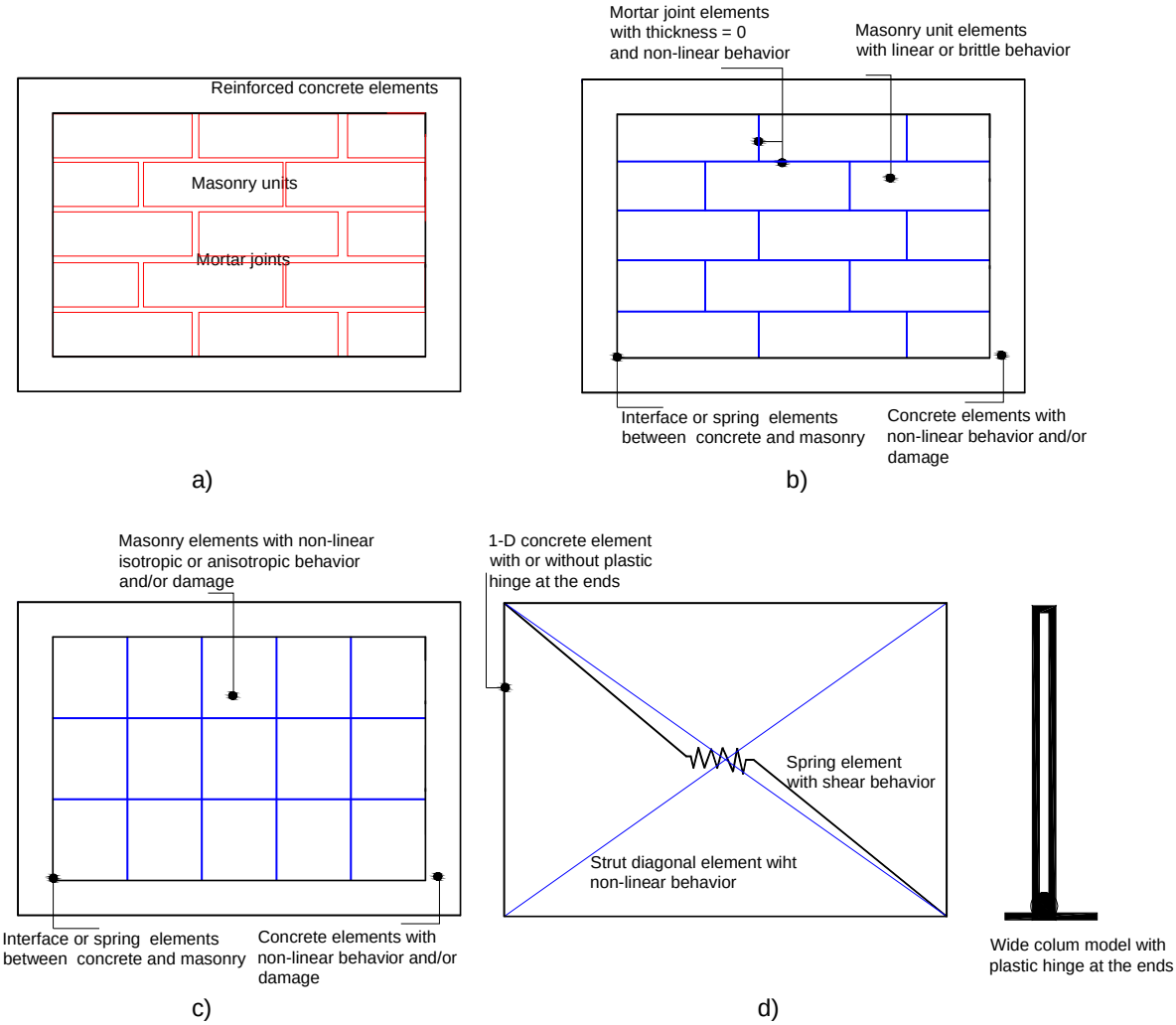

Figure 3.1: Kinds of numerical models of masonry: a) Confined masonry wall, b) Micro-model [8][57], c) Macro-model level one [12] [50], d) Macro-model level two [101] [114]

3.3 Masonry micro-models

- Lourenco and Rots (1997) proposed a model that assumes five forms for the failure of the system joint-units. They are: a) joint failure by tension stress, b) joint failure by shear effect, c) units cracking by tension effect, d) units failure by diagonal tension, and e)

failure of the system joint-units by compression effect. To consider all possibilities, the authors propose an envelope defined by three surfaces. The first surface related to Mode I and valid in the tension-shear area type cut-off, the second surface associated to Mode II that considers a linear model of Mohr-Coulomb in shear-compression, and the third associated to the compression failure by means of an ellipsoidal surface cap, Figure 3.2.

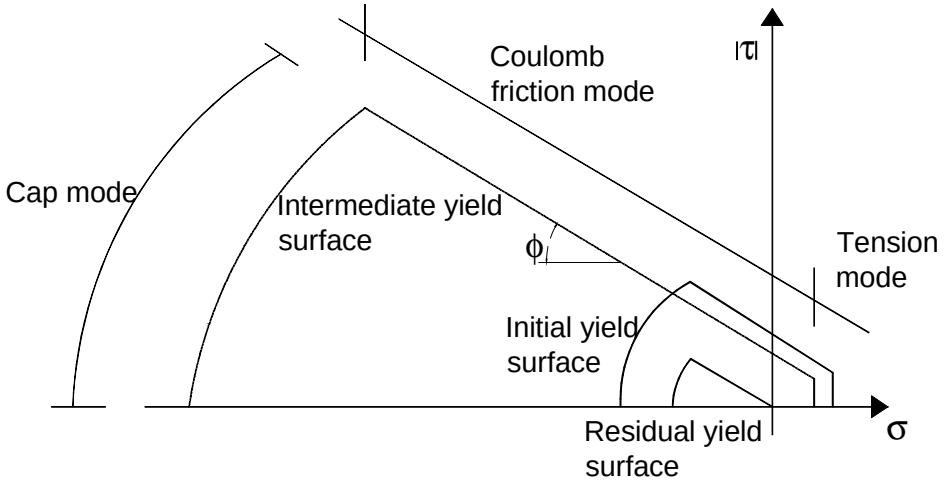

Figure 3.2: Two-dimensional interface model proposed by Lourenco and Rots (1997)

The model requires joints of zero thickness and vertical interfaces at the central plane of the units; these have an elastic behavior until the tensile strength with degradation after the peak. For Mode I, the tensile strength has exponential softening by considering plasticity associated with strain softening, Equation 3.1. For Mode II, the cohesion has exponential softening while the initial value of the friction angle decreases during the charging process to reach a residual value. Mode II has a non-associated plasticity function *g* by considering the dilatancy angle different to zero with strain softening hypothesis, Equation 3.2 and Equation 3.3. Equation 3.4 shows the yield function for the cap mode. The model considers coupling between Mode I and Mode II with strain softening.

$$f_1 = \sigma - \sigma_t \tag{3.1}$$

$$f_2 = |\tau| + \sigma\Phi - c \tag{3.2}$$

$$g = |\tau| + \sigma\Psi - c \tag{3.3}$$

$$f_3 = \sigma^2 + C_s\tau^2 - \sigma_c^2 \tag{3.4}$$

Were:

f_1 Yield surface function in tension mode

σ_t Tensile stress of the joint

f_2 Yield surface function in Mohr-Coulomb mode

Φ Tangent of the variable friction angle

c Cohesion of the joint

Ψ Tangent of variable dilatancy angle

f_3 Yield function in cap mode

g Potential flow function in Mohr-Coulomb mode

C_s Parameter to control the shear distribution

σ, τ Acting normal and shear stress on the joint

Experimental results of two types of masonry walls built from clay solid bricks with joints 10 mm thickness and vertical uniform stress were used to compare the numerical results. The tests were carried out under lateral load [90][111], Figure 3.3. Figure 3.4 shows the numerical and experimental results, where it can be seen a good concordance except for the test with maximum vertical stress. In addition, both failure modes were similar.

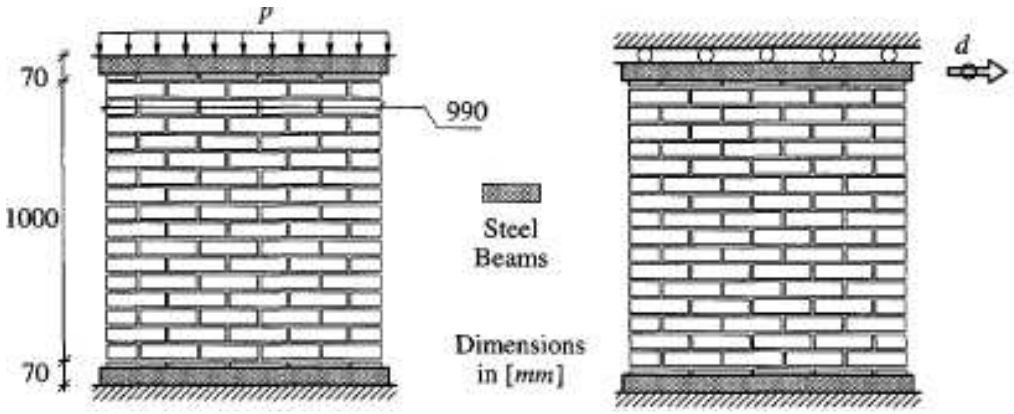

Figure 3.3: Tests on masonry wall referenced by Lourenco and Rots (1997)

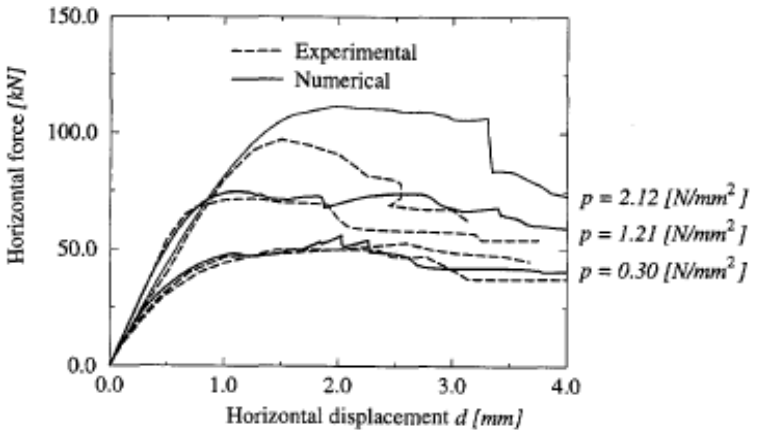

Figure 3.4: Numerical simulations and experimental results by Lourenco and Rots (1996)

- Alfaiate and Almeida (2004) modified the model proposed by Lourenco and Rots (1997) by means of a continuous parabolic surface of yield, Equation 3.5 and Figure 3.5. To facilitate the numerical development, the authors proposed an exponential variation of the cohesion in function of the tensile strength and a constant value of the friction angle. The plastic flow function *g* has two non-associated plasticity functions: one applied in tension zone, and other applied in compression zone. Both expressions are functions of the dilatancy angle ψ, the tensile strength σ_t and the joint cohesion *c*, Equation 3.6.

$$f = \tau^2 - \frac{\sigma_t + 2\,c\,\Phi\,\sigma_t - c^2}{\sigma_t^2}\,\sigma^2 - c^2\left(1+\Phi^2\right) + \left(\sigma + \Phi c\right)^2 \tag{3.5}$$

$$g = \begin{cases} \tau^2 + \left(\sigma\Psi - c_o\right)^2 & if\ \sigma \le 0 \\ \tau^2 - \dfrac{\sigma_{to}^2 + 2\,c_o\,\Psi\,\sigma_{to} - c_o^2}{\sigma_{to}^2}\,\sigma^2 - \left(1+\Psi^2\right)c_o^2 + \left(\sigma + c_o\,\Psi\right)^2 & if\ \sigma \ge 0 \end{cases} \tag{3.6}$$

Were:

f	Yield surface function
σ_t	Tensile stress of the joint
σ_{to}	Initial tensile stress of the joint
Φ	Tangent of variable friction angle
c	Cohesion of the joint
c_o	Initial cohesion of the joint
Ψ	Tangent of variable dilatancy angle
g	Potential flow function
σ, τ	Acting normal stress and acting shear stress on the joint

With regard to units, this model considers a linear elastic and isotropic behavior when the tensile stress is less than the tensile strength. After, the pieces show perpendicular cracks to the direction of the principal tensile stress. The authors consider a rotating crack model. Because of the fragile behavior of the pieces, the model does not suppose transferring shear after the cracking. A bilinear isotropic and perfectly elastic model resulting from Von Mises criterion describes the compression behavior of the masonry units. The results show that the inclusion of the rotating crack model is important to evaluate the behavior of unconfined masonry walls.

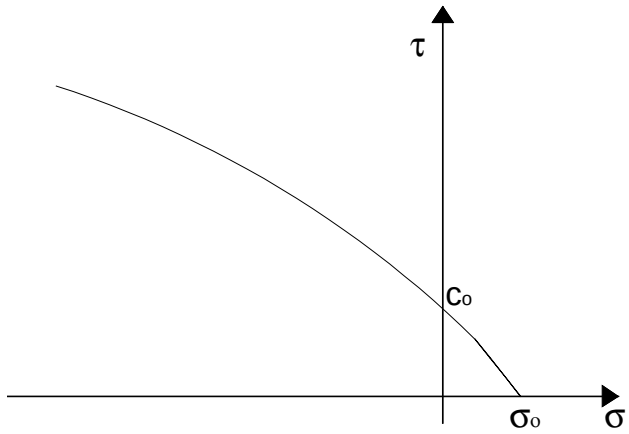

Figure 3.5: Two-dimensional interface model proposed by Alfaiate and Almeida (2004)

- Lofti and Shing (1994) proposed a hyperbolic model of yield with smooth transition between the criterion of yield tension cut-off and that of Mohr-Coulomb, Equation 3.7 and Figure 3.6. Tensile strength decreases depending on the equivalent strain and energy fracture associated to Modes II and I.

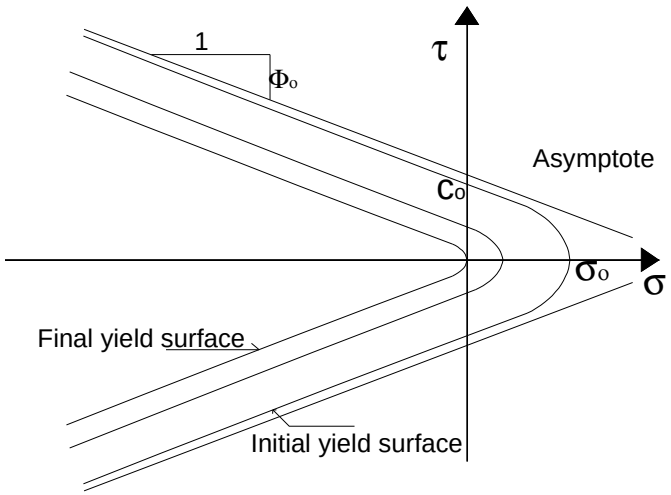

Figure 3.6: Two-dimensional interface model proposed by Lofti and Sing (1994)

On the other hand, the asymptotic slope decreases exponentially, as well as the curvature radius of the yield surface that is function of the friction angle Φ, the cohesion c, and the tensile strength σ_t. In order to avoid excessive dilatancy, a non-associated plasticity function g was proposed, Equation 3.8.

$$f = \tau^2 - (\sigma - \sigma_t)^2 \Phi^2 + 2r(\sigma - \sigma_t) \tag{3.7}$$

$$g = \eta\tau^2 + (r - r_r)(\sigma - \sigma_t) \tag{3.8}$$

Where:

f	Yield surface function
g	Non-associated plasticity function
σ_t	Tensile stress of the joint
Φ	Tangent of variable friction
r	Curvature radius of yield surface at the hyperbola vertex
r_r	Residual curvature radius of yield surface at the hyperbola vertex
η	Scale factor of dilatancy
σ, τ	Acting normal stress and acting shear stress on the joint

The authors proposed a combined criterion of Rankine-Von Mises to describe the yield surface of the units. It has linear elastic behavior under tension stress and parabolic behavior under compression stress with exponential degradation after the peak in both cases. Besides, the joints have zero thickness.

The numerical model was applied for two unreinforced, ungrouted hollow concrete block masonry walls, 1.62 m X 1.62 m (Height X Length), where the normal load was applied first and kept constant during the test. On top of the wall restrained against rotation was applied in-plane lateral displacement. Figure 3.7 shows the finite element mesh used and Figure 3.8 presents the numerical and experimental results of the wall subjected to 264 KN of vertical load. It can be seen a good correlation of both curves except for the final stage. One cause of discrepancy may be the deficiency of the smeared crack model that modifies the shear resistance at top and bottom compression toes of the wall.

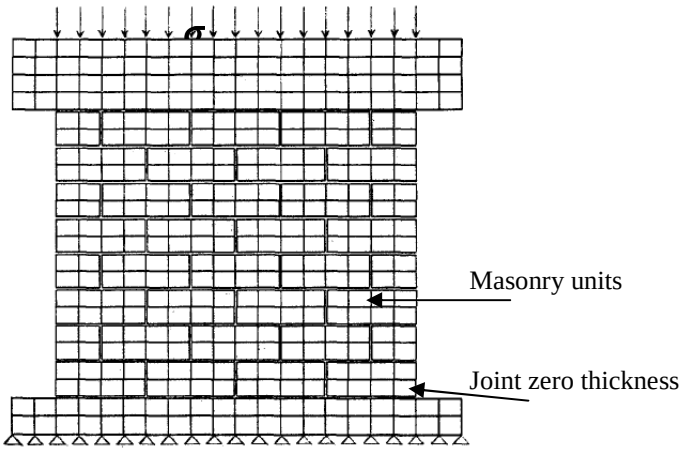

Figure 3.7: Finite element mesh proposed by Lofti and Sing (1994) for an unreinforced masonry wall

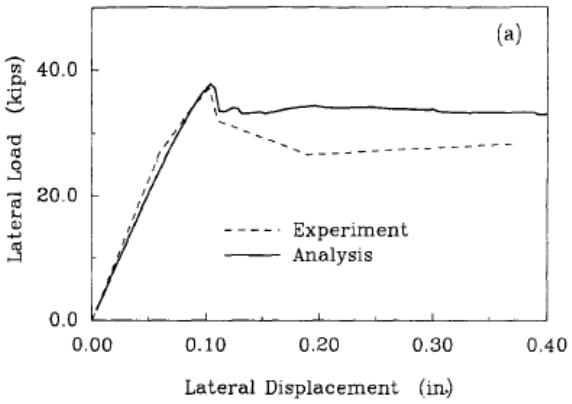

Figure 3.8: Load vs. displacement curves under 264 KN of vertical load by Lofti and Sing (1994)

In order to evaluate the masonry behavior, additional micro-models have been developed by Giambanco, Spallino and Rizo (2001), Merabi and Shing (1997), and Abdou (2005).

3.4 Masonry macro-models

3.4.1 Level-one macro-models

- Ishibashi and Kastumata (1994) conducted numerical modeling of five specimens, each one composed by two walls 2.50 m height coupled by means of different systems. Even if the walls were tested under cyclic lateral load, the authors developed the study assuming an incremental monotonic loading because the cracks in masonry walls are difficult to simulate The proposed hypotheses were:

  a) There was no influence of the slab foundation on the walls behavior,

  b) To model the masonry, homogeneous elements with mechanical properties obtained on tests were used. Its size was approximately square with two courses height,

  c) Horizontal joints between masonry elements were modeled by using spring elements, which had a tensile strength equal to three times the masonry strength,

  d) Two types of spring elements were placed at frame-masonry interface, one in normal direction, and other in perpendicular direction.

  The failure surface of masonry and concrete was modeled under biaxial stress by using a stress vs. elastic strain relationship with brittle failure in tension zone by means of the Kupfer et al. (1973) approach. However, in compression zone was used a stress vs. linear-parabolic-exponential strain relationship, Figure 3.9.

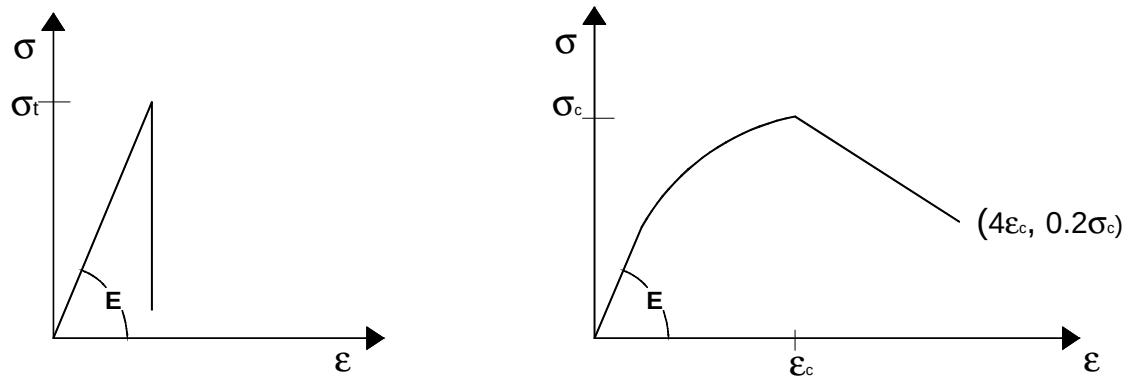

a) b)

Figure 3.9: Stress vs. strain relationship of concrete and masonry, a) Tension, b) Compression [50]

Two spring elements at frame-masonry interface were placed, one in normal direction with elastic behavior until the tensile stress and posterior brittle failure, and the other in parallel direction with elasto-plastic behavior by considering an elastic sliding equal to 0.1 mm, Figure 3.10. At the beginning, the vertical load is applied followed by increments of lateral displacement.

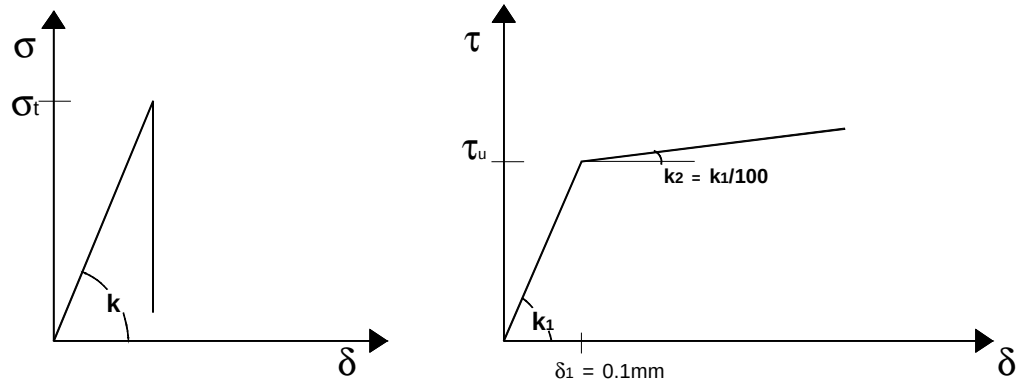

a) b)

Figure 3.10: Stress vs. strain relationship at frame-masonry interface, a) Normal spring elements, b) Tangential spring elements [50]

Figure 3.11 shows two of three structural systems analyzed composed by two walls built from solid clay brick 0.15 m thickness, 2.5 m X 2.4 m and 2.5 m X 1.6 m, composed these. Connection element between them was different in each system, one had a steel bar, other had a beam-slab concrete, and another had a beam-slab concrete plus a parapet on top of the wall. In addition, reinforcement steel inside the horizontal joints was placed in two systems. Tests were carried out under vertical constant load and lateral cyclic load.

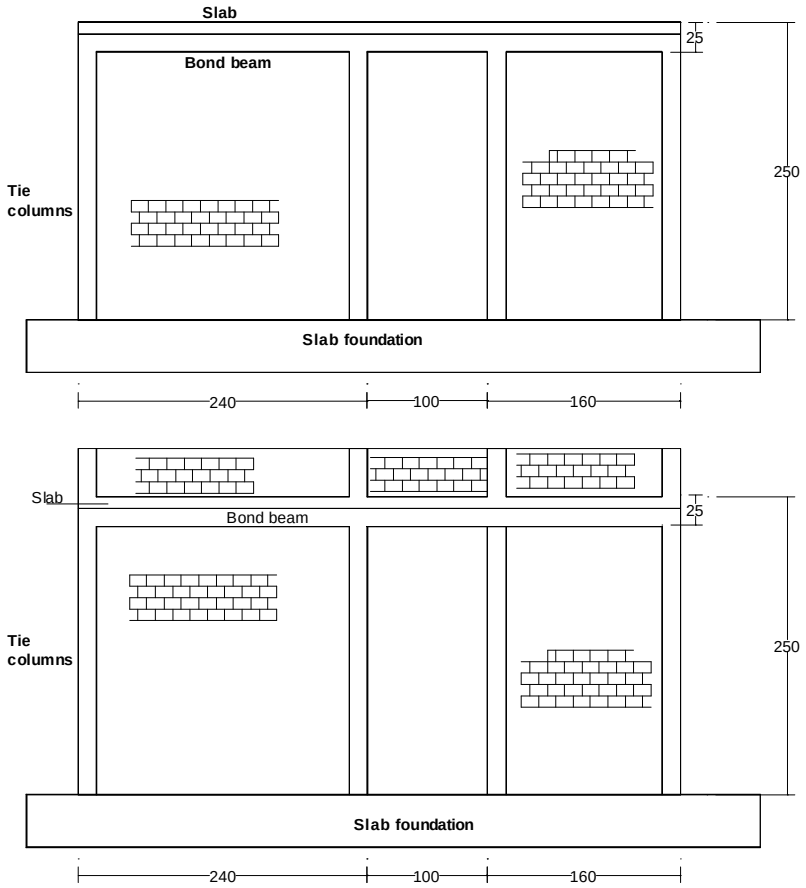

Figure 3.11: Confined masonry walls analyzed by Ishibashi and Kastumata (1994)

In general, the numerical models were able to simulate the experimental cracking of the units, sliding of the joints, and opening of frame-masonry interface, Figure 3.12. Besides, the ratio numerical resistance vs. experimental resistance ranged from 0.72 to 1.06.

- According to experimental results, Andreus (1996) classified the failure modes of the masonry subject to biaxial stress state. The author proposed ten failure mechanisms classified into three groups: a) slipping of the joint c) splitting of the bricks with slipping of the joint, and c) spalling of the bricks by compression effect. Under principal stresses normal and parallel to the horizontal joints with null shear stress, the model supposes the first failure caused by slipping of the joints. Then the second failure may occur by the splitting of units and slipping of the joints and at the end happens the spalling of the pieces.

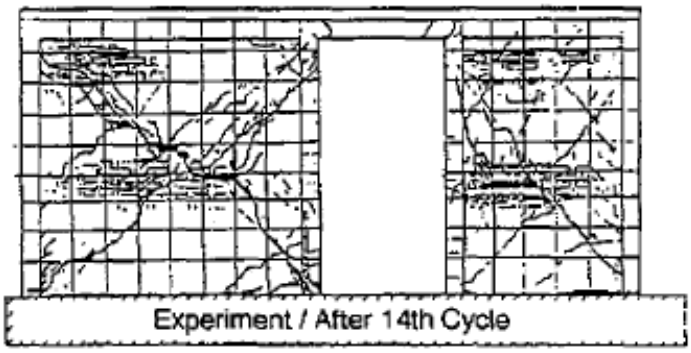

a)

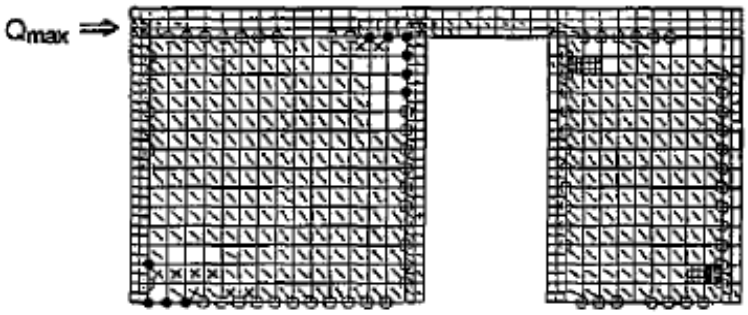

b)

Figure 3.12: Damage state to maximum lateral load, a) Experimental failure pattern [6], b) Numerical failure pattern [50]

The author proposed the Mohr-Coulomb modified criterion to evaluate the slipping of the joint, Equation 3.9. The anisotropic linear elastic Saint Venant criterion is used to analyze the normal cracking with respect to the principal tension stress of the units. It supposes that the slipping started at the vertical joints becomes as units' normal cracking, Equation 3.10. Finally, the criterion of maximum compression stress modeled the failure of the units, Equation 3.11.

$$f_1 = \tau^2 - \left(c_e - \sigma_n \Phi\right)^2 \tag{3.9}$$

$$f_2 = \tau^2 - G^2 \left\{ \left[\varepsilon_u - \frac{1}{2}\left(\frac{1-\nu_{pn}}{E_p}\sigma_p + \frac{1-\nu_{np}}{E_n}\sigma_n \right) \right]^2 - \frac{1}{4}\left(\frac{1+\upsilon_{pn}}{E_p}\sigma_p - \frac{1+\nu_{np}}{E_n}\sigma_n \right)^2 \right\} \tag{3.10}$$

$$f_3 = \tau^2 - \left(\sigma_p - f_c^{'}\right)\left(\sigma_n - f_{cn}^{'}\right) \tag{3.11}$$

Where:

f_i Yield function of surface *i*

c_e Effective cohesion

Φ Friction coefficient of slipping in direction parallel to the bed joints

G Modulus of rigidity

ε_u Ultimate strain in direction of the tensile maximum stress before the crack opening

E_p Modulus of elasticity in parallel direction

E_n Modulus of elasticity in perpendicular direction

ν_{pn} Poisson's ratio

ν_{np} Poisson's ratio

f'_c Biaxial compressive strength in direction of the minimum principal stress

f'_{cn} Biaxial compressive strength in normal direction

σ_n Stress normal to bed joints

σ_p Stress parallel to bed joints

τ Absolute value of shear stress

In each state and for each integration point are reviewed the stress conditions and the stress-strain criteria to evaluate which criterion fails. The model showed good agreement with experimental results of the solid-units panels tested by Dhanasekar et al (1985).

- Another model to simulate the masonry behavior by means of the tension-compression multi-surfaces criterion is the combination of the Rankine modified model in tension and the model of Tsai Hill in compression. It considers the anisotropy of the masonry and the variation of the shear stress. For this model, the tension stress varies in both directions in function of the tensile strength, characteristic length of finite element, and fracture energy. Its application requires at least six tests on masonry panels to obtain the necessary parameters. Abdou (2005) implemented this model combined with damage criterion to evaluate the masonry wall behavior, which results were acceptable.

3.4.1 Level-two macro-models

- Zúniga and Terán (2008) proposed a non-linear analysis procedure based on the wide column model to estimate the cyclic behavior of masonry buildings. The model replaces the masonry walls by a wide column element with identical properties, while an element (with infinite stiffness to flexion and shear) substitutes the concrete slab, Figure 3.13. The authors defined three phases of the wall behavior dominated by shear deformations. The

first phase has an elastic behavior until the masonry diagonal cracking. Then, the second phase presents stiffness degradation until the maximum lateral load. The last phase has stiffness and resistance degradation until the wall failure. From experimental evidence, they proposed three pairs of values of lateral load and distortion to define the envelope curve.

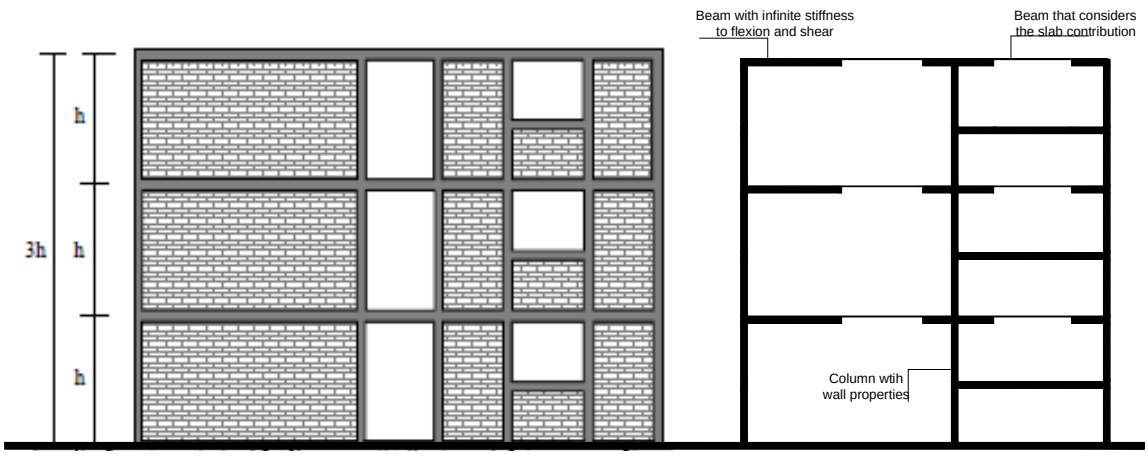

Figure 3.13: Masonry building and model of wide column [114]

They proposed also an equation to define the stiffness degradation that considers the cycle stiffness vs. initial stiffness relationship as long as the flexural stiffness is constant during the analysis. The application to individual walls and two-level masonry building shows good precision with respect to experimental results, Figure 3.14.

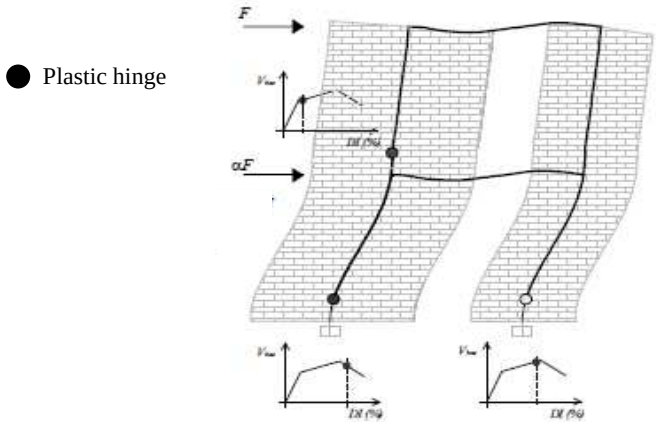

Figure 3.14: Damage on wide column model for two-level masonry building [114]

- To evaluate the response of the confined masonry subjected to dynamic loading, Smyrou (2006) developed a numerical model, where five linear elements replace the masonry wall. Two strut elements parallel to each diagonal have hysteretic behavior defined by Crisafulli et. al (2000). A spring element under shear solicitation, which joints opposite corners, has hysteretic bilinear behavior depending of the panel deformation and can

withstand compression effects. Each strut element linked a wall corner with a fictitious point defined by the width of the diagonal to simulate the contact between masonry and frame, Figure 3.15.

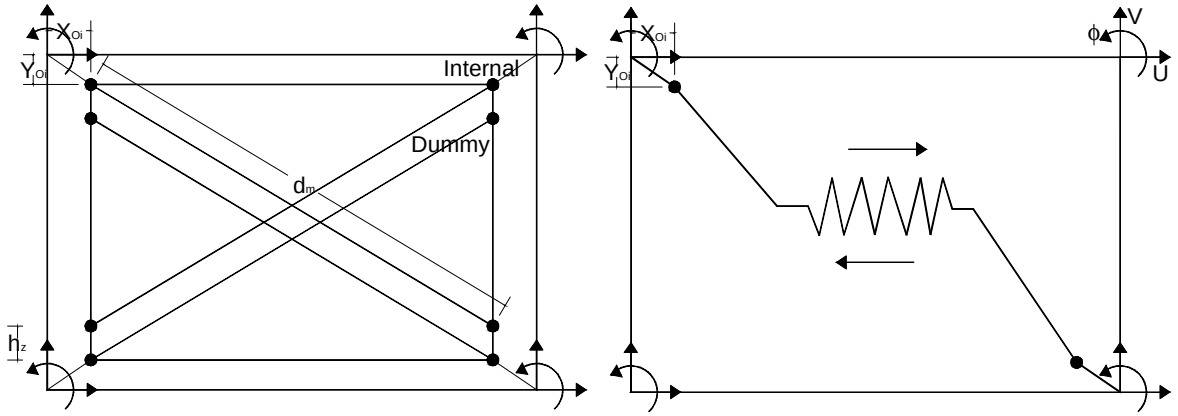

a) b)

Figure 3.15: Masonry wall model: a) Four diagonal elements, b) Spring elements with shear behavior [101]

The system stiffness obtained from equilibrium and compatibility of loads and displacements is the sum of the spring element stiffness and the struts elements stiffness. The model application requires many geometrical-mechanical and empirical parameters such as: a) compressive strength, modulus of elasticity, and tensile strength of the masonry, b) cohesion, friction and shear strength of the joint, d) size of the concrete columns, e) vertical separation and area of the strut elements. Empirical parameters have been proposed according to masonry walls behavior. The model proposes to reduce the strut elements area according to empirical factors in order to analyze walls with doors or windows.

A full-scale test with, four storey, three-bay reinforced concrete building with infilled brick walls under pseudo-dynamic loads was used to compare both results. They show a good agreement.

Mandan et al (1997) and Puglisi (2007) have proposed also numerical models level two for assessing the hysteretic behavior of confined masonry walls.

3.5 Simplified models

The aim of these models is to assess the masonry walls resistance regardless of the distortion. Some models evaluate only the masonry resistance whereas others take also account the

external frame resistance and/or the reinforcement steel resistance. Most models require the mechanical properties of masonry obtained on prism tests or panel tests and other models require the mechanical properties of joints and units.

Tomazevic (2000) evaluates the lateral resistance of confined masonry walls by means of Equation 3.12 that considers the masonry resistance and the concrete frame resistance.

$$V = C_R V_{u1} + V_{u,fr} \tag{3.12}$$

Where:

- V_{u1} Masonry resistance related with the cross-sectional area of masonry, tensile strength, acting vertical load, and an interaction coefficient that considers the distribution of forces as well as the variation of the shear stress on the wall horizontal section
- C_R Reduction factor ranging from 0.5 to 0.7
- $V_{u,fr}$ Concrete frame resistance evaluated as the sum of shear resistance of the stirrups and shear resistance associated to the flexural moments of the columns

Mexican codes [42][45] consider only the masonry resistance and neglect the concrete frame resistance by means of Equation 3.13

$$V = \min \begin{cases} A_T \left(0.5\tau_m^* + 0.30\sigma\right) \\ 1.5\ \tau_m^* A_T \end{cases} \tag{3.13}$$

Where:

- A_T Cross-sectional horizontal area of the wall
- τ^*_m Reduced shear strength obtained on diagonal tension test
- σ Vertical stress generated by gravitational loads

From experimental results of walls built with hollow concrete blocks and different Height/Length ratios tested under cyclic loading, Castilla and Marinilli (2003) proposed Equation 3.14.

$$V = A_T (0.22\sigma / f_m + 0.50) \tag{3.14}$$

Where:

A_T	Cross-sectional horizontal area of the wall
σ	Vertical stress generated by gravitational loads
f_m	Compressive strength of the masonry
0.50	Shear strength in MPa

Besides, other type of models supposes that only one part of the wall resists the lateral load and the failure occurs by compression effect of the diagonal equivalent element. Thus, Cruz (2002) proposed Equation 3.15, where the diagonal strut slope is equal to either the wall diagonal slope for vertical full joints or the units' diagonal slope for vertical empty joints.

$$V = f_m t l_c \cos\alpha \tag{3.15}$$

Where:

f_m	Compressive strength of the masonry
t	Wall thickness
l_c	Width of the equivalent diagonal obtained by an empirical equation
α	Diagonal angle of the diagonal strut

Mebarki et al. (2009) avoid the use of the diagonal strut and consider the presence of the normal tension stress along the wall diagonal. Thus, the wall failure occurs by induced tension when it overcomes the tensile strength of the masonry. Equation 3.16 requires a fitting function $f(\gamma)$ related to the angle of the wall diagonal.

$$V = A_d \sigma_t \, f(\gamma) \tag{3.16}$$

Where:

A_d	Failure diagonal area
σ_t	Tensile strength of masonry
$f(\gamma)$	Fitting function

3.6 Conclusions

This chapter describes the numeric models commonly used to evaluate the masonry behavior. The existing models have been divided into three groups: micro-models, macro-models, and simplified models. The micro-models represent the masonry units, joints, and concrete elements by means of finite elements, where each component has a constitutive law. In this way, it is possible to take in account, with particular accuracy, the characteristics of the joints that play an important role in the masonry global behavior. However, the principal limitation of these models is the high computational effort required. In general, this type of model analyzes specimens under monotonic lateral load.

In this project, the macro-models have been divided into two levels. The “level-one” macro-models assume that the masonry is a continuum material to which it is necessary to define the behavior criterion, the yield function, and the plastic flow function. Tests on masonry prisms or homogenization process are useful to evaluate the mechanical properties. Then, without high computational effort, these become possible the analysis of the masonry walls. This type of model is able to carry out the analysis under monotonic lateral loads.

The “level-two” macro-models represent the masonry by means of several struts elements or spring elements. Most models assume the failure by compression effect of the strut elements, which characteristics are measured on masonry prism tests or on masonry walls tests. Other models require additional mechanical properties of the masonry joints. This type of model simulates the masonry walls behavior subject to monotonic lateral or cyclic load.

By contrast, the simplified models evaluate the masonry walls resistance regardless of the deformation. Most models measure only the masonry resistance and neglect the frame resistance. Their application requires mechanical properties of the masonry and units, as well as the vertical acting stress.

CHAPTER 4

Experimental program and results

4.1 Introduction

The high seismic forces used for the structural design of masonry structures [26], the large use of this type of constructions [49], and the wide variation of this material generate high seismic risk for these type of structures built in Guerrero State [46]. One additional factor that should also notice is the lack of experimental data of the pieces and masonry used in this zone.

For this reason, it was necessary to developed a wide experimental program that: a) measures the mechanical properties of pieces, masonry and joints, b) assesses the increment of shear strength caused for the metallic reinforcement inside the joints, and c) evaluates the behavior of various confined masonry walls: unreinforced, reinforced and repaired with metallic reinforcement-mortar. Thus, this chapter contains the description and results of the tests, some of them used to build the numerical models and the simulations presented in chapter 5 and 6.

Compressive strength and modulus of elasticity of units and masonry, cohesion and friction angle of the joint, horizontal stiffness of the joint, modulus of rigidity of the masonry, and Poisson's ratio of units and masonry are among others, the required mechanical properties for the numerical models developed in chapter 5. In addition, the simplified models of the chapter 6 require the shear strength and tensile strength. Even if there are some references of the mechanical properties of the joints [7] [65] and masonry units [4] [64] in Mexico, some tests are still required.

In addition, this project is the first work developed in Guerrero State to evaluate the modulus of elasticity and rigidity of the masonry. Furthermore, testing of the walls depicted herein are the first tests conducted at the Laboratory Structures in University of Guerrero.

The experimental program shows two innovations for this type of masonry in Mexico: a) placement of the metallic reinforcement inside the joints, b) placement of the metallic hexagonal mesh-mortar coat on the wall faces.

With respect to the second reinforcement, a similar type composed by metallic wire-welded mesh bolted to wall faces and mortar has been used in Mexico [87][93]. However, the wires of the hexagonal mesh proposed herein are not welded and their diameter is smaller. Thus, this metallic reinforcement is cheap, flexible to guarantee its placement, and currently used in the rural areas for other type of activities.

For the metallic reinforcement inside the joints, the selection criteria were the flexibility to placement and the perfect bond to mortar in order to guarantee its yield. Its collocation does not require additional mortar. Then, the wall faces can stay without mortar layer, as this is a common situation in developing countries.

Two important points of this experimental program should be noticed.

- Measurement of the modulus of elasticity of the units of which that has not any national reference,
- Usefulness of the resistance of confined masonry walls from which is evaluated the resistance of the masonry buildings according to experimental evidence and local code [45] [96].

4.2 Description of the experimental program

The tests were carried out on three types of specimens: tests on masonry units, mortar samples, and concrete cylinders as the first type, tests on masonry panels and masonry prisms with different arrangements as the second type, and tests of three full-scale confined masonry walls are the third type. The local specifications defined the number of samples for each type.

Table 4.1 summarizes the experimental program, the first column shows the specimen tested, the second column defines the number of samples tested, and the third column shows the minimum quantity of samples to be tested according to local specifications. The fourth column defines the mechanical properties to evaluate as the last column describes their use.

Tests for elasticity modulus and rigidity modulus were developed at the CENAPRED Laboratory and the remaining tests were conducted at the Guerrero University laboratories.

Table 4.1 Experimental program developed

Specimen	Samples	Number of samples according to Mexican specifications [42], [70],[72],[83]	Mechanical properties evaluated	Use of mechanical property or technical information
Masonry units	30	30 pieces for compressive strength; for modulus of elasticity there are not specification	Compressive strength and modulus of elasticity	Micro-models and design
Mortar	31	9 samples for wall, 27 samples in total	Compressive strength	Design
Concrete cylinder	23	12 samples for wall	Compressive strength, modulus of elasticity and Poisson' ratio	Micro-models, macro-models and simplified models
Metallic reinforcement mesh	9	3 samples for set	Tensile stress and load-strain relationship	Micro-models, macro-models
Longitudinal steel bar	3	3 samples for set	Tensile stress and stress-strain relationship	Micro-models, macro-models and simplified models
Mortar joint	11	There is no specification	Cohesion, friction angle and horizontal stiffness	Micro-models
Unreinforced masonry panels	12	9 samples	Shear strength to several types of load	Macro-models, simplified models and design
Reinforced masonry panels	8	9 samples	Shear strength and influence of metallic reinforcement	Micro-models, macro-models and simplified models
Masonry panels associated to walls	13	9 samples	Shear strength and modulus of rigidity	Macro-models, simplified models and design
Masonry prisms	12	9 samples	Compressive strength and modulus of elasticity	Macro-models, simplified models and design
Circular masonry specimen	5	There is no specification	Tensile strength	Macro-models and simplified models
Wall MUR1	1	1 specimen	Shear resistance and failure model	Micro-models, macro-models, simplified models and design
Wall MUR2	1	1 specimen	Shear resistance, failure model and hysteretic behavior	Micro-models, macro-models, simplified models and design
Wall MRM2	1	1 specimen	Shear resistance, failure model and hysteretic behavior of confined-repaired masonry walls	Micro-models, macro-models, simplified models and design
Wall MRM3	1	1 specimen	Shear resistance, failure model and hysteretic behavior of confined-reinforced masonry walls	Micro-models, macro-models, simplified models and design

4.3 Tests on elements

4.3.1 Compressive strength of solid clay bricks

To evaluate the compressive strength of masonry units, thirty specimens of solid clay bricks, 0.13 m X 0.13 m X 0.05 m, were tested according to local specifications [71][73][74]. Six specimens instrumented with strain-gages provided the elasticity modulus, Figure 4.1. The compressive strength had mean value f_p = 9.4 MPa and coefficient of variation, CV = 0.17, Table 4.2 and Figure 4.2a. However, the manual elaboration of the units causes a large variation. Thus, Figure 4.2b presents the results of 297 tests where the mean value decreases to f_p = 6.5 MPa and the coefficient of variation rises up to CV = 0.43 [108].

Figure 4.1: Experimental setup of compressive test on solid clay bricks and tested specimen

The masonry prisms specification was used for assessing the units' modulus of elasticity because there is not local specification to measure it [75]. It considers the coordinates at 5% and 40% of the maximum stress according to Figure 4.3. Then Table 4.2 presents the mean value E_2 = 25, 099 MPa and coefficient of variation CV = 0.34. A second option proposed herein aims to evaluate the secant modulus of elasticity between the origin point and the peak. In this case, the mean value was E_1 = 5257 MPa while the coefficient of variation was CV = 0.20. Figure 4.3 presents the compressive stress vs. axial strain relationship, where was measured a mean value of axial strain ε_{max} = 0.002 for the peak.

Although the compressive mean strength is acceptable, after the test can be seen that the core of the specimens had some preexistent holes and different colors, both probably associated to the non-uniform process of firing which indicates bad quality of the units.

Table 4.2 Mechanical properties of masonry units

Parameter	f_p , [MPa]	E_1, [MPa]	E_2, [MPa]	ε_{max}
Mean value	9.4	5257	25099	0.0020
C. of variation	0.17	0.20	0.34	0.11

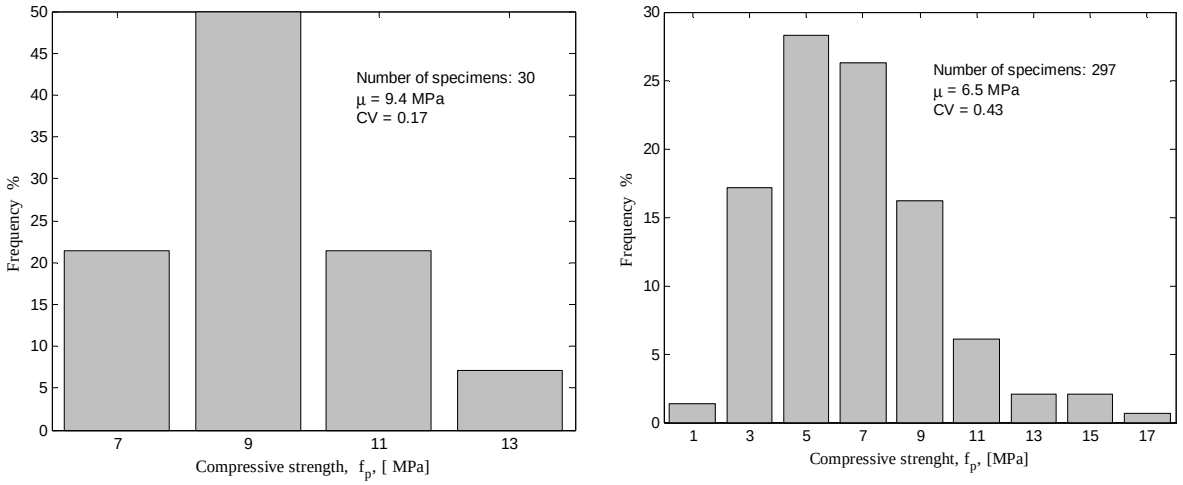

a) b)

Figure 4.2: Histogram of compressive strength, a) In this project, b) With large size of sample [108]

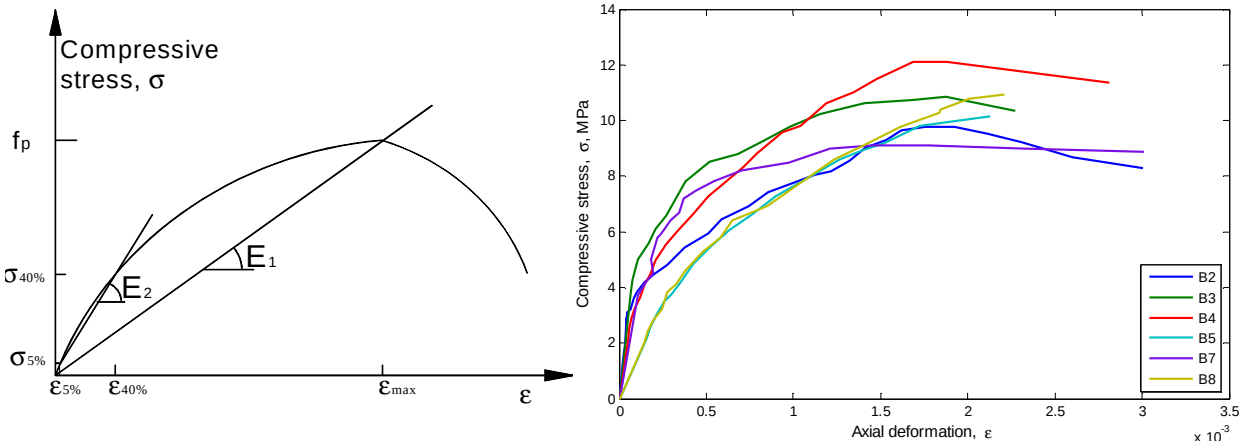

Figure 4.3 Definition of elastic modulus and compressive stress vs. axial deformation relationship

It is common to define the modulus of elasticity in function of the compressive strength [42][45]. Then data of Table 4.2 defines Equation 4.1 and Equation 4.2.

$$E_1 = 559 f_p \tag{4.1}$$

$$E_2 = 2670\, f_p \qquad (4.2)$$

4.3.2 Mortars

Mortar type I with dose by volume 1:3 cement-sand [45] was used for the specimens and walls tested herein. It has high compressive strength and reduces the influence of the compressive strength of the units on the masonry behavior. Tests on 31 samples were carried out according to local specifications [76] with mean value of the compressive strength f_j = 28.0 MPa and coefficient of variation CV = 0.11.

Mortar specimens show better behavior than the solid clay brick. Thus, the design compressive strength is f^*_p = 21.9 MPa by using the normative equation [45]. This value is 75 % greater than the design compressive strength value. Besides, the coefficient of variation is less than the specified value.

4.4 Test on specimens

4.4.1 Mechanical properties of mortar joints

The numerical modeling of the masonry by means of micro-models requires the joint mechanical properties: cohesion (τ), friction angle (ϕ), and horizontal and vertical stiffness (k_s, k_n). Although the two first parameters have some references in Mexico [7][65] and the stiffness joint has been evaluated in international studies [2][3].

Figure 4.4a shows the test specimen of three masonry units. Three samples under vertical load and confining stress equal to 0.25 MPa and eight samples under vertical load were tested. In order to measure the joint displacement, a linear variable differential transformer (LDVT) precision equal to 0.01 mm was used, Figure 4.4b. The cohesion (τ) was equal to 0.41 MPa, the friction angle (ϕ) and shear stiffness (k_s) were 35.7° and 28.0 N / mm, Table 4.3. The failure modes of the system joint –units were similar to those reported in previous works [2][3]. Figure 4.5 shows the shear stress vs. joint slip relationship for samples p15 and p17. According to Meli and Reyes (1971) and CEN (2002), the joint cohesion (τ) is a linear function of the confining stress σ, then data of Table 4.3 defines Equation 4.3 [MPa].

$$\tau = 0.41 + 0.72\,\sigma \qquad (4.3)$$

Table 4.3 Mechanical properties of mortar joints

Number of test	σ, [MPa]	τ_m, [MPa]	k_s, [N/mm]
8	0.00	0.41	
3	0.25	0.59	28.0
Friction angle ϕ = 35.7 °, tg (ϕ) = 0.72			

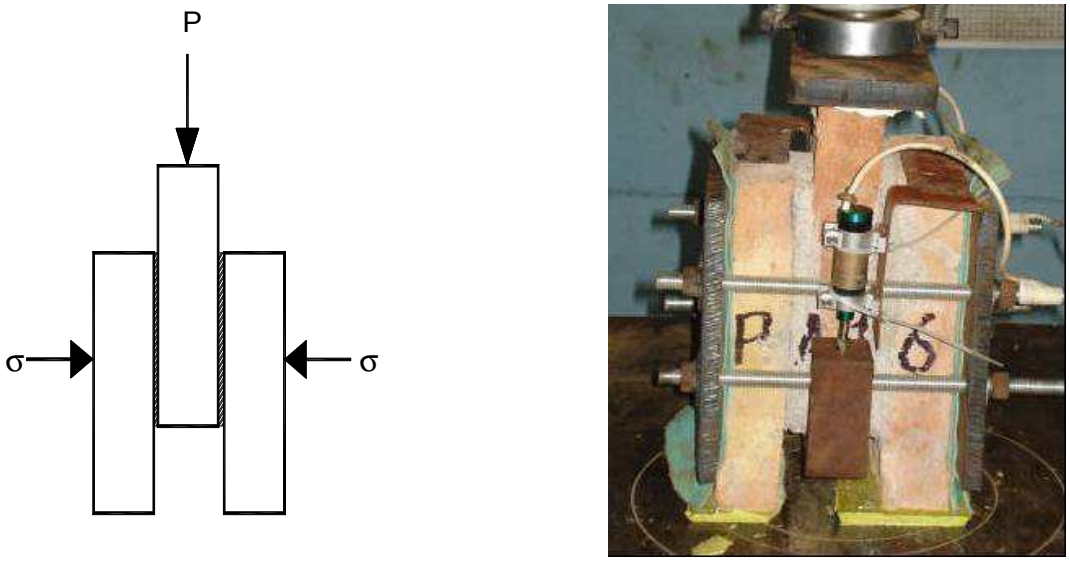

a) b)

Figure 4.4: a) Schema of mortar joint test, b) Experimental setup for mortar joint test

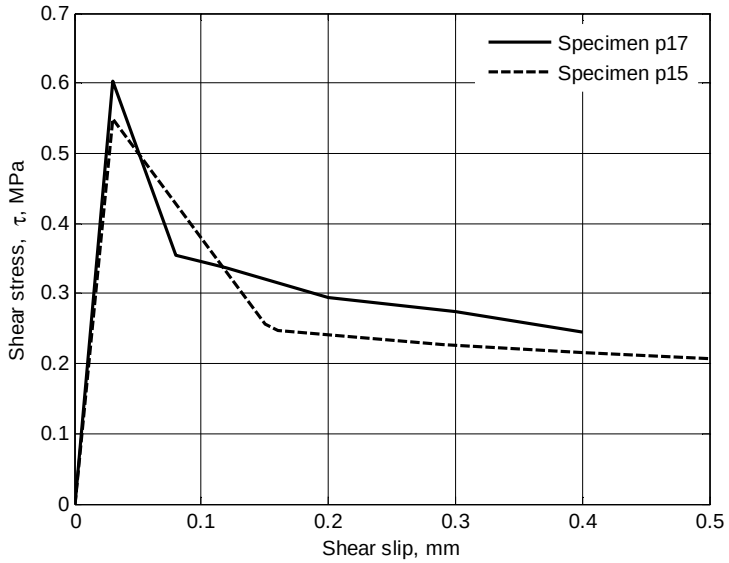

Figure 4.5: Mortar joint behavior with confining stress σ = 0.25 MPa

From results, it can be seen that the excellent quality of mortar raises the cohesion up to 0.41 MPa. It is greater than 0.25 MPa obtained by Meli and Reyes (1971), who used lower resistant mortar. Other reference parameter in Mexico is the value equal to 0.65 MPa for joints elaborated with compressive strength of mortar f_j = 7.6 MPa and confining stress equal to 0.55 MPa according to Alcocer et. al (1999). However, the cohesion evaluated herein is approximately equal to one third of that evaluated in other countries [1][38].

With reference to the friction angle, the value (ϕ = 35.7°) is smaller than that obtained by Meli y Reyes (1971), Abdou (2005), and Gabor et. al (2006b), ϕ = 36.8°, ϕ = 45°, ϕ = 39.6°, respectively. The horizontal stiffness of the joint (k_s) has no variation with respect to the referenced values [1][57].

4.4.2 Shear strength of masonry panels

In order to increase the shear strength of the masonry panels, two options were proposed: a) use of high compressive strength mortar, b) place metallic reinforcement mesh inside the joints [99]. For this purpose, twenty panels were tested (0.41 m X 0.41 m X 0.13 m, 0.55 m X 0.55 m X 0.13 m, and 0.63 m X 0.63 m X 0.13 m). Eleven panels tested under monotonic loading (panels MM and MR), six panels tested under loading-unloading cycles (panels MCD), and three panels tested under alternate loading along their diagonals (panels MCC). The characteristics of the units and mortar have been defined in section 4.3 and the size of panels satisfies the local code specifications [42].

Figure 4.6 shows the size of the panels and location of the metallic reinforcement mesh, which behavior is defined in Annex A1. Tests were carried out in a machine 1000 KN capacity, Figure 4.7. Two metallic “shoes” placed at the corners of the vertical diagonal are placed to guarantee the uniform distribution of the load during the test. Equation 4.4 evaluates the shear stress [42], Figure 4.6a.

$$\tau = F / L_v\, t \tag{4.4}$$

Where:

τ	Shear stress
F	Ultimate load
L_v	Vertical diagonal length
t	Thickness panel

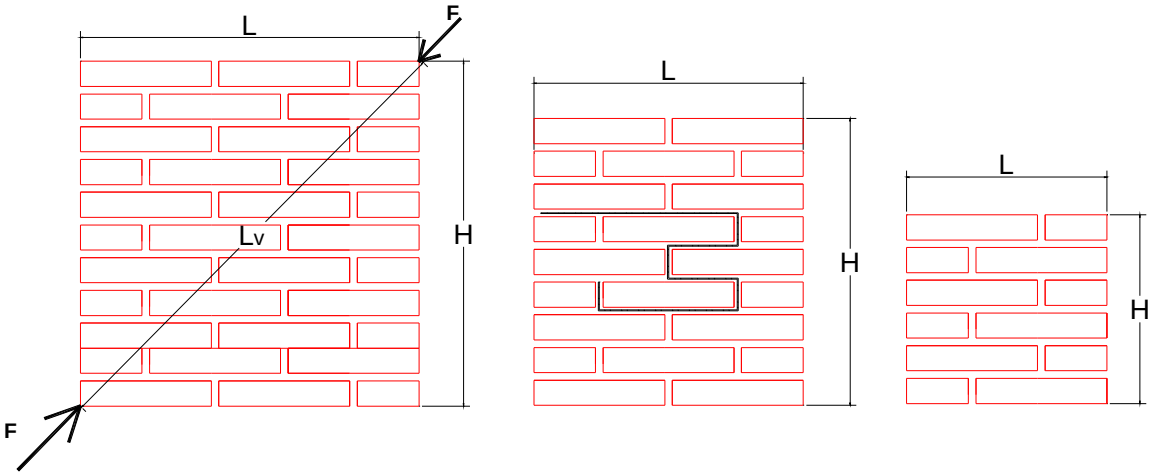

a) b) c)

Figure 4.6: Size of specimens: a) Panel MM and CD, b) Panel MR with metallic reinforcement mesh, c) Panel MM and MCC

Figure 4.7: Experimental setup of diagonal tension test

4.4.2.1 Behavior of unreinforced panels

Twelve unreinforced panels under three types of loads were tested. The control specimens MM1, MM5, and MM6 were tested under monotonic loading according to local code [45][75] while three loading-unloading cycles were applied to specimens MCD7-MCD12, Figure 4.8. One third of the maximum theoretical load along the first diagonal before applying the maximum theoretical load along the second diagonal was applied for specimens MCC2 and MCC3. For specimen MCC4, two thirds of the maximum theoretical load along the first

diagonal before applying the maximum theoretical load along the second diagonal was applied.

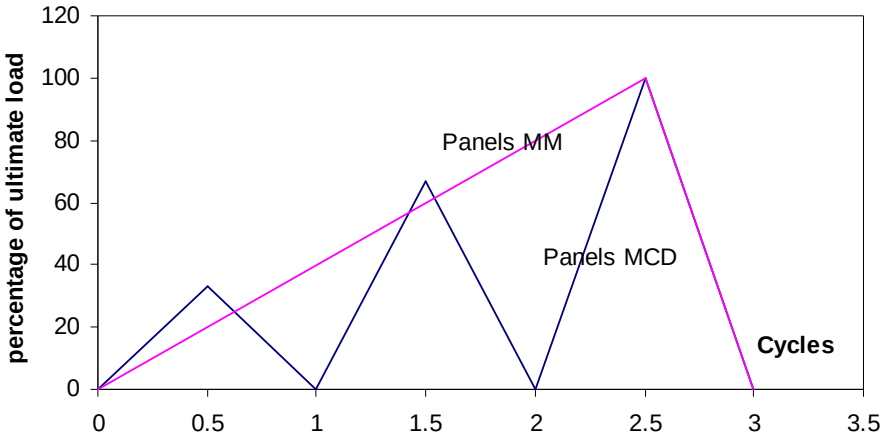

Figure 4.8: Load history applied to panels MM and MCD

The load applied on panels MCD and MCC aims to simulate the seismic actions developed in masonry walls. Then the loading-unloading cycles applied to panels MCD simulate the seismic load on masonry near the corners. Alternate loads along two diagonals of the panels MCC represent the load conditions in the middle of the wall, Figure 4.9.

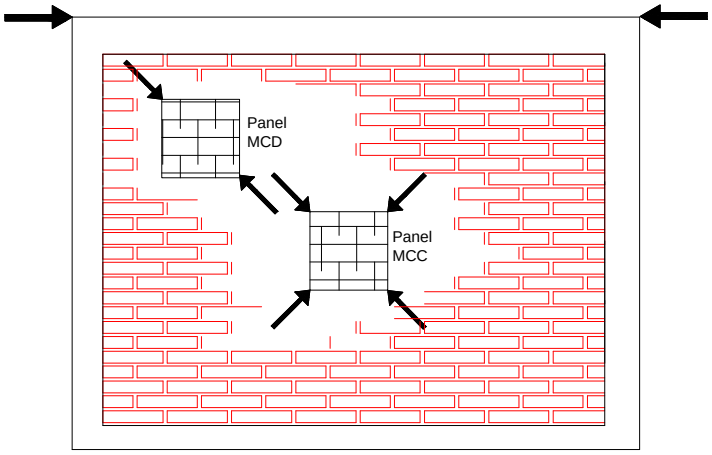

Figure 4.9: Types of load applied to panels MCC and MCD

Table 4.4 shows the independence of the shear strength with respect to the type of load and size of panel. Then the mean value is τ_m = 0.70 MPa. Table 4.5 presents the angle of the main crack measured at the end of the test with respect to the panel base. The highest values correspond to failure panels caused by diagonal cracking of the bricks, MCD11, MCD7, and MCC3, Figure 4.10 and Figure 4.11. The mean value is close to the masonry friction angle, ϕ = 33.20°.

Most panels had a combined failure of masonry units cracking and joints slipping. Masonry units present parallel cracks to the load direction with angle of 45° with respect to its base. Another casual failure of pieces is the parallel crack to the horizontal joints generated by shear effect. The failure by compression effect appeared only in panel MCD7 whereas panel MM6 presented several failure zones by slipping of the joints. In some specimens, the joints had vertical cracks generated by the fragmentation of the wall. Figure 4.10 and 4.11 show the final crack patterns.

Table 4.4 Mean shear strength according to type of load and size of panel

Type of load	τ_m, [MPa]	Size, [m]	τ_m, [MPa]
MM (Figure 4.8)	0.70	0.41 x 0.41 x0.13	0.70
CC	0.68	0.66 x 0.66 x0.13	0.70
CD	0.70		

Table 4.5 Angle of the failure plane

Specimen	Angle ϕ, degrees	Specimen	Angle ϕ, degrees	Specimen	Angle ϕ, degrees
MM1	29.7	MM5	29.3	MCD9	32.2
MCC2	33.7	MM6	32.0	MCD10	25.8
MCC3	39.0	MCD7	38.6	MCD11	44.9
MCC4	30.3	MCD8	33.7	MCD12	29.3

.

a)

b)

Figure 4.10: a) Failure mode of the panel MM1, b) Failure mode of the panel MM5

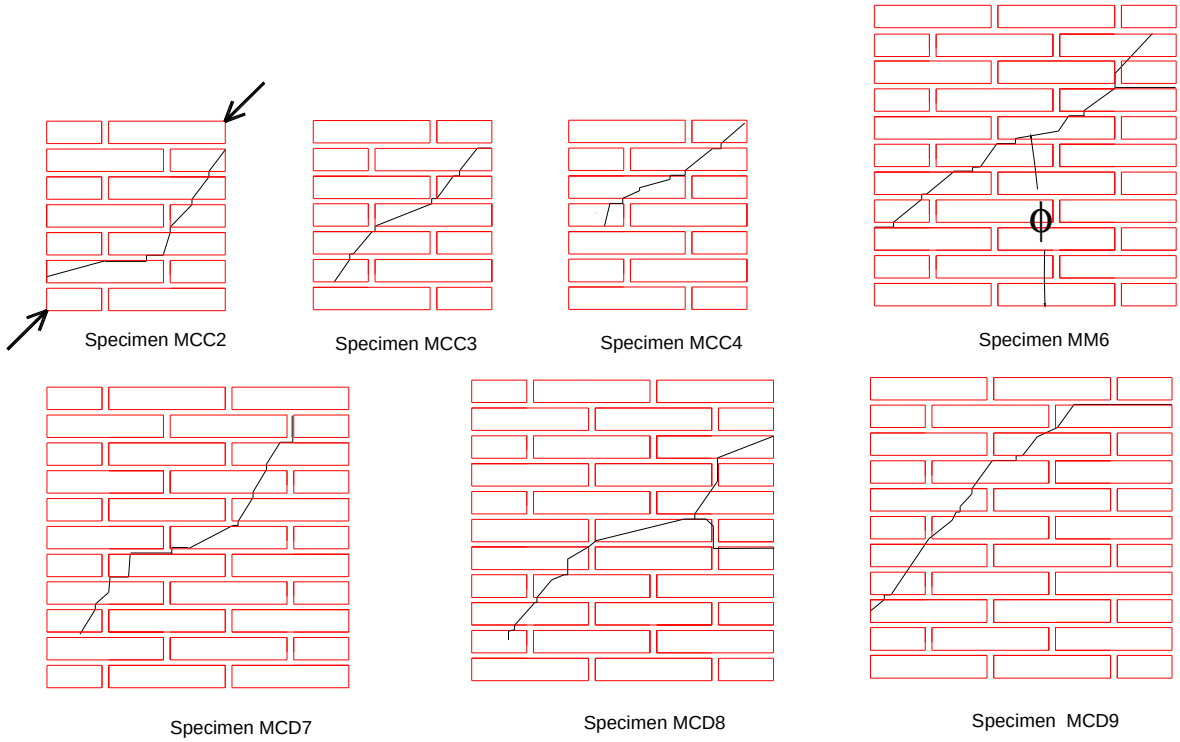

Figure 4.11: Failure modes of un-reinforced panels and definition of failure angle

4.4.2.2 Behavior of reinforced panels

In order to increase the shear resistance, a strap of metallic reinforcement mesh was placed inside the vertical and horizontal joints of eight panels [35], 0.55 m X 0.55 m X 0.125m. Location of the metallic reinforcement aims to confine the panels' core in order to induce the presence of the cracks across the reinforced joints. Thus, the reinforcement absorbs tension stress on the horizontal joints. It improves the joint resistance and generates the cracking of the piece, the ideal mechanism to obtain highest shear strength. The position of the metallic reinforcement mesh at middle of the joint ensures the perfect adherence with the mortar, Figure 4.12. Tests were carried out under monotonic loading according to specifications [45] [75] and Annex A1 summarizes the mechanical properties of the metallic reinforcement mesh.

The mean shear strength was τ_m = 0.85 MPa and the results present predominant failure modes of the units cracking by diagonal tension. In addition, the cracks crossed the metallic reinforcement mesh except for specimen MR17. The shear strength is still high for the panels MR17 and MR19 where there was slipping of the reinforced joints. Figure 4.13a shows the failure by tension effect of the metallic reinforcement mesh on the horizontal joint of the panel MR18, which pieces had a failure angle approximately equal to 45°. Figure 4.13b presents cracks across two reinforced joints of the panel MR23 while Figure 4.14 contains the

remaining failure patterns. Finally, Figure 4.15 presents the vertical load vs. vertical displacement relationships and the mean experimental curve.

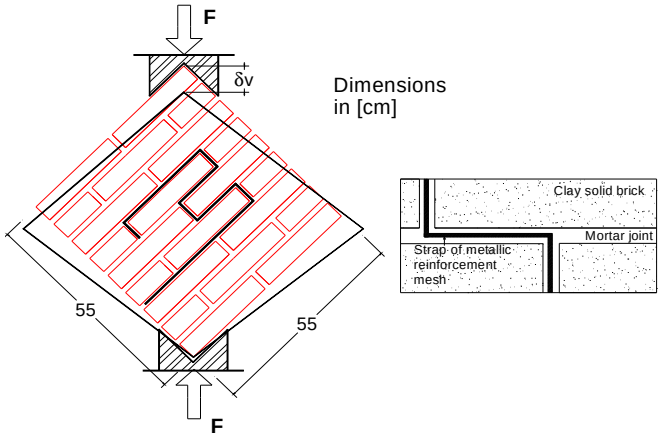

Figure 4.12: Position of metallic reinforcement mesh inside the mortar joint

a) b)

Figure 4.13: a) Tension failure of metallic reinforcement mesh in panel MR18, b) Failure mode of the panel MR23

The collocation of the metallic reinforcement had the following benefits:

- Increased the shear strength from 0.71 MPa to 0.85 MPa (20% of increase) ,
- Changed the failure modes with respect to that presented in unreinforced panels. Almost panels failed by diagonal cracking of the units and the cracks crossed at least once the metallic reinforcement, and
- Strengthened the joints and avoided the failure by shear effect.

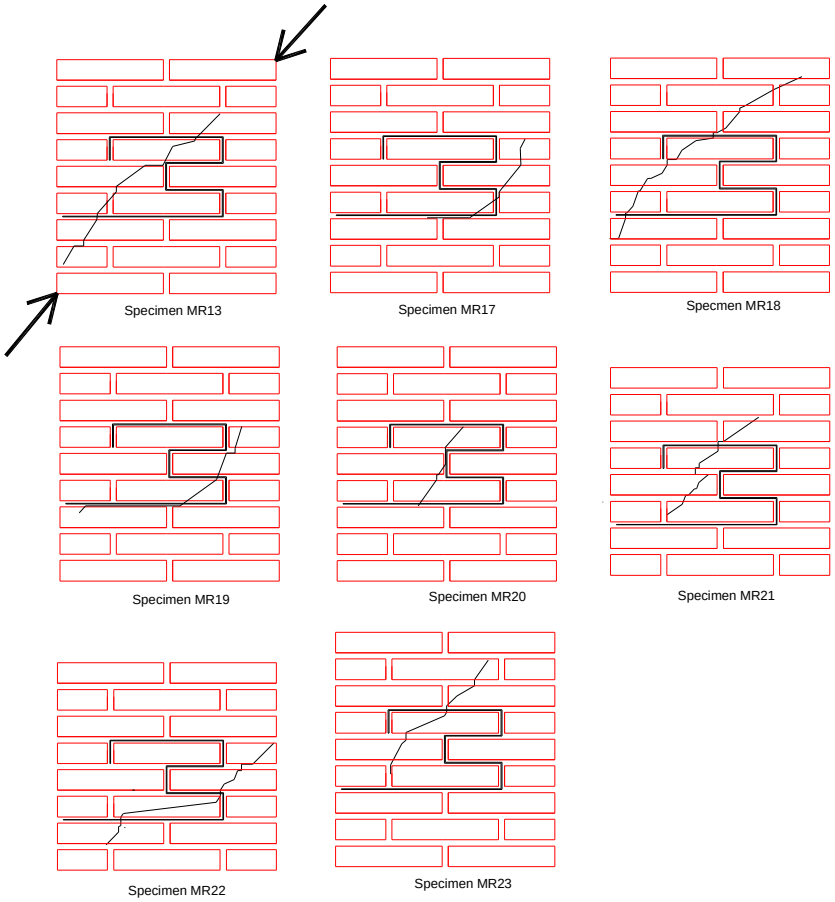

Figure 4.14: Failure modes of reinforced panels

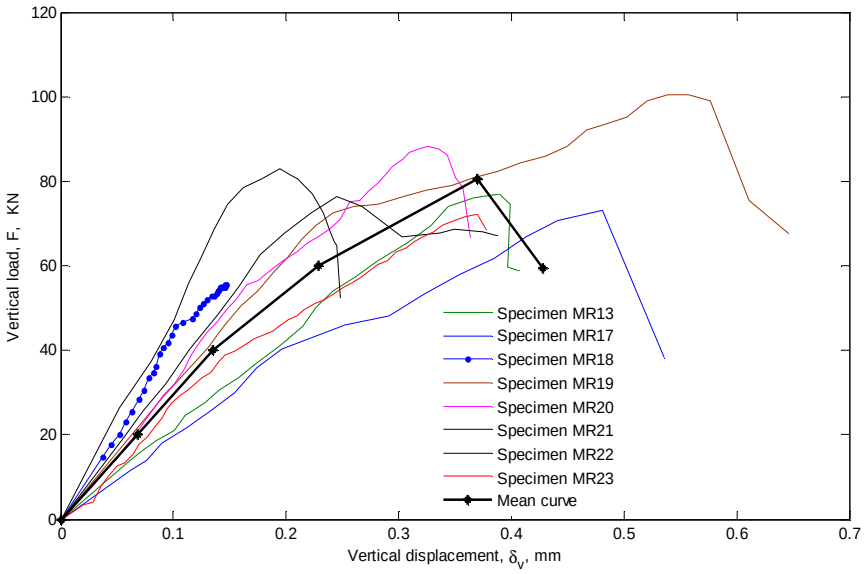

Figure 4.15: Vertical displacement vs. vertical load relationship of reinforced panels

In addition, the behavior and the cracking patterns of the reinforced panels indicate an adequate adherence between mortar and metallic reinforcement mesh.

4.4.2.3 Panels associated to masonry walls

As part of the tests on confined masonry walls presented in section 4.5, diagonal tension tests were also carried out on thirteen panels, 0.40 m X 0.40 m X 0.13 m, for assessing the shear strength and the modulus of rigidity [11][42][75]. Thus, the men value of shear strength calculated by Equation 4.4 is τ_m =0.71 MPa, while the modulus of rigidity calculated by Equation 4.5 had a mean value G_m = 1013 MPa [11]. Table 4.6 and Figure 4.16 show additional mean values of the mechanical properties.

$$G = \tau / \gamma \tag{4.5}$$

Where:

G Modulus of rigidity

τ Shear strength

$\gamma = \delta_v / L_v + \delta_h / L_h$ Shear strain [11]

L_v Control vertical length, Figure 4.16

L_h Control horizontal length, Figure 4.16

δ_v Vertical shortening

δ_h Horizontal extension

Table 4.6 Mechanical properties on diagonal tension test

Parameter	τ_m, [MPa]	G_m, [MPa]	γ_m	γ_u	G_m / τ^*_m
Mean value	0.71	1013	0.0007	0.0015	2110
C. of variation	0.26	0.27			0.21

Figure 4.16 shows the shear stress vs. tangential strain relationship of eight specimens. The curves have an important variation of its initial slope that determines a coefficient of variation *CV*= 0.27. These are characteristics of brittle materials with a sudden failure followed by a horizontal part that ranges from γ_m = 0.0007 to γ_u = 0.0015. Figure 4.17 shows the histogram by considering all results including those of § 4.4.2.1, then the coefficient of variation was *CV* =0.19. In order to describe the shear stress vs. shear strain relationship is proposed Equation 4.6.

$$\tau = \begin{cases} G_m \gamma & if \ \gamma \leq \gamma_m \\ \tau_m & if \ \gamma_m \leq \gamma \leq \gamma_u \end{cases} \quad (4.6)$$

Where:

τ Shear stress

τ_m Mean of the shear strength,

γ Shear strain

G_m Mean of the modulus of rigidity

γ_m, Mean of shear strain used to evaluate the modulus of rigidity

γ_u, Ultimate shear strain

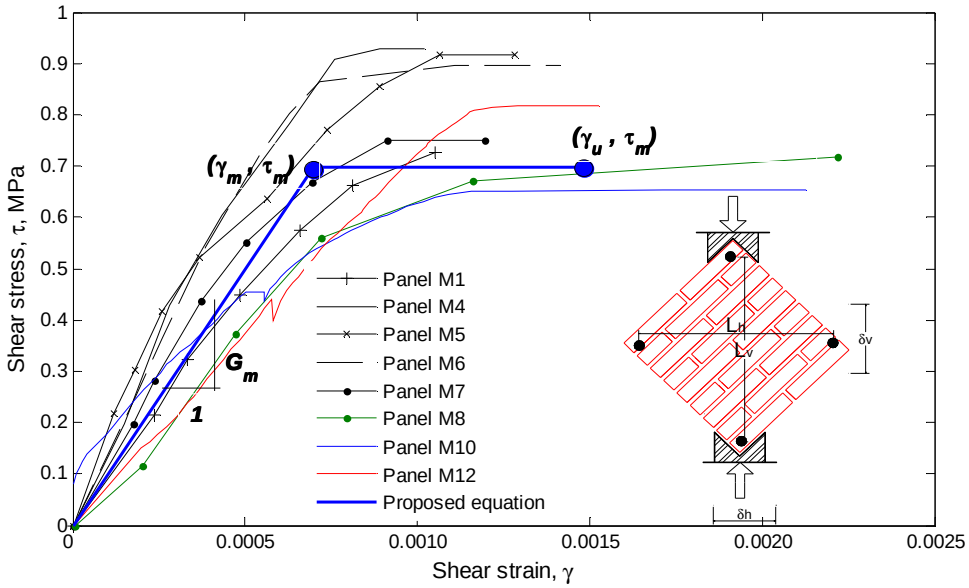

Figure 4.16: Shear stress vs. shear strain relationship of masonry panels

In general, the joint slipping by shear effect, the diagonal cracking of the units by induced tension and the cracking of masonry units by compression are the independent failure modes observed. Almost panels presented the failure mode caused by diagonal cracking indicating the presence of weak units and strong joints. Others presented a combination of diagonal cracking and joint slipping. Furthermore, the failure mode by diagonal cracking provides the highest value of shear strength. The behavior is similar to that described by Meli and Reyes (1971) and Salgado (2000).

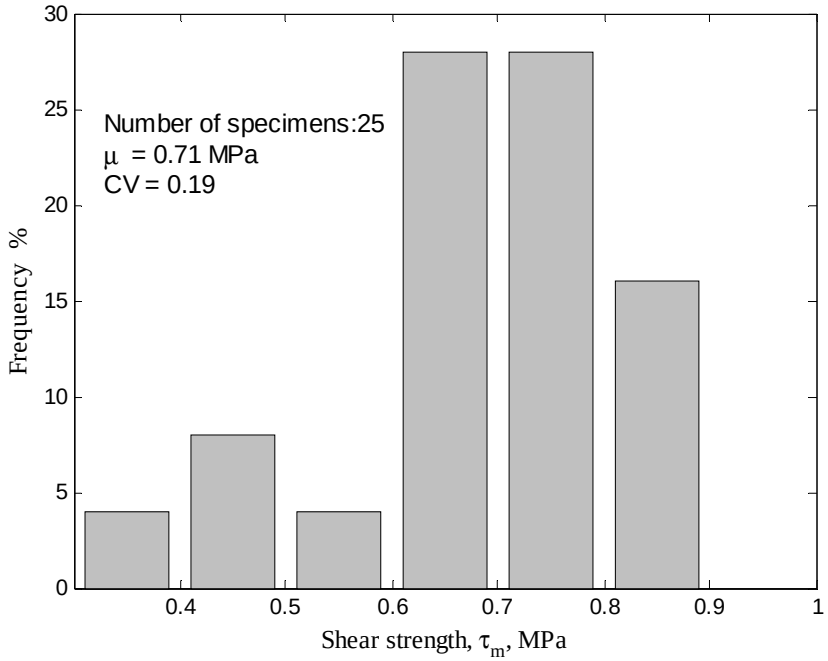

Figure 4.17: Histogram of shear strength

The design shear strength computed by normative Equation 4.7[45] for the 25 specimens is τ^*_m = 0.48 MPa by considering τ_m = 0.71 MPa and *CV* = 0.19. This value is 37 % greater than the specified shear strength τ^*_m = 0.35 MPa [45].

$$\tau^*_m = \tau_m / (1+2.5CV) \tag{4.7}$$

The experimental values of the design shear strength in Mexico ranges from 0.19 MPa to 0.35 MPa [4] [48][65] [69][107] but one referenced value equal to 1.20 MPa for the masonry panels constructed with multi-hollow concrete blocks [86]. Then, the shear strength calculated in this project is greater than all values previously obtained.

4.4.3 Compressive strength of masonry prisms

During the construction of the walls twelve masonry prisms with six pieces each one were tested according to specifications [75], in order to assess the compressive strength and the elastic modulus of the masonry, Figure 4.18. The mean values expressed in Table 4.7 are f_m = 4.5 MPa, E_m = 2426 MPa, and ε_m = 0.0029, where f_m is the compressive strength, E_m is the modulus of elasticity, and ε_m is the normal strain related to the compressive strength. Figure 4.19 shows the normal stress vs. normal strain relationship of nine masonry prisms and the parameters of Table 4.7.

Table 4.7 Mechanical properties on compression tests

Parameter	f_m, [MPa]	f_u, [MPa]	E_m, [MPa]	ε_m	ε_u	E_m/f^*_m
Mean value	4.5	4.0	2426	0.0029	0.0052	809
C. of variation	0.20	0.16	0.21	0.25	0.31	0.34

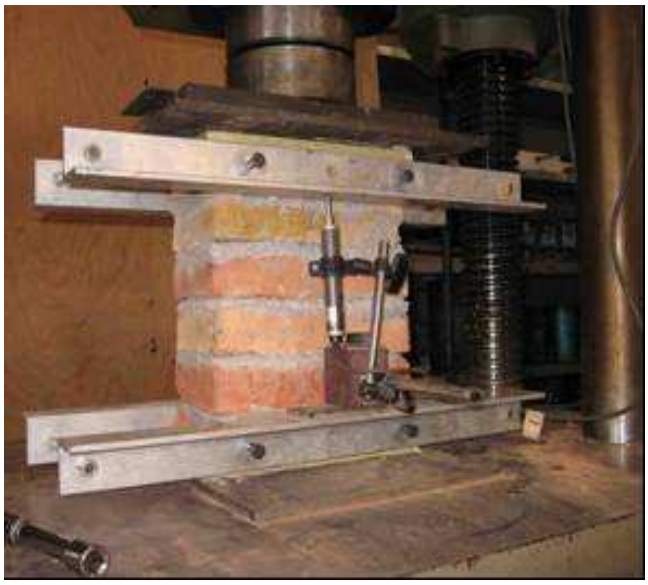

Figure 4.18: Experimental setup for compression test

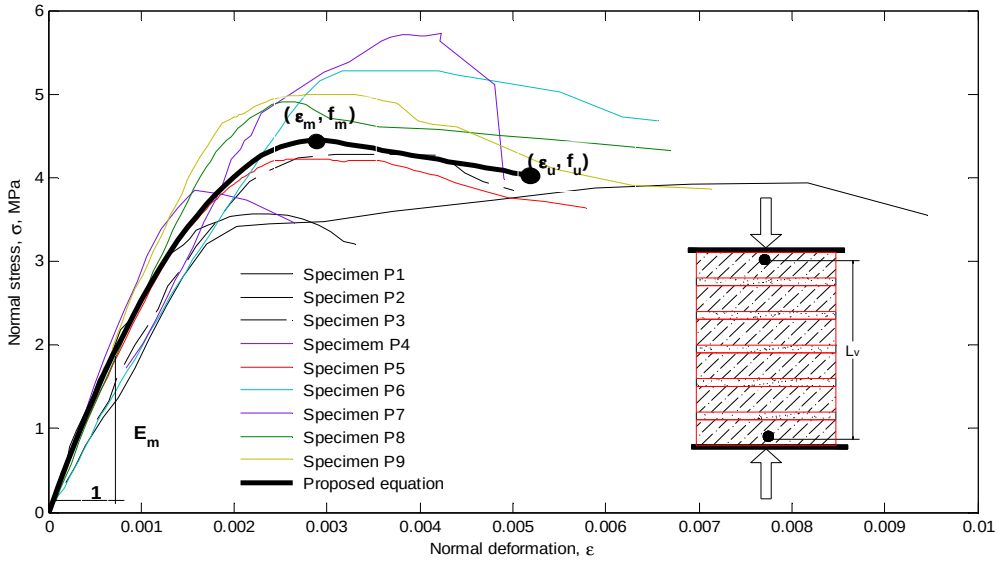

Figure 4.19: Compression stress vs. normal strain relationship for masonry prisms

Besides, to define the behavior of masonry prisms subject to axial stress Equation 4.8 has been proposed. The first part defines a parabolic variation of the axial stress until the maximum load and the second part proposes a linear variation.

$$f = \begin{cases} f_m \left[\dfrac{2\varepsilon}{\varepsilon_m} - \left(\dfrac{\varepsilon}{\varepsilon_m} \right)^2 \right] & if \ \ \varepsilon \leq \varepsilon_m \\ f_m - \left[\dfrac{f_u - f_m}{\varepsilon_u - \varepsilon_m} \right] \varepsilon & if \ \ \varepsilon > \varepsilon_m \end{cases} \tag{4.8}$$

Where:

f	Normal stress
f_m	Mean of the compressive strength
ε	Normal strain
ε_m	Normal strain related to mean compressive strength
f_u,	Ultimate compressive strength
ε_u,	Ultimate compressive strain

The evaluated compressive strength is similar to that obtained by Navez (2000) for the same kind of masonry units and mortar. Therefore, this value is slightly greater than that presented by Meli and Reyes (1971) and Aguilar (1997).

In other way, the mean and ultimate normal strains are identical to those values obtained by Meli and Reyes (1971). However, the modulus of elasticity is twice the referenced values. The normative Equation 4.7 provides the design compressive strength f^*_m = 3.0 MPa by using f_m = 4.5 MPa and CV = 0.20. Then the ratio E_m / f^*_m = 809 is different to that proposed by the local building code. Finally, the Poisson's ratio is ν = 0.19 according to Equation 4.9 and data given in Table 4.6 and Table 4.7.

$$\upsilon = \frac{E_m}{2G_m} - 1 \tag{4.9}$$

4.5 Test on confined masonry walls

Technical errors during the first test caused the loss of the experimental data for the wall MUR1, from which only the maximum load and the failure mode were obtained. The following paragraphs describe the characteristics of the systems used [27], the construction of the walls, its instrumentation, the development of the tests, and the results.

4.5.1 Description of the mechanical-electronic devices and apparatus

The load device is a metallic frame anchored to a reaction slab, 9.0 m X 9. 0 m X 0.7 m. The frame elements consist in two columns, one beam, and one strut element. Two lateral actuators 500 KN capacity can move vertically along the columns to apply alternate lateral load in opposite directions, Figure 4.20. A load cycle includes: a) opening of the left actuator, b) loading by the left actuator during 15 seconds, c) unloading and retraction of the left actuator, d) opening of the right actuator, e) loading by the right actuator during 15 seconds, f) unloading and retraction of the right actuator.

The hydraulic system for the load application includes the following components: a) 10 horsepower engine, b) pump for injecting oil 2.1 MPa capacity, c) valves of pressure control and tank capacity equal to 80 oil's liters. The electronic system operates by means of three-phase current at 220 V and 60 Hz. It develops and controls the tests through a programmed load history that is automatically applied, Figure 4.21. The system does not have any option to develop tests under displacement control.

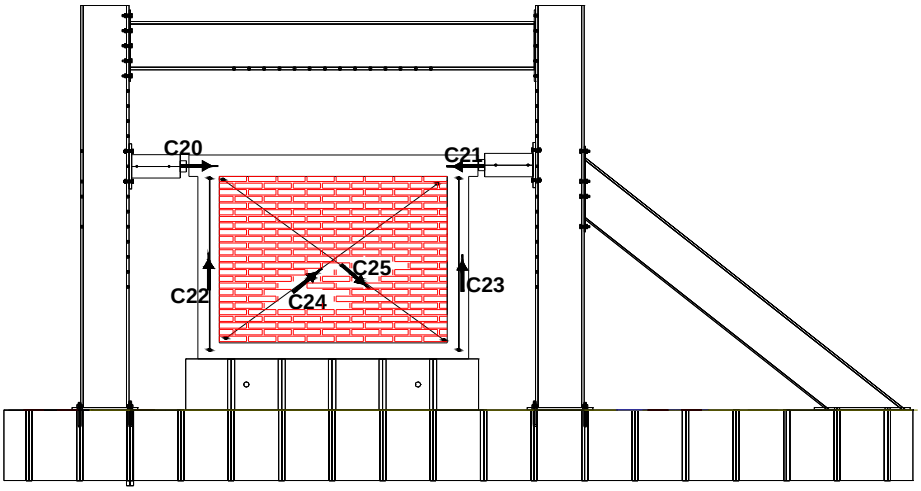

Figure 4.20: Foundation slab, mechanical apparatus, and LDVT's position

Figure 4.21: Mechanical-electronic devices for load application

4.5.2 Building process and characteristics of walls

The next steps define the construction process of the whole walls, Figure 4.22.

1. Placing the reinforcement steel within the support block hole and placing the columns reinforcement steel,
2. Placing the formwork and pouring the bottom concrete beam,
3. Placing the solid clay brick up to the required height,
4. Placing the formwork and pouring the concrete columns,
5. Placing the top beam reinforcement steel,
6. Placing the formwork and pouring the top concrete beam.

Figure 4.22: Construction process of confined masonry walls

The three walls (MUR1, MUR2/MMR2, MMR3) have the same size, 2.0 m X 2.50 m X 0.125 m (Height X Length X Thickness), Figure 4.23. Solid clay bricks, 0.048 m X 0.25 m X 0.125 m, were assembled by using the mortar defined in 4.3.2. Thirteen masonry panels and twelve masonry prisms built during the walls construction to carry out diagonal tension tests and compression tests guaranteed the quality control.

The concrete elements have four longitudinal bars 9 mm diameter yield stress f_y = 46 MPa. Besides, stirrups 6 mm diameter and yield stress f_y = 25 MPa were placed every 10 cm at the ends of the columns, Figure 4.24. Table 4.8 shows the compressive strength of the concrete elements and Annex A1 contains additional information about the mechanical properties of the concrete and reinforcement steel.

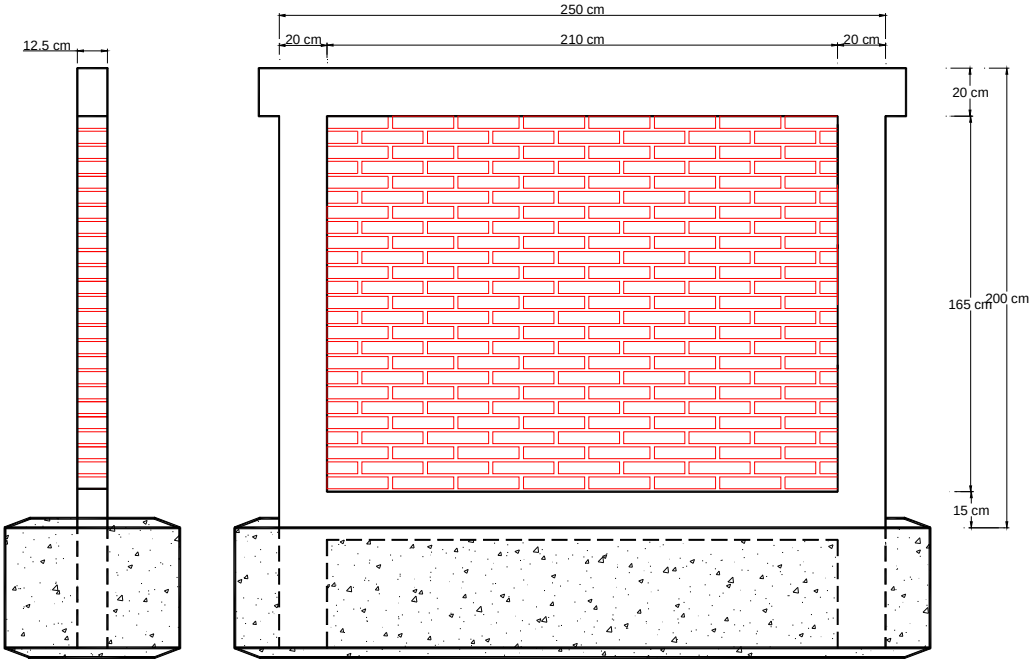

Figure 4.23: Size of confined masonry walls

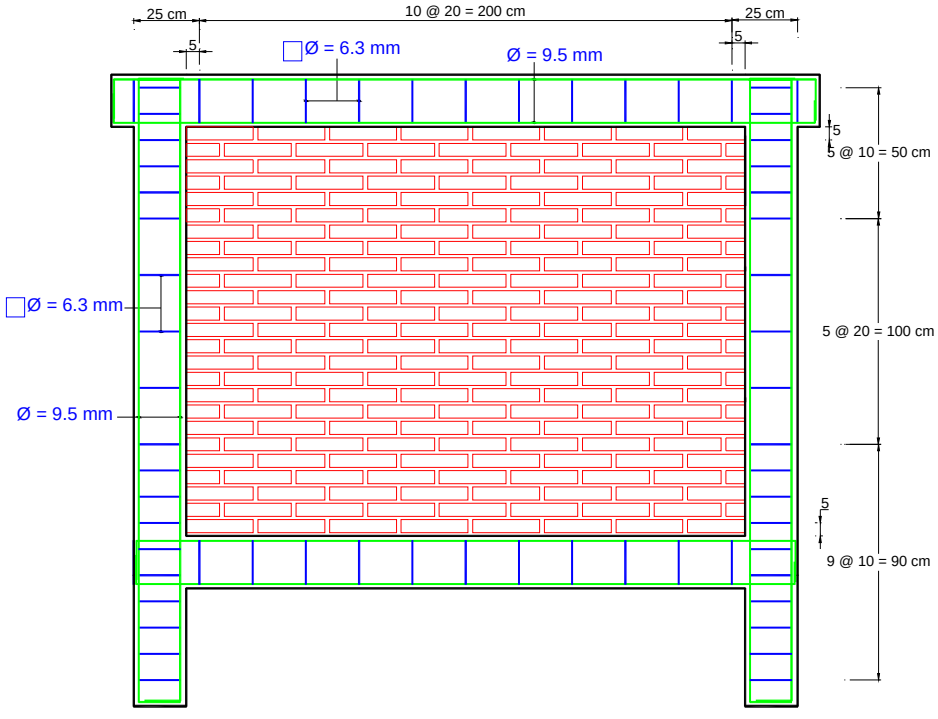

Figure 4.24: Characteristics of reinforcement steel

Table 4.8 Compressive strength of concrete elements, [MPa]

Walls MUR1, MUR2/MMR2	Wall MMR3
24	14

4.5.3 Instrumentation of walls

Six linear variable differential transformers (LVDT) displacement capacity equal to 30 mm measured the wall displacements. Two LVDT measured the shortening-extension of the columns and two LVDTs measured the lateral displacements on top of the wall. In addition, two LVDTs measured the shortening-expansion of the wall diagonals, Figure 4.26a. To define the walls behavior, it was necessary to measure the control length of the LVDTs presented in Figure 4.25. Pressure transducers connected to the actuators hoses measured indirectly the load, Figure 4.26b. These devices and the LDVTs were connected to an electronic module in order to record data.

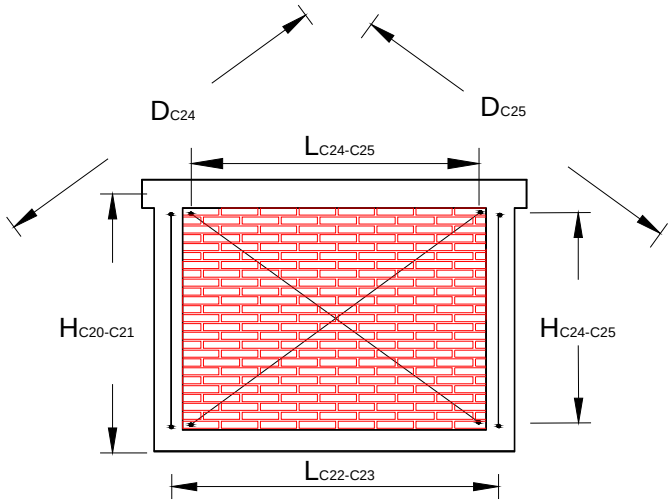

Figure 4.25: LVDTs' control length to define the wall behavior

a) b)

Figure 4.26: a) LVDT to measure the displacement b) Pressure sensor to measure the load

4.5.4 Test on wall MUR1

Due to failures in instrumentation for this wall, it was not possible to measure the hysteretic behavior during the tests. The load history applied had fifteen cycles with a maximum value of 105 KN, Figure A2.4a (Annex A2). Figures 4.27 and 4.28 show different levels of damage that are described here after.

The first flexural cracks appeared at the lower third of the right column and reached the masonry units in cycle 3^+ with load V^+ = 40 KN. Subsequent cracks appeared on bottom of the both columns that spread in the lower joints, Figure 4.27a. Afterwards, the force acting V^+ = 80 KN in cycle 12^+ increased the cracking, which began on top of the right column to cross the masonry units. One zone at the right side of the wall presented vertical cracks that dropped at the centre of the wall before continuing in the lower joint until the left column. For this stage, the wall was divided in two blocks and the flexural cracks of both columns increased until to extend into the masonry, Figure 4.27b.

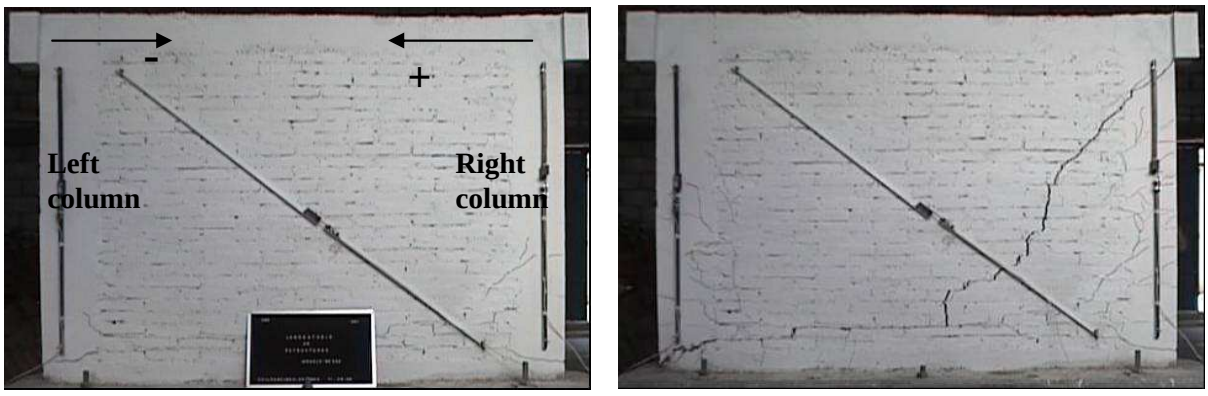

a) b)

Figure 4.27: a) First flexural crack, V^+ = 40 KN (Cycle 3^+), b) Damage state, V^+ = 80 KN (Cycle 12^+)

The left column cracking reached the masonry units increasing their width and length during cycle 14^- when the load was V^- = 80 KN, Figure 4.28a. The main quasi-vertical crack started on top of the frame-masonry left interface and penetrated the masonry causing the cracking of the joints and units by compression effect.

Figure 4.28b shows the final stage for the maximum load V^+ = 105 KN, the increase of the cracking of units and columns caused the slipping of the top block with respect to the bottom block. The extreme sections of the right column and lower section of the left column showed cracking by shear effect.

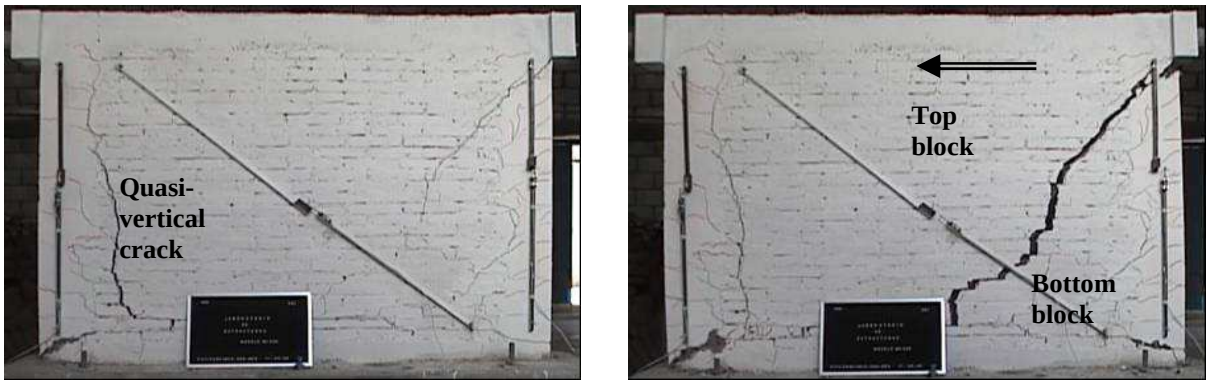

a) b)

Figure 4.28: a) Damage state, V^- = 80 KN (Cycle 14^-), b) Damage state, maximum lateral load V^+ = 105 KN (Cycle 15^+)

4.5.5 Test on wall MUR2

The second specimen, called MUR2, was tested under the load history shown in Figure A2.4b (Annex A2) to 28 days after its construction. This wall showed a linear behavior up to the cycle 9^+ for distortion R^+ = 0.090% and lateral load V^+ = 114 KN, at this point appeared the first flexural cracks at the central part of the right column that penetrated the masonry. The diagonal cracking of the units and slipping of the joints occurred suddenly with distortion R^- = 0.1% and lateral load V^- = 101 KN in cycle 9^-. Simultaneously, the left column showed flexural cracks at the central part and shear cracks at the upper end, Figure 4.29a.

The positive resistance was V^+ = 137 KN with distortion R^+ = 0.47% in cycle 11^+. At this point, Figure 4.29b shows the cracking at the upper right interface masonry-column that continued along the diagonal until it become vertical at the wall central area. Then it changed its direction and caused the failure of the horizontal joint, after the cracking continued on masonry until the end of the left column. A second crack appeared beneath the main crack on the right side of the wall.

a) b)

Figure 4.29: a) First diagonal cracking, R^- = 0.10 % and V^- = 101 KN (cycle 9^-), b) Damage state, maximum lateral load, R^+ = 0.47% and V^+ = 137 KN (cycle 11^+)

Figure 4.30a shows the cracking by compression effect of the load application zone and the extension of the cracks into the masonry. At the end of the test, the longitudinal steel of the left column reached its yield stress and the concrete column failed by shear effect with lateral load and distortion were equal to V^+ = 122 KN and R^+ = 0.99%, Figure 4.30b. In addition, the right column lost its vertical alignment, Figure 4.29a.

a) b)

Figure 4.30: a) Compression failure at the load application zone, b) Flexural failure of the longitudinal reinforcement and shear failure of the concrete section

Figure 4.31 presents the hysteretic cycles and important points that define the behavior of the wall MUR2, where *R* is the rotation evaluated by Equation A2.2. The red line is the resistance envelope obtained with the maximum lateral force and maximum rotation of each cycle, the resistance evaluated by means of Equation 4.10 proposed by the local code is also plotted [45]. Herein, τ^*_m is the design shear strength, § 4.4.2.4. Table 4.9 summarizes the values of the lateral load and distortion for the wall MUR2.

$$V_{NTCM} = 0.5\,\tau^*_m\,A_T \qquad (4.10)$$

Where:

V_{NTCM}	Normative lateral resistance according to local code [45]
τ^*_m	Design shear strength
A_T	Cross-sectional horizontal area of the wall

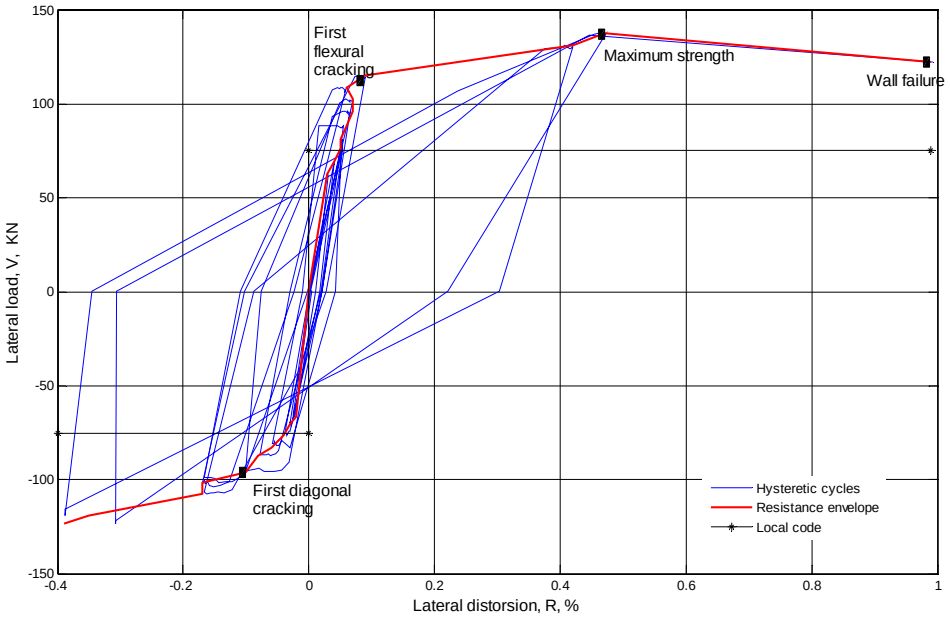

Figure 4.31: Hysteretic behavior and resistance envelope of the wall MUR2

With regard to distortion, the shear distortion dominates during the first four cycles while the flexural distortion dominates during the following six cycles. At the end of the test, both distortions were equal. Equation A2.4 and Equation A2.5 calculated the distortion history shown in Figure 4.32. Sometimes, masonry modeling needs to limit the concrete columns deformation caused by tension then the maximum elongation measured was 2.0 mm at the right column according to Figure 4.33.

Figure 4.32: Rotation caused by shear effect and flexural effect

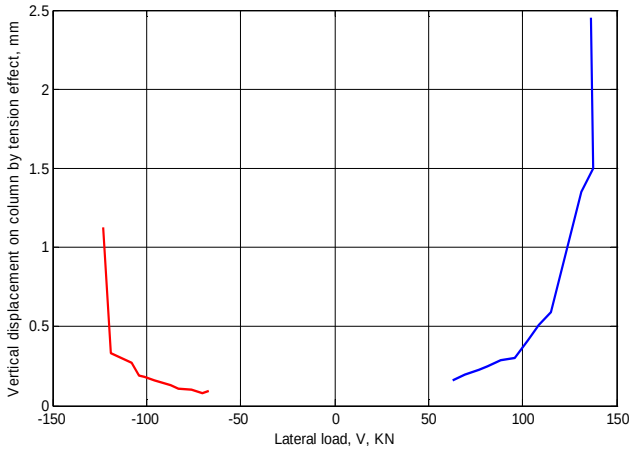

Figure 4.33: Extension of concrete columns by tension effect

4.5.6 Test on retrofitted wall MRM2

4.5.6.1 Retrofit process

The wall MUR2 repaired by means of metallic wire mesh and mortar coat was named MRM2. Figure 4.34 shows the reinforcement process summarized as follows:

1. Fill all cracks with mortar
2. Scarify the masonry and concrete surfaces to ensure perfect bond between the mortar coat and the original surfaces
3. Place and anchor the metallic wire mesh by means of nine steel nails/m^2
4. Place two mortar layer 12 mm thickness on the wall surfaces

Figure 4.34: Retrofit process of the wall MMR2

Mortar characteristics have been specified in § 4.3.2. The metallic wire mesh has a hexagonal form with wires 0.90 mm diameter which yield stress is f_y = 891 MPa [34]. The reinforcement ratio is ρ = 0.0004 according to Mexico City Code [42]. The test was carried out 28 days after the mortar was placed in order to ensure an adequate resistance [76].

4.5.6.2 Description of behavior and failure mode

Alternate load was applied up to the cycle 17^+, for which the diagonal most damaged in previous test showed re-cracking. After the cycle 17^+, the load was applied only in negative direction to generate cracking along the other diagonal; Figure A2.4c (Annex A2) shows this load history.

The diagonal with highest residual damage showed the first diagonal crack, Figure 4.35a, for R^+ = 0.20% and V^+ = 51 KN (Cycle 3^+). Then the load increment caused increase of the diagonal crack width and generated two cracks by shear effect on top of the right column. The positive resistance was V^+ = 133 KN with R^+ = 0.73% in cycle 17^+, when a wide crack generated on top of the right column continued into masonry, Figure 4.35b. Besides, the cracking of the mortar coat at upper right corner indicated the yield of the metallic wire mesh. The reinforcement prevented the cracking of the mortar coat along the other diagonal and over areas previously damaged. After the cycle 17^+, only the load was registered.

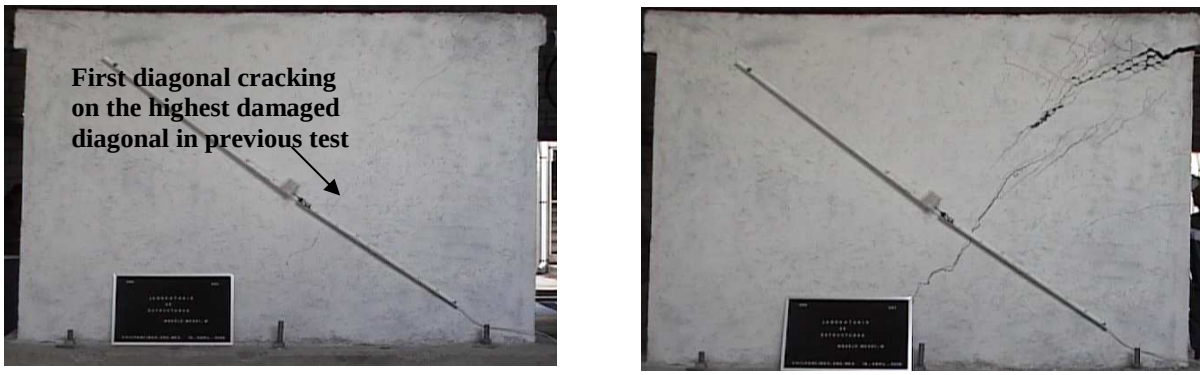

a) b)

Figure 4.35: a) First diagonal cracking, R^+ = 0.20 % and V^+ = 51 KN (Cycle 3^+), b) Damage state, maximum lateral load, R^+ = 0.73 % and V^+ = 133 KN (Cycle $17^{+)}$

After the maximum positive load, the force was applied only in negative direction to cause the diagonal cracking load V^- = 124 KN as it is shown in Figure 4.36a. At the end of the test, the maximum load V^- = 133 KN caused the cracking of the same surface damaged in previous test (wall MUR2). However, the metallic wire mesh generated the change of the cracks direction and prevented the cracking of the low section of right column. The left column presented flexural cracking along its length and shear cracking on top, Figure 4.36b. Because the

metallic reinforcement lost adherence and the coat mortar cracked, the reinforcement at both upper corners showed considerable damage, Figure 4.37.

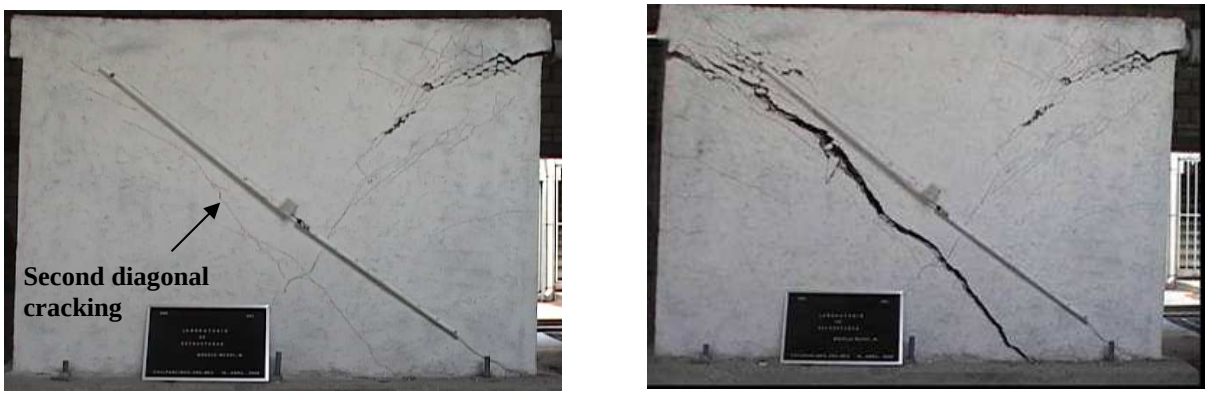

a) b)

Figure 4.36: a) Second diagonal cracking, V^- = 124 KN, b) Damage state, maximum lateral load, V^- = 133 KN

Figure 4.37: Final damage state of reinforcement at the upper corners

Figure 4.38 presents the hysteretic behavior until the cycle 17^+ and the resistance envelope, which marks the first positive diagonal cracking and the maximum load reached. The hysteretic cycles are asymmetric and the wall shows the highest deformation along the direction of the greater residual damage. Figure 4.39 shows the predominance of the flexural rotations with respect to the shear rotations except for the loads close to the maximum positive load. This behavior is opposite to that observed in wall MUR2. Table 4.9 and Table 4.10 summarize the wall behavior. The shear and flexural distortion presented in Figure 4.39 were evaluated by means of Equations A2.4 and A2.5.

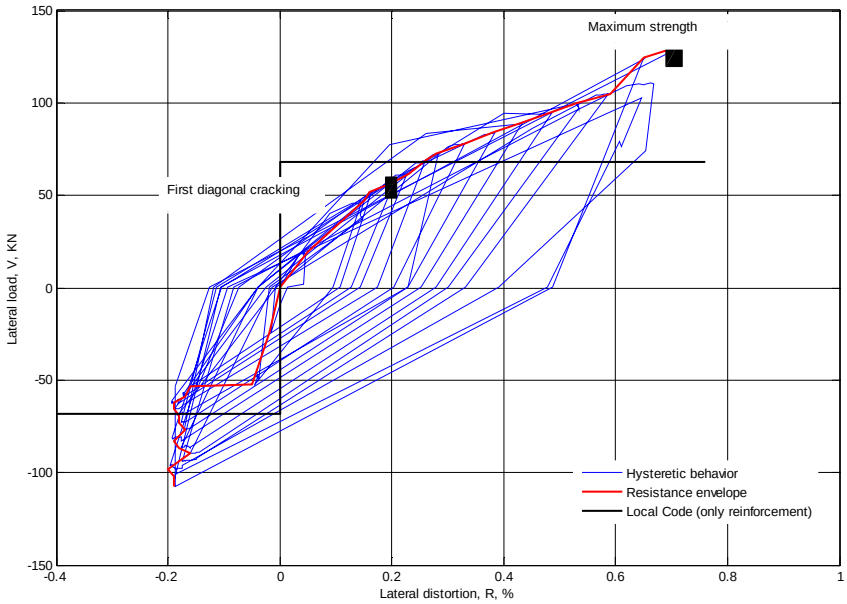

Figure 4.38: Hysteretic behavior and resistance envelope of the wall MMR2

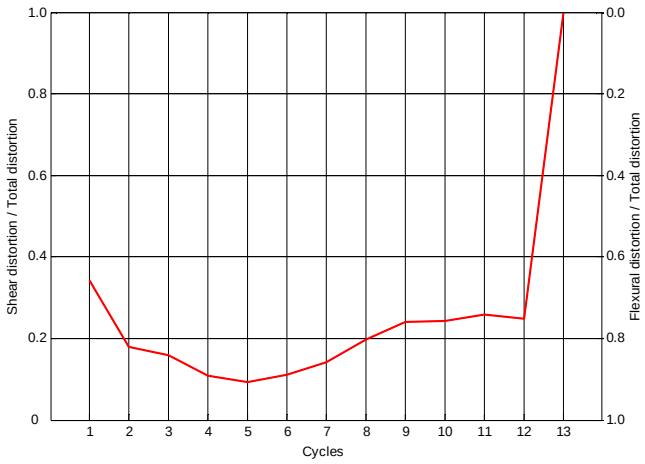

Figure 4.39: Rotation caused by shear effect and flexural effect

4.5.7 Test on rehabilitated wall MMR3

4.5.7.1 Rehabilitation process

This wall had the same constructive process than the precedent walls. However, unlike the wall MUR2, the metallic wire mesh was placed before the test and fixed by means of steel nails (nine pieces/m^2). Then mortar with 25 mm thicknesses was placed on the wall surfaces. To ensure an adequate strength, the test was carried out 28 days after the mortar placement according to local code [76].

4.5.7.2 Description of behavior and failure mode

The load history applied to wall MMR3 contains more cycles than those applied to precedent tests according to Figure A2.4d (Annex A2). Concerning to the wall behavior, it can be seen that the metallic reinforcement changed the behavior and raise the wall resistance. Thus, it showed the first flexural cracks on bottom of the right column and slipping of the lower joints until the cycle 13^+ related with a high lateral load V^+ = 135 KN and R^+ = 0.19%, Figure 4.40a. In subsequent cycles there was no visible damage up to cycle 22^+, where the loading area (upper right corner) failed by compression effect with V^+ = 181 KN and R^+ = 0.67%, Figure 4.40b. In semi-cycle 23^-, the loading area of the left actuator showed cracking by compression. However and according to Figure 4.41, the rest of the wall showed no damage except the lower joints and the lower right corner. Figure 4.42 presents the hysteretic behavior with wide, stable, and symmetrical cycles that indicates an excellent performance of the wall. The red line is the resistance envelope curve.

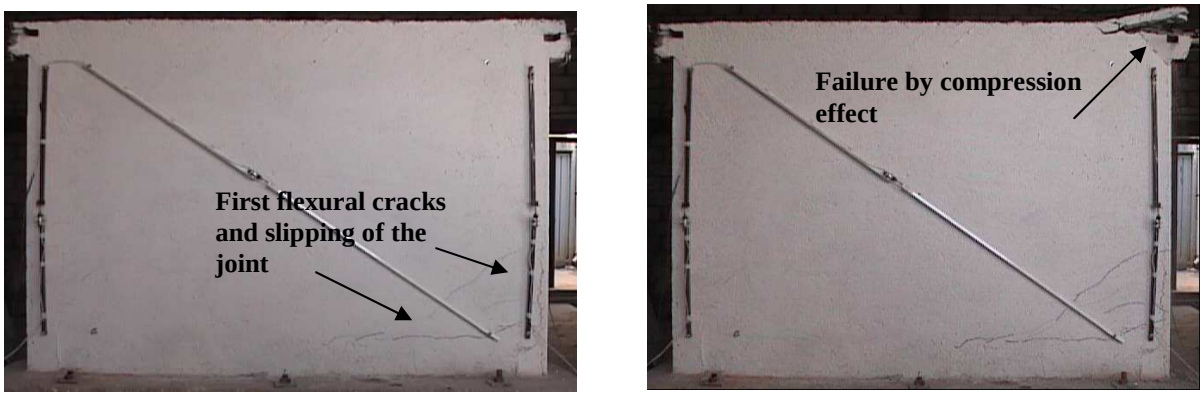

a) b)

Figure 4.40: a) First flexural cracking, R^+ = 0.19 % and V^+ = 135 KN (Cycle 13^+), b) Damage state, maximum lateral load, R^+ = 0.67 % and V^+ = 181 KN (Cycle 22^+)

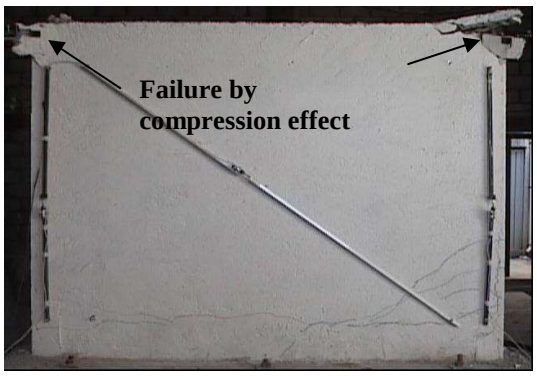

Figure 4.41: Damage state, maximum lateral load, R^- = 0.55 % and V^- = 156 KN (Cycle 22^-)

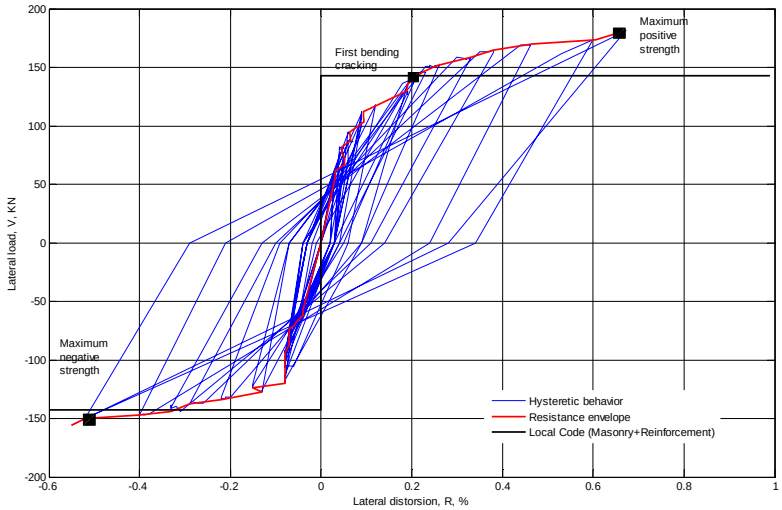

Figure 4.42 Hysteretic behavior and resistance envelope of the wall MMR3

4.5.8 Comments about the behavior of confined masonry walls

The parameters that describe the wall behavior have been defined in Annex A2 and their values are described on next paragraphs.

Hence, Figure 4.43 shows the ratio cycle stiffness vs. initial elastic stiffness as function of the distortion. Because of the different characteristics of the three walls (confined wall MUR2, confined-retrofitted wall MMR2, and rehabilitated-confined wall MMR3), it is not possible to define an equation to determine the stiffness reduction for all walls. In general, there is symmetrical degradation of stiffness for the walls MUR2 and MMR3, while the behavior of the wall MMR2 presents the influence of the residual damage. At the end of the tests, the walls stiffness ranged from 10 to 20% of the elastic stiffness.

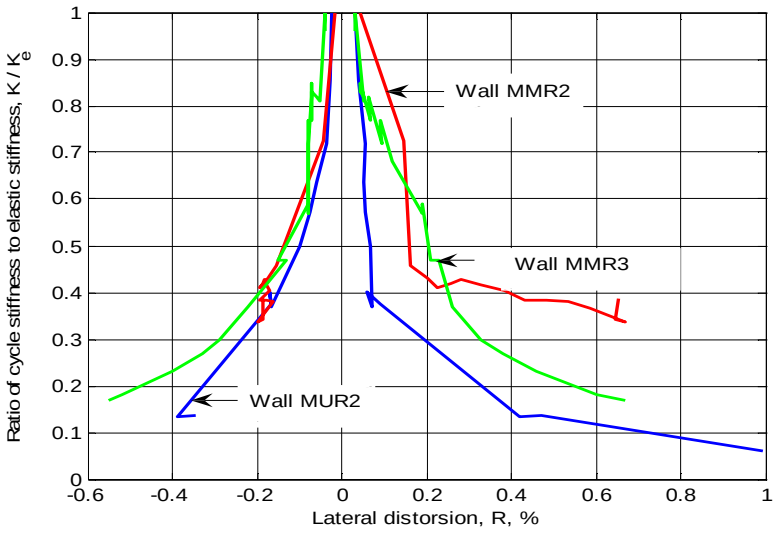

Figure 4.43: Stiffness variation with respect to distortion

The elastic stiffness of the walls is function of the elastic stiffness of the masonry and the elastic stiffness of the concrete columns. Then, the columns of the wall MUR2 provide greater stiffness than the columns of the wall MMR3, which concrete compressive strength was small. Thus, K_e was 135 KN / mm, 42 KN / mm and 93 KN / mm for walls MUR2, MMR2 and MMR3. For the wall MMR2, the reinforcement does not increase the elastic stiffness and its value was one third of the elastic stiffness of the wall MUR2, Table 4.10.

Although the metallic wire mesh does not raise the initial stiffness, it modifies the quantity of dissipated energy. Then walls MMR2 and MMR3 dissipated a quantity of energy approximately equal to twice the energy of the unreinforced wall MUR2, which developed hysteretic cycles with reduced area, Figure 4.44. Furthermore, the residual damage of the wall MMR2 generates an asymmetric curve of dissipated energy vs. lateral displacement different from the curve of the wall MUR2 and MMR3.

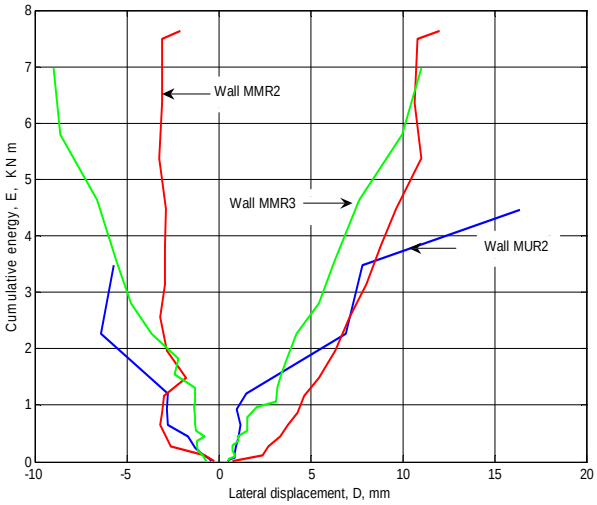

Figure 4.44 Cumulative dissipated energy

Figure 4.45 shows the envelope curves of the resistance obtained with the maximum load and maximum distortion of each load cycle. The curve of the wall MMR2 in negative zone did not register the maximum negative resistance V^- = 133 KN because the LDVT associated cannot register the displacement. It can be seen that the reinforcement placed on wall MMR2 has adequate structural efficiency because its resistance was equal to that of the undamaged wall MUR2.

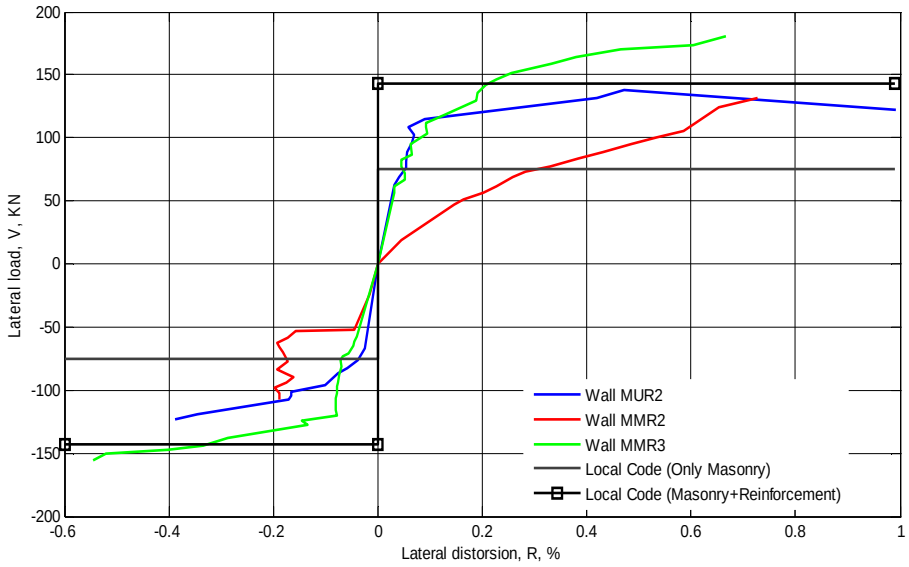

Figure 4.45: Lateral load vs. lateral distortion relationship for all walls

Low compressive strength of the concrete elements in the wall MMR3 generated the failure by compression effects at the load application zones and prevented to reach a greater resistance and deformation. However, this wall had the best behavior than the rest according to Table 4.9. For walls MMR2 and MMR3, the point of maximum load and the point of failure are similar.

Table 4.9 Lateral load and distortion from different stages

Wall	First flexural cracking	First diagonal cracking	Maximum load	Failure of the wall
MUR2	V^+ =114 KN, R^+ = 0.09 %	V^- = 97 KN, R^- = 0.10 %	V^+ =137 KN, R^+ = 0.47 %	V^+ =122 KN, R^+ = 0.99 %
MMR2		V^+ =51 KN, R^+ = 0.20 %	V^+ =133 KN, R^+ = 0.73 %	
MMR3	V^+ =135 KN, R^+ = 0.19 %		V^+ =181 KN, R^+ = 0.67 %	

Table 4.10 shows the experimental resistance (V^+ or V), the resistance computed by local code considering a unitary reduction factor (V_D), and the elastic stiffness (K_e). By considering only the contribution of the metallic wire mesh, the resistance of the wall MMR2 is greater than the theoretical resistance according to local code. It may mean two aspects: a) the mortar layer resists lateral load, and/or b) the cracked masonry has residual resistance. For wall MMR3, the experimental resistance is close to the theoretical resistance, which considers the contribution of the metallic wire mesh and masonry. The mean of two experimental values, positive and negative, have been used in order to evaluate the increment with respect to the

normative resistance. The theoretical resistance with and without metallic reinforcement are drawn in Figure 4.45.

Table 4.10 Theoretical and experimental resistance and elastic stiffness

Wall	$V_{D,}$ [KN]	V^+, [KN]	V^-, KN]	Increment / local code %	K_e, [KN/ mm]
MUR1	75	105	97	35	
MUR2	75	137	122	73	135
MMR2	68	133	133	96	42
MMR3	143	181	156	18	93

Figure 4.46 shows the deformed position of the wall MUR2 for the maximum load. The upper bond beam has rigid body behavior because both extremes have similar lateral displacement. However, the columns situation is different because the left column has greater tension effect than the right column. Moreover, one diagonal suffers extension, and the other suffers compression. Figure 4.47 presents the influence of the reinforcement on the wall MMR3 behavior. Therefore, the horizontal displacement on top of the wall is greater than that of the wall MUR2 while the expansion of columns decreases but the deformation of the diagonals has no variation.

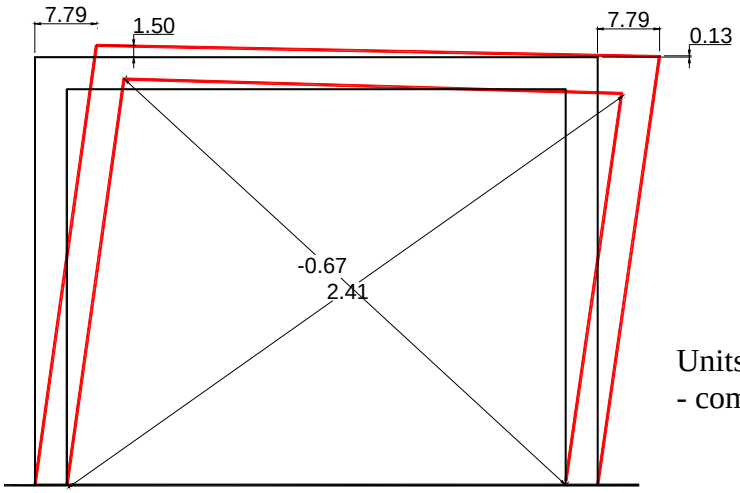

Figure 4.46: Deformed position of the wall MUR2 under maximum load V^+ = 133 KN, R^+ = 0.73 %

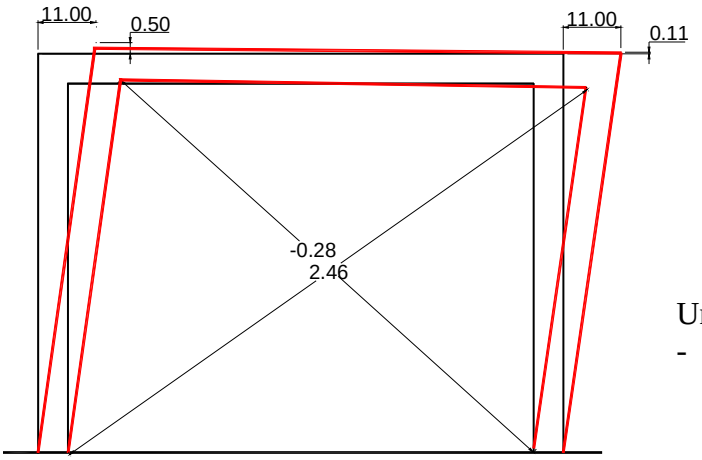

Figure 4.47: Deformed position of the wall MMR3 under maximum load V^+ = 181 KN, R^+ = 0.67 %

Table 4.11 shows the values of the ductility by using the Park and Paulay criterion in both directions, see Annex A2 [84]. Because of errors affecting the instrumentation during the tests, the displacements of the wall MMR3 and negative displacement of the wall MUR2 related to maximum load were used in Equation A2.6 (Annex A2) instead of the ultimate displacement. Even so, it had adequate values.

Table 4.11 Ductility according to Park and Paulay criterion (1989)

Wall	Positive direction	Negative direction
MUR2	12.4	6.13
MMR3	4.06	5.21

Table 4.12 and Figure 4.48 present the equivalent viscous damping computed in both directions. These values are similar to those obtained by Aguilar (1997) and Barragan (2005) except for the negative direction of the wall MMR2, which reached a damping equal to 34% caused by the highest residual damage of the wall diagonal during the test of the wall MUR2.

Table 4.12 Equivalent viscous damping [%]

Wall	Positive direction	Negative direction
MUR2	21	17
MMR2	14	34
MMR3	12	15

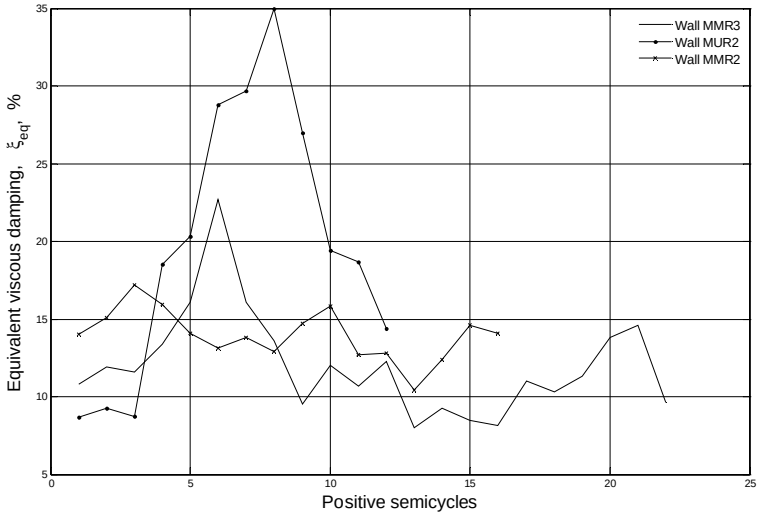

Figure 4.48: Equivalent viscous damping in positive semi cycles

4.6 Conclusions

The lack of available experimental data for masonry units and masonry specimens required a large experimental program in order to evaluate their main properties to be used in the design as input data and for numeric analysis. Besides, three full-scale walls were built and tested. The first two walls were tested without reinforcement; after having been tested and damaged, the second wall was repaired and tested again. Finally, the third wall was reinforced before the test.

From the obtained results, it can be seen that the deficient quality control of materials and production process of the masonry units generate high variation of the compressive strength, CV = 0.43. For this reason, a mortar type I with design compressive strength equal to 21.9 MPa (i. e. 75 % greater than the normative value) were used to build all specimens and walls.

With respect to the cohesion and friction angle of the joint, the values are similar to those obtained in other national research programs. However, the cohesion is approximately one third of the common values measured in Europe. With respect to horizontal stiffness, its value is equal to those referenced.

Results from unreinforced panel tests show that the shear strength is independent of the type of load and damage level on the perpendicular diagonal. Moreover, two independent failure patterns were identified: slipping of the joint and diagonal cracking of the units, with possible combination of these independent modes. Thus, the highest shear strength was associated to the diagonal cracking of units. In addition, the rigidity modulus and shear stress vs. tangential

strain ratio were obtained. Finally, it can be concluded that a high compressive strength of mortar gives an adequate cohesion of the joint and high shear strength of panels. It is greater than the common values registered in Mexico.

Shear strength of the reinforced panels increased by 20% with respect to that of unreinforced panels and the predominant failure pattern was the diagonal cracking of the units. The reinforcement proposed herein is flexible and can easily be placed inside the joints. Besides, its reduced thickness and the spaces between wires filled with mortar guarantee a good adherence, inducing its failure by tension effect. Due to its low cost, easy placement and structural efficiency, this reinforcement is an excellent alternative compared to carbon fibers or fiberglass.

In the same way, compression tests on masonry prisms provided a compression stress vs. axial strain relationship. Thus, one parabolic function up to the compressive strength and other linear function to descendent zone have been proposed with an axial strain associated to compressive strength ε_m = 0.0029. However, the modulus of elasticity is twice the common values reference for this type of the units.

In general, the walls MUR1 and MUR2 show diagonal cracking of masonry units, slipping of the joints, shear failure at the end of the columns, and failure of longitudinal reinforcement. For these walls, the first crack occurs on the columns by flexural effect. The wall MUR1 shows an atypical failure pattern with a main quasi-vertical crack near to left masonry-columns interface. The other direction shows diagonal cracking on the central area.

In the first cycles, the wall MUR2 had rigid behavior and reduced deformation energy until the first flexural crack and then two large cycles appear before the maximum load. At this peak point, occurred the cracking by shear effect at the end of the columns with posterior failure of the longitudinal reinforcement. The positive tri-linear envelope is similar to that defined by Flores (1995).

The metallic reinforcement placed on walls MMR2 and MMR3 had two main functions: to fix the mortar layer and to spread the stress on the wall surface. Unlike the fibers carbon, this reinforcement has a low cost and does not require a qualified workmanship. Besides, it has good structural efficiency shown in wall MMR2, which reached the same resistance of the wall MUR2, even if the initial damage was considerable.

For the wall MMR3, with reinforcement placed before the test and low compressive strength of the concrete frame, the failure by compressive effect occurred in the load application zone preventing the increment of resistance. Related figures show no other damaged zone.

For the walls MUR2 and MMR3, the same lateral displacement on top of the wall for the maximum load indicates a rigid body behavior of the upper beam. In other way, the wall MMR3 had better behavior than the wall MUR2 because the reinforcement raised the lateral displacement and reduced the expansion of the columns.

With respect to the building local code by considering a unitary factor of resistance, the increase of resistance is equal to 35%, 73%, 96%, and 18 % for walls MUR1, MUR2, MMR2, and MMR3. Thus, one can conclude that the walls had an adequate resistance as long as the proposed reinforcement guaranteed an excellent behavior under lateral load.

CHAPTER 5

Numeric simulations of masonry walls behavior

5.1 Introduction

The goal of this chapter is to reproduce, by means of numerical models, the experimental behavior of the masonry panels and masonry walls presented in the previous chapter by using the mechanical properties evaluated herein. Unlike of the walls MMR2 and MMR3, the wall MUR2 represents the typical masonry walls used to build the masonry structures in Guerrero State, consequently it has been chosen to be modeled among the whole set of walls.

In order to analyze different specimens through the micro-models, the first part of the chapter describes the theoretical behavior of the whole materials: joint, masonry units, and concrete frame. The second part describes the main characteristics of the numerical models of the unreinforced and reinforced panels and the results comparison. The third part presents the numerical model of the masonry wall MUR2 as well as the principal characteristics of its behavior. One additional model considers the case of metallic reinforcement mesh inside the joints.

Although the analysis requires a large computational effort, the main advantage of micro-models is those allow the analysis and visualization of the deformations and stress for the different elements at each load level. The implementation of these models by considering the 2-D plane non-linear stress analysis was developed in TNO DIANA program, which is a general-purpose finite element code based on the displacement method [103].

The last part present a macro-model developed herein from a simplified model that supposes the masonry failure by shear effect (chapter 6) by using the experimental data of chapter 4. The macro-model is applied to wall MUR2 but additional experimental results of the other walls are used for assessing its performance.

5.2 Masonry modeling by using micro-models

5.2.1 Behavior of the mortar joint

In order to evaluate the joint behavior, we adopt the multi-surface model developed by Lourenco (1996), Lourenco and Rots (1997) and improved by Van Zijl (2000). It considers the Coulomb friction model combined with a tension cut-off mode, and an elliptical compression cap according to Figure 5.1. The threes modes consider the strain-softening hypothesis, adding hardening for the cap mode.

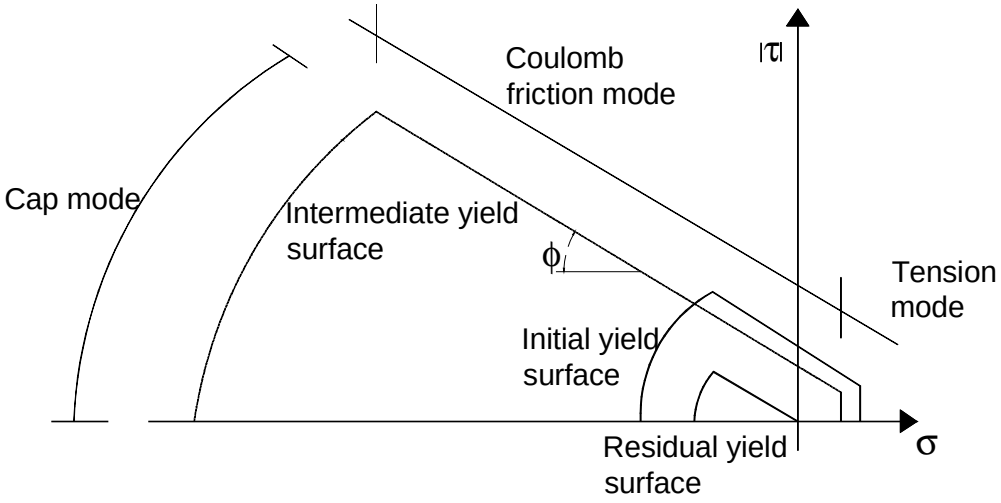

Figure 5.1: Two-dimensional interface model [59]

The interface model is derived in terms of the generalized stress and strain vector ***(σ, ε)*** defined by Equation 5.1 and 5.2 [102]. Thus, an interface four-node element in a two-dimensional configuration zero thickness is adopted at the joint model. The local xy axes for displacements are evaluated in the first node with x from node 1 to node 2 and the variables (stress and displacements) oriented in the xy axes, Figure 5.2. The element has linear interpolation functions with an integration scheme for 3-point Newton-Cotes [104]. In addition, Equation 5.3 describes the elastic regime of the constitutive behavior, where *D* is the diagonal stiffness matrix defined by Equation 5.4.

$$\boldsymbol{\sigma}=\begin{Bmatrix}\sigma\\ \tau\end{Bmatrix} \tag{5.1}$$

$$\boldsymbol{\varepsilon}=\begin{Bmatrix}\Delta u\\ \Delta v\end{Bmatrix} \tag{5.2}$$

$$\boldsymbol{\sigma}=\mathbf{D}\,\boldsymbol{\varepsilon} \tag{5.3}$$

$$\mathbf{D} = diag\left[k_n \quad k_s\right] \tag{5.4}$$

Where:

$\boldsymbol{\sigma}$	Generalized vector of stress
$\boldsymbol{\varepsilon}$	Generalized vector of strain
σ	Normal stress
τ	Shear stress
Δu	Relative displacement in the interface normal direction
Δv	Relative displacement in the interface parallel direction
$\boldsymbol{D}$	Diagonal stiffness matrix
k_n	Normal stiffness of the joint proposed with experimental data of chapter 4
k_s	Tangential stiffness of the joint, § 4.4.1

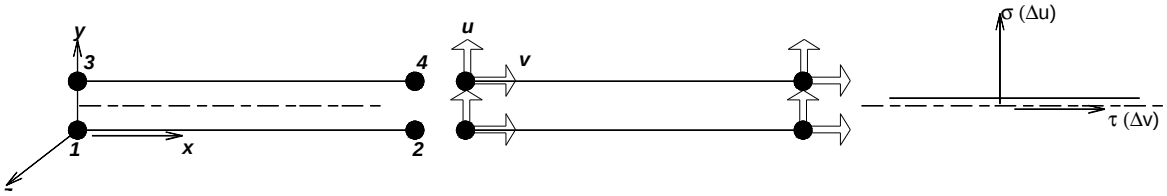

a) b) c)

Figure 5.2: Interface 4-nodes element, a) Topology, b) Displacements, c) Stress [102] [103]

5.2.1.1 Shear slipping mode

Equation 5.5 represents the Coulomb friction mode that describes the shear slipping at the joints. Herein, the cohesion *c* shows softening expressed by Equation 5.6 [59].

$$f_1 = |\tau| + \sigma\Phi - c \tag{5.5}$$

$$c(\sigma, \kappa_1) = c_o\, e^{\frac{-c_o \kappa_1}{G_f^{II}}} \tag{5.6}$$

Where:

f_1	Yield function surface for the Coulomb friction mode
$\lvert\tau\rvert$	Absolute value of shear stress
σ	Normal stress
Φ	Effective friction angle defined by Equation 5.7
c	Effective cohesion defined by Equation 5.6
c_o	Initial cohesion of the joint, § 4.4.1
G^{II}_f	Shear-slip fracture energy

κ_1 Internal softening parameter

The friction softening is coupled to the cohesion softening by means of Equation 5.7. The cohesion and friction parameters are proposed from the experimental program while the fracture energy is determined by the appropriate integration of the load vs. displacement relationship [16] [57]

$$\Phi(\sigma,\kappa_1)=\phi_o+(\phi_r-\phi_o)\frac{c_o-c}{c_o} \tag{5.7}$$

Where:

Φ Effective friction angle

ϕ_o Initial friction angle, § 4.4.1

ϕ_r Residual friction angle

c_o Initial cohesion of the joint, § 4.4.1

c Effective cohesion evaluated by Equation 5.6

The flow rule expressed by Equation 5.8 [30] provides a way of describing the dilatancy by a choice of a suitable potential function expressed by Equation 5.9, where $\Psi = \tan\psi$ is the dilatancy coefficient. From Equations 5.8 and 5.9, one obtains Equation 5.10 and u_p can be given by integration of Equation 5.11. This is one experimental evidence that dilatancy depends on the confining stress and the shear-slip [102] .

$$\dot{\boldsymbol{\varepsilon}}=\begin{Bmatrix}\dot{u}_p\\ \dot{v}_p\end{Bmatrix}=\dot{\lambda}\frac{\partial g}{\partial\sigma} \tag{5.8}$$

$$\frac{\partial g}{\partial\sigma}=\begin{Bmatrix}\Psi\\ sign(\tau)\end{Bmatrix} \tag{5.9}$$

$$\Psi=\frac{\dot{u}_p}{\dot{v}_p}\,sign(\tau) \tag{5.10}$$

$$u_p=\int\Psi\,d\left|\Delta v_p\right| \tag{5.11}$$

Where:

$\dot{\boldsymbol{\varepsilon}}$ Plastic strain rate vector

$\dot{\lambda}$ Plastic strain-rate multiplier

$\frac{\partial g}{\partial \boldsymbol{\sigma}}$ Normal vector to yield surface, derivate of no associated potential function with respect to stress vector

$\Psi = \text{tg } \psi$ Dilatancy coefficient

$sign(\tau)$ Sign of shear stress

$\dot{u}_p$ Displacement rate in the interface normal direction

$\dot{v}_p$ Displacement rate in the interface parallel direction

u_p Displacement in the interface normal direction

Δv_p Displacement increment in the interface parallel direction

A dilatancy formulation of separate variables expressed by Equation 5.12 simplifies the curve fitting and ensures convexity of the potential function g, Equation 5.13. Therefore, a description of the normal uplift upon shear slipping is chosen in function of normal stress and the dilatancy, Equation 5.14. It can be seen that for tensile stress, a stress-independent dilatancy is assumed [102].

$$\Psi = \Psi_1(\sigma)\Psi_2(v_p) \tag{5.12}$$

$$g = \int \left(\frac{\partial g}{\partial \sigma}\right)^T d\sigma = |\tau| + \Psi_2(v_p) \int \Psi_1(\sigma)\, d\sigma \tag{5.13}$$

$$\frac{\partial g}{\partial \sigma} = \begin{cases} 0 & if\ \sigma < \sigma_u \\ \frac{\psi_o}{\delta}\left(1 - \frac{\sigma}{\sigma_u}\right)\left(1 - e^{-\delta v_p}\right) & if\ \sigma_u \le \sigma < 0 \\ \frac{\psi_o}{\delta}\left(1 - e^{-\delta v_p}\right) & if\ \sigma \ge 0 \end{cases} \tag{5.14}$$

Where:

$\Psi = \text{tg } \psi$ Dilatancy coefficient

$\Psi_1(\sigma)$ Dilatancy function related with normal stress

$\Psi_2(v_p)$ Dilatancy function related with the displacement in the interface parallel direction

g No associated potential function

$\frac{\partial g}{\partial \boldsymbol{\sigma}}$ Normal vector to yield surface, derivative of no associated potential function

σ Normal stress

v_p Plastic displacement in the interface parallel direction

ψ_o Value of dilatancy associated with zero confining stress and null shear-slip from experimental test

σ_u Compressive stress when dilatancy becomes zero from experimental test

δ Dilatancy shear-slip degradation from experimental test

A strain-softening hypothesis is adopted, where the softening is governed by shear slipping through Equation 5.15 by considering Equations 5.8 and 5.9. The stress-update can be cast in the standard plasticity predictor-corrector form and the corrected stresses, together with the plastic strain increment $\Delta\kappa$; or $\Delta\lambda$ can be solved by a Newton-Raphson iterative scheme. A consistent tangent modulus is employed for the global convergence iterations, which ensures quadratic convergence [59][109].

$$\Delta\kappa_1 = \left|\Delta v_p\right| = \Delta\lambda_1 \tag{5.15}$$

Where:

$\Delta\kappa_1$ Increment of internal softening parameter

Δv_p Increment of displacement in the interface parallel direction

$\Delta\lambda_1$ Increment of plastic strain multiplier

5.2.1.2 Tension cut-off mode

Equation 5.16 defines the yield function for the tension cut-off mode, where the tensile stress σ_t of the joint has an exponential softening defined by Equation 5.17 while Equation 5.18 shows the softening governed by the strain-softening hypothesis. Thus, assuming an associated flow rule, Equation 5.19 leads to Equation 5.20 [102].

$$f_2 = \sigma - \sigma_t \tag{5.16}$$

$$\sigma_t(\sigma,\kappa_2) = f_t e^{-\frac{f_t}{G_f^I}\kappa_2} \tag{5.17}$$

$$\Delta\kappa_2 = \left|\Delta u_p\right| \tag{5.18}$$

$$\Delta\varepsilon_p = \Delta\lambda_2 \frac{\partial f_2}{\partial\sigma} \tag{5.19}$$

$$\Delta\kappa_2 = \Delta\lambda_2 \tag{5.20}$$

Where:

f_2	Yield function surface for tension cut-off mode
σ	Normal stress
σ_t	Effective tensile stress
f_t	Tensile stress of mortar joint
G_f^I	Fracture energy of tension cut-off mode
κ_2	Internal softening parameter
$\Delta\kappa_2$	Increment of internal softening parameter
Δu_p	Increment of displacement in the interface normal direction
$\Delta\varepsilon_p$	Increment of plastic strain vector
$\Delta\lambda_2$	Increment of plastic strain multiplier
$\frac{\partial f_2}{\partial\sigma}$	Normal vector to yield surface, derivative of the associated potential function

5.2.1.3 Compression cap mode

Equation 5.21, where C_s is a parameter controlling the shear distribution to failure and σ_c is the compressive strength, defines the yield function for the compression cap. If it assumes the strain-hardening hypothesis of Equation 5.22 with an associated flow rule defined by Equation 5.23, then Equation 5.24 evaluates the softening-hardening for this mode [102].

$$f_3 = \sigma^2 + C_s\tau^2 - \sigma_c^2 \tag{5.21}$$

$$\Delta\kappa_3 = \sqrt{\Delta\varepsilon_p^T \Delta\varepsilon_p} \tag{5.22}$$

$$\Delta\varepsilon_p = \Delta\lambda_3 \frac{\partial f_3}{\partial\sigma} \tag{5.23}$$

$$\Delta\kappa_3 = 2\Delta\lambda_3\sqrt{\sigma^2 + (C_s\tau)^2} \tag{5.24}$$

Where:

f_3	Yield function surface for compression cap mode
σ	Normal stress
τ	Shear stress
C_s	Materials parameter controlling the shear distribution to failure
σ_c	Effective normal stress
$\Delta\kappa_3$	Increment of internal softening parameter
$\Delta\varepsilon_p$	Increment of plastic strain vector
$\Delta\lambda_3$	Increment of plastic strain multiplier
$\frac{\partial f_3}{\partial\sigma}$	Normal vector to yield surface and derivative of the associated potential function

After the yield surface hardening there is a parabolic/exponential softening, Figure 5.3. The peak strength f_c is reached at the plastic strain κ_p. Subsequently, the softening branch is governed by the fracture energy $G_{fc.}$ For practical reasons, all stress values in Figure 5.3 are related to the compressive strength f_c according to Equation 5.25. Equation 5.26 defines the three regions of this hardening-softening rule [102].

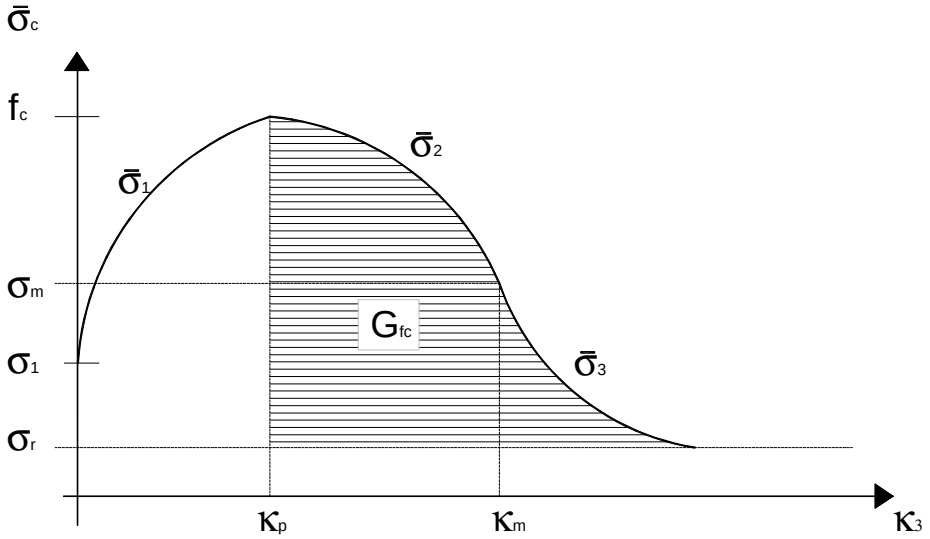

Figure 5.3: Hardening-softening relationship for compression cap mode [102]

$$\sigma_1 = \frac{1}{3} f_c$$
$$\sigma_m = \frac{1}{2} f_c \qquad (5.25)$$
$$\sigma_r = \frac{1}{7} f_c$$

$$\bar{\sigma}_1(\kappa_3) = \sigma_1 + \left(f_c - \sigma_1 \right) \sqrt{\frac{2\kappa_3}{\kappa_p} - \frac{\kappa_3^2}{\kappa_p^2}}$$
$$\bar{\sigma}_2(\kappa_3) = f_c + \left(\sigma_m - f_c \right) \left(\frac{\kappa_3 - \kappa_p}{\kappa_m - \kappa_p} \right)^2 \qquad (5.26)$$
$$\bar{\sigma}_3(\kappa_3) = \sigma_r + \left(\sigma_m - \sigma_r \right) exp \left[2 \left(\frac{\sigma_m - f_c}{\kappa_m - \kappa_p} \right) \left(\frac{\kappa_3 - \kappa_m}{\sigma_m - \sigma_r} \right) \right]$$

Where:

- σ_1 Normal stress at the beginning of the joint non-linear behavior
- f_c Compressive strength of the system units-joint
- σ_m Normal stress related with the change point from parabolic softening to exponential softening
- σ_r Residual normal stress
- $\bar{\sigma}_i$ Normal stress for different zones: hardening, parabolic softening, or exponential softening
- κ_3 Internal softening parameter
- κ_p Internal softening parameter associated to normal stress f_c
- κ_m Internal softening parameter associated to normal stress σ_m

5.2.1.4 Corners

At each of the intersections of the Coulomb friction criterion with the tension cut-off and the compression cap, the plastic strain increment is given by Equation 5.27, where the subscript 1 refers to the shear criterion and *i* refers to tension cut-off (*i*=2) and to compression cap (*i*=3). Then the corners are analyzed consistently. In both shear/tension corner and the shear/compression corner, the stress corrections can be written in standard predictor-corrector form and solved for, together with two plastic strain increments $\Delta\lambda_1$ and $\Delta\lambda_i$, by a Newton-

Raphson iterative scheme [53]. In addition, the consistent tangent moduli are employed for the global convergence iterations to ensure quadratic convergence [102]

$$\Delta\varepsilon_p = \Delta\lambda_1 \frac{\partial g_1}{\partial g} + \Delta\lambda_i \frac{\partial g_i}{\partial g} \tag{5.27}$$

5.2.2 Behavior of masonry units

The previous model of the system joint-unit considers the failure surfaces by tension-shear, shear-compression, and compression. For this reason, the behavior model of the pieces only considers the tension capacity by means of Rankine model, Equation 5.28. Then, Equation 5.29 shows the plastic strain rate vector by considering an associated flow rule and the relation between the internal state variable κ_1 and the plastic process is given by the strain hardening hypotheses expressed by Equation 5.30 [53] [102]. Figure 5.4 shows the yield function surface and the stress vs. strain relationship, which has linear behavior up to the tensile strength and then it shows linear softening until ε_{ult}.

$$f_1(\boldsymbol{\sigma}, \kappa_1) = \sqrt{\frac{1}{2}\boldsymbol{\sigma}^T \mathbf{P}\boldsymbol{\sigma}} + \frac{1}{2}\pi_1^T \boldsymbol{\sigma} - \bar{\sigma}_1(\kappa_1) \tag{5.28}$$

$$\boldsymbol{\Delta\varepsilon}_\mathbf{p} = \Delta\lambda_1 \left\{ \frac{\mathbf{P}\boldsymbol{\sigma}}{2\psi} + \alpha_1 \pi_1 \right\} \tag{5.29}$$

$$\Delta\kappa_1 = \Delta\lambda_1 \tag{5.30}$$

Where:

$f_1(\boldsymbol{\sigma}, \kappa_1)$ Yield function surface for Rankine model

$\boldsymbol{\sigma} =$ $[\sigma_x\ \sigma_y\ \sigma_z\ \tau_{xy}\ \tau_{yz}\ \tau_{zx}]^T$

$\boldsymbol{P}$ Projection matrix, Equation 5.31

$\pi_1 =$ $[1\ 1\ 0\ 0\ 0\ 0]^T$

$\sigma(\kappa_1) = f_t$, Tensile strength of masonry unit, Figure 5.4

$\psi = \sqrt{(1/2)\boldsymbol{\sigma}^T \mathbf{P}\boldsymbol{\sigma}}$

$\boldsymbol{\Delta\varepsilon_p}$ Increment of plastic strain vector

$\Delta\lambda_1$ Increment of plastic strain multiplier

$\Delta\kappa_1$ Increment of internal softening parameter

$$\mathbf{P}=\begin{bmatrix} 1/2 & -1/2 & 0 & 0 & 0 & 0 \\ -1/2 & 1/2 & 0 & 0 & 0 & 0 \\ 0 & 0 & 0 & 0 & 0 & 0 \\ 0 & 0 & 0 & 2 & 0 & 0 \\ 0 & 0 & 0 & 0 & 0 & 0 \\ 0 & 0 & 0 & 0 & 0 & 0 \end{bmatrix} \tag{5.31}$$

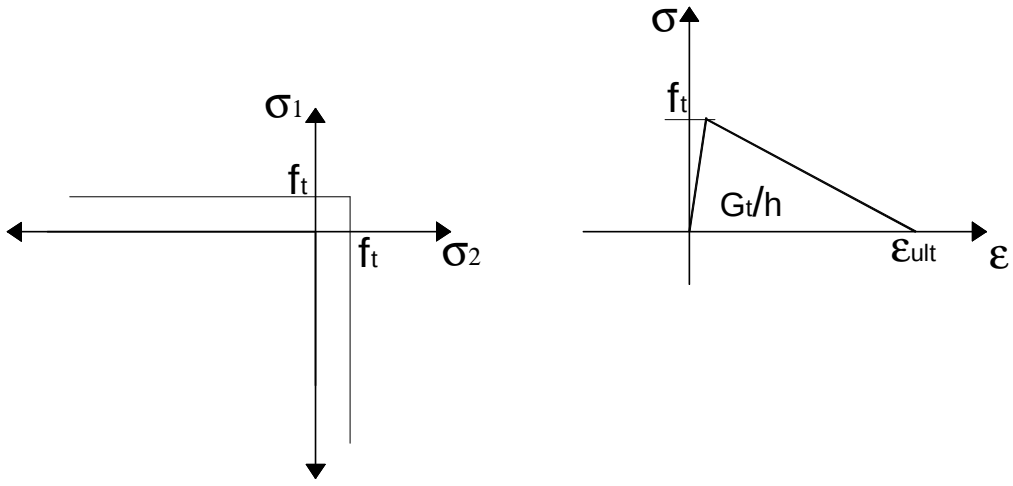

a) b)

Figure 5.4: Behavior of masonry units: a) Yield function surface, b) Stress vs. strain relationship [102]

5.2.3 Behavior of concrete elements

A multi-surface plasticity model defines the mechanical behavior of concrete elements, one surface type Von Mises model the compression failure and other type Rankine model the tension failure. This last model has been presented in the previous section whereas Equation 5.32 defines the Von Mises model. Then, Equation 5.33 proposes the plastic strain rate vector by considering an associated flow rule $g \cong f_2$, while the relation between the internal state variable κ_2 and the plastic process, by considering strain hardening, is defined by Equation 5.34 [102]. For points close to corners, the summation of the inelastic strain of each yield function can be performed by means of Koiter's rule [53].

$$f_2(\boldsymbol{\sigma}, \kappa_2) = \sqrt{\frac{1}{2}\boldsymbol{\sigma}^T \mathbf{P}\boldsymbol{\sigma}} - \bar{\sigma}_2(\kappa_2) \tag{5.32}$$

$$\boldsymbol{\Delta\varepsilon_p} = \Delta\lambda_2 \left\{ \frac{\mathbf{P}\boldsymbol{\sigma}}{2\psi} \right\} \tag{5.33}$$

$$\Delta\kappa_2=\sqrt{\frac{2}{3}\left[\left(\Delta\varepsilon_1^p\right)^2+\left(\Delta\varepsilon_2^p\right)^2\right]} \tag{5.34}$$

Where:

$f_2(\boldsymbol{\sigma},\kappa_2)$ Yield function surface for the Von Mises model

$\boldsymbol{\sigma}=$ $[\sigma_x\ \sigma_y\ \sigma_z\ \tau_{xy}\ \tau_{yz}\ \tau_{zx}]^T$

$\boldsymbol{P}$ Projection matrix, Equation 5.35

$\sigma(\kappa_2)=f'_c$, Compressive strength, Figure 5.5

$\psi=\sqrt{(1/2)\boldsymbol{\sigma}^T\mathbf{P}\boldsymbol{\sigma}}$

$\boldsymbol{\Delta\varepsilon_p}$ Increment of plastic strain vector

$\Delta\varepsilon^p_i$ Increment of plastic strain for direction i

$\Delta\lambda_2$ Increment of plastic strain multiplier

$\Delta\kappa_2$ Increment of internal softening parameter

$$\mathbf{P}=\begin{bmatrix} 2 & -1 & -1 & 0 & 0 & 0 \\ -1 & 2 & -1 & 0 & 0 & 0 \\ -1 & -1 & 2 & 0 & 0 & 0 \\ 0 & 0 & 0 & 6 & 0 & 0 \\ 0 & 0 & 0 & 0 & 6 & 0 \\ 0 & 0 & 0 & 0 & 0 & 6 \end{bmatrix} \tag{5.35}$$

Figure 5.5a shows this combined model, where σ_1 and σ_2 are the principal stress, f_t is the tensile strength, and f'_c is the compressive strength. Figure 5.5b presents the stress vs. strain relationship, where the compression zone has a linear-parabolic curve and the tension zone has a linear-exponential curve.

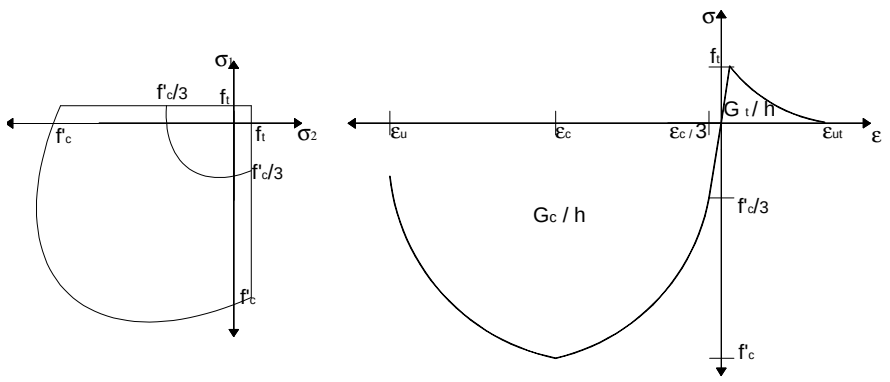

a) b)

Figure 5.5: Failure model of concrete elements: a) Yield function surface, b) Stress vs. strain relationship [102]

The compression stress vs. strain relationship has three characteristic values: the strain $\varepsilon_c/3$ that corresponds to one-third of the compressive strength f'_c, the strain ε_c related to compressive strength f'_c, and the ultimate strain ε_u at which the material is completely softened in compression, Figure 5.5b and Equation 5.36. It can be seen that $\varepsilon_c/3$ and ε_c are independents of the element size or compressive fracture energy [102]. Equation 5.37 describes now the parabolic compression curve, while the relation between the fracture energy G_c and the characteristic element length h for softening part is governed by last expression of Equation 5.36.

$$\begin{aligned}
\varepsilon_1 &= \frac{f_c^{'}}{3E_c} \\
\varepsilon_c &= -\frac{5f_c^{'}}{3E} \\
\varepsilon_u &= \varepsilon_c - \frac{3G_c}{2hf_c^{'}}
\end{aligned} \tag{5.36}$$

$$f = \begin{cases}
-f_c^{'}\dfrac{\varepsilon}{3\varepsilon_1} & if\ \varepsilon_1 < \varepsilon \le 0 \\
-f_c^{'}\left[\dfrac{1}{3}+\dfrac{4}{3}\left(\dfrac{\varepsilon-\varepsilon_1}{\varepsilon_c-\varepsilon_1}\right)-\dfrac{2}{3}\left(\dfrac{\varepsilon-\varepsilon_1}{\varepsilon_c-\varepsilon_1}\right)^2\right] & if\ \varepsilon_c < \varepsilon \le \varepsilon \\
-f_c^{'}\left[1-\left(\dfrac{\varepsilon-\varepsilon_c}{\varepsilon_u-\varepsilon_c}\right)^2\right] & if\ \varepsilon_u < \varepsilon \le \varepsilon_c \\
0 & if\ \varepsilon \le \varepsilon_u
\end{cases} \tag{5.37}$$

For masonry plasticity models, concrete plasticity models and smeared cracking models, the crack bandwidth h of the quadrilateral elements can be evaluated by Equation 5.38, where A is the total area of the element [102].

$$h = \sqrt{A} \tag{5.38}$$

5.3 Micro-models for the masonry panels

5.3.1 Unreinforced masonry panel MM1

5.3.1.1 Modeling

The numeric model of the unreinforced panel MM1 aims to simulate its experimental behavior under monotonic load and to evaluate the influence of different variables. For this purpose, three different models were constructed in order to measure the mesh sensitivity, Figure 5.6. Then the masonry units have been modeled by means of four 8-nodes elements (case 1), four 4-nodes elements (case 2), and sixteen 4-nodes elements (case 3).

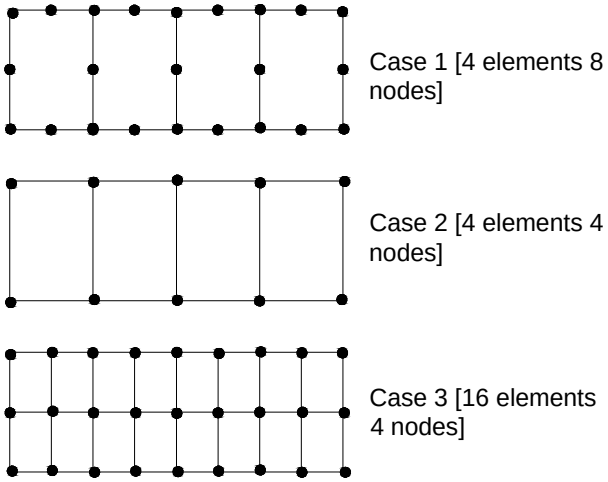

Figure 5.6: Different meshes to model the masonry unit

Figure 5.7 shows the finite element mesh for the panel MM1 presented in § 4.4.2.1. The size of the model is 0.40 m X 0.40 m X 0.125 m (Height X Length X Thickness) and the size of the masonry units rises to 0.06 m X 0.28 m X 0.125 m in order to consider the joint thickness. Sixteen 4-node elements with linear interpolation and 2 X 2 Gauss integration points model each unit, case 3 in Figure 5.6. Besides, interface 4-node element zero thickness models the joint.

5.3.1.2 Mechanical properties

According to experimental data (chapter 4 and annexes) and references presented herein, the mechanical properties of the masonry units and joints were proposed. Table 5.1 shows the characteristics of the joints, which have been defined in § 5.2.1.

In Mexico there are not references about the normal stiffness k_n, then an underestimated value by considering the modulus of elasticity of the system units-joint equal to E_1= 5227 MPa was

proposed, § 4.3.1. It is associated to the height (H) of one piece plus a joint according to Figure 5.8. Then Equation 5.39 proposed by Lotfi and Shing (1994) calculates k_n.

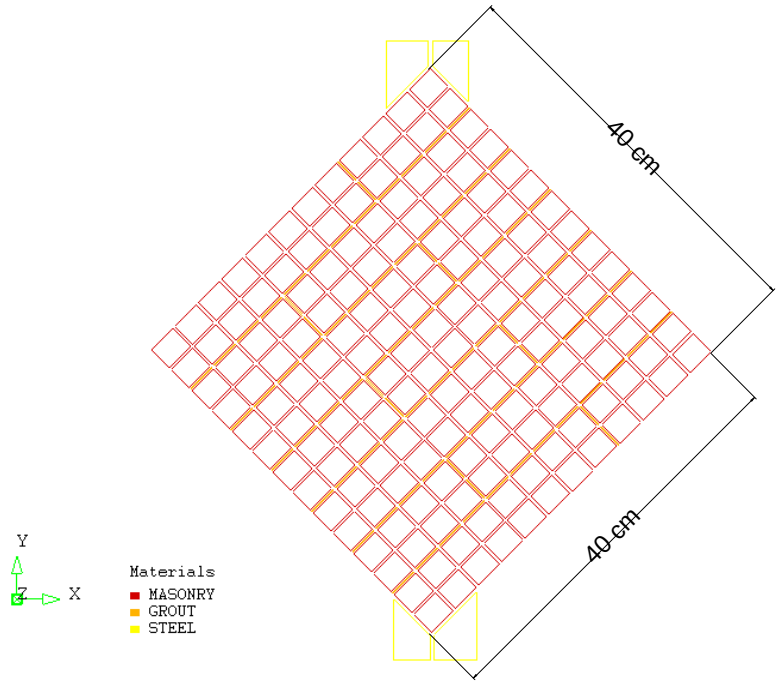

Figure 5.7: Finite element mesh of the masonry panel MM1, case 3

$$k_n = \frac{E_1}{H} \tag{5.39}$$

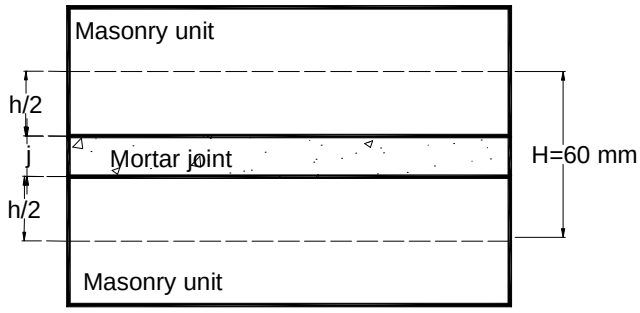

Figure 5.8: System units-joint to compute the vertical stiffness k_n

Other unknown parameter is f_c that represents the compressive strength of the system units-joint. For this case, Equation 5.40 obtained by Atkinson and Noland (1983) has been used.

$$f_c = f_p \frac{\left(f_{tp} + \alpha f_j \right)}{U_u \left(f_{tp} + \alpha f_p \right)} \tag{5.40}$$

$$\alpha = j/4.1h \tag{5.41}$$

Where:

f_c	Compressive strength of the system units-joint
f_p	Compressive strength of the units, § 4.3.1
f_{tp}	Tensile strength of the units, Annex A1
f_j	Compressive strength of the mortar, § 4.3.2
U_u	Uniformity coefficient equal to 1.5
j	Joint thickness
h	Masonry unit height

The numerical model requires additional mechanical properties of the joint. Thus, the values of the joint tensile strength f_t, the fracture energy of the three modes (tension, shear and compression: G^I_t, G^{II}_f , G_{fc}), the scalar parameter of hardening-softening to compressive strength κ_p, and the controlling parameter of shear C_s have been proposed according to typical values collected from the references. In the same way, the dilatancy angle had a close value to zero [1][59]

Table 5.1 Mechanical properties of mortar joints

k_n, [N/mm]	k_s, [N/mm]	f_t, [MPa]	G^I_f, [N/mm]	c_o, [MPa]	$tg(\phi_o)$	$tg(\psi_o)$	$tg(\phi_r)$
87	28	0.35	0.018	0.41	0.72	0.09	0.72
σ_u, [MPa]	δ	f_c, [MPa]	C_s	G_{fc}, [N/mm]	κ_p	G^{II}_f, [N/mm]	
-1.3	5	12.0	9	5.0	0.093	0.05	

Tensile strength f_{tp} = 0.40 MPa according to experimental data (Annex A1) and fracture energy in tension G^I_f = 0.02 N/mm [59] were supposed for the masonry units.

5.3.1.3 Results

From Figure 5.9, it can be seen that the cases 2 and 3 showed best approximation to experimental results. The ultimate vertical displacement related to maximum vertical load is D_v = 0.29 mm that has an error E = 11 % with respect to experimental value. The ultimate vertical numerical load was F_{the} = 50 KN while the experimental value was F_{exp} = 53 KN, it has an error E = 6%.

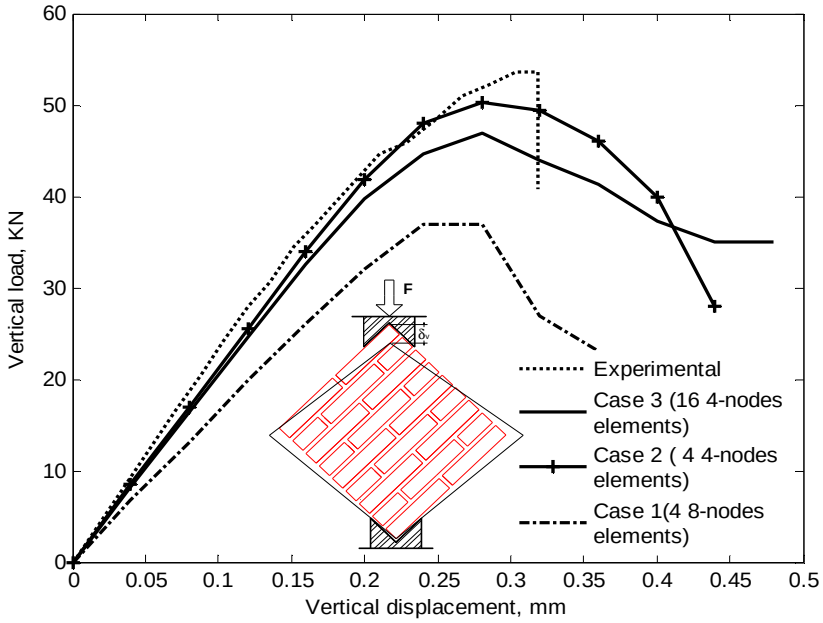

Figure 5.9: Experimental behavior and numerical simulation of the panel MM1

The numeric simulations show concentration of the units cracking in accordance with the experimental failure pattern, Figure 5.10a. Besides, the joint theoretical slipping is in good agreement with the experimental results, Figure 5.10b.

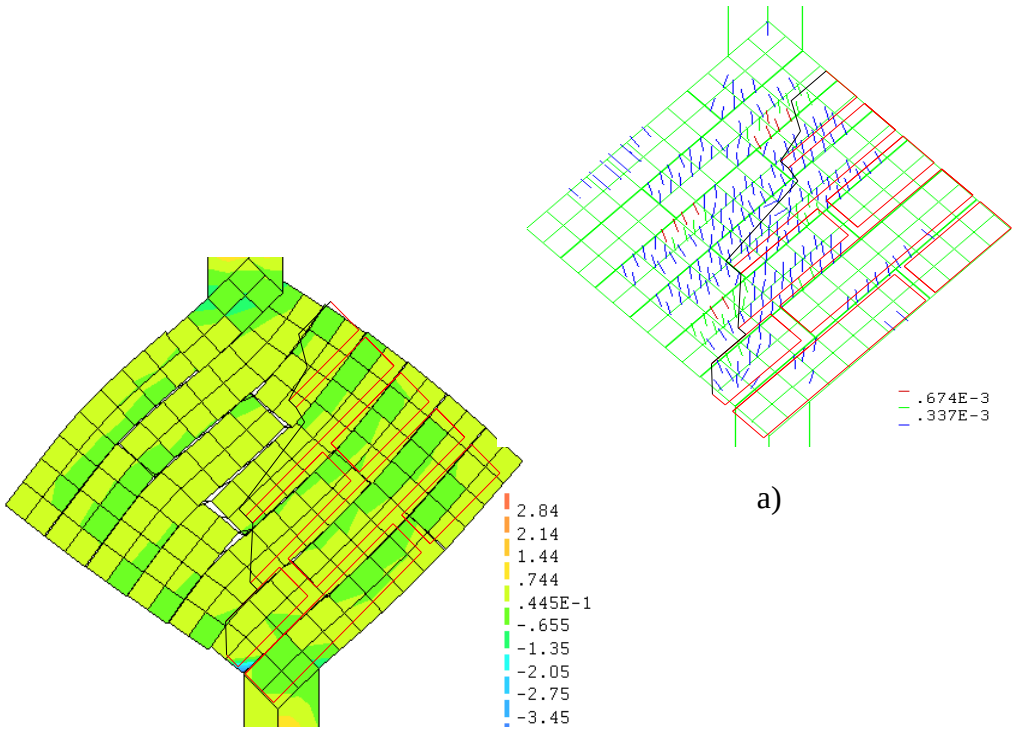

a)

b)

Figure 5.10: Numerical simulation and experimental failure pattern to *Dv* = 0.29 mm, case 3, a) Units cracking, b) Joints slipping and principal stress [MPa]

In order to evaluate the influence of two principal mechanical characteristics of the masonry, the tensile strength of the units and the cohesion of the joint, two additional analyses were developed. Figure 5.11 indicates that the cohesion of the joint has greater influence than the tensile strength of the units on the panel behavior. Considering the criterion defined by Lourenco (2009) both parameters were increased by 25 %.

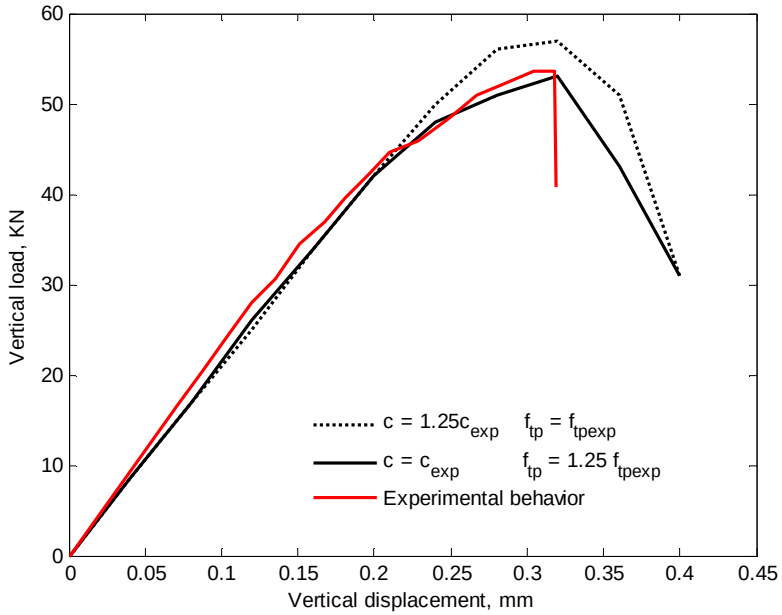

Figure 5.11: Influence of the units' tensile strength and joints' cohesion for case 2

5.3.2 Reinforced masonry panel

5.3.2.1 Modeling

A numeric model, 0.55 m X 0.55 m X 0.125m, was elaborated by using eight 4-nodes elements for each brick, Figure 5.12. Their mechanical properties were similar to those presented in Table 5.1. Additional metallic reinforcement mesh or modified cohesion were placed at the joints according to experimental data, incise 4.4.2 and Annex A1. The reinforcement contribution to the panel resistance was modeled in two ways:

1. By an increment of the initial cohesion *c* according to Equation 5.42. Annex A1 and Table 5.2 presents the experimental data. Then the additional cohesion is c_a = 0.15 MPa.

$$c_a = F_{ult} / (Lt) \qquad (5.42)$$

2. By means of a 1-D element that simulates the behavior of the metallic reinforcement mesh bonded to adjacent elements by considering the Von Mises model. The

mechanical properties summarized in Table 5.2 have been presented in Annex A1. In addition, Figure 5.13 shows the hardening strain vs. stress experimental relationship for the metallic reinforcement mesh.

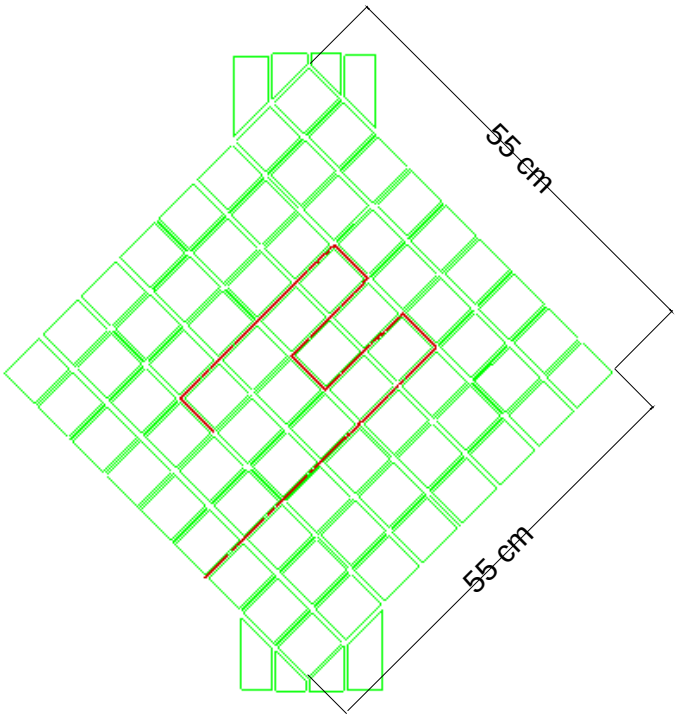

Figure 5.12: Numerical model of reinforced panel

Table 5.2 Mechanical properties of metallic reinforcement mesh

E_s, [MPa]	L, [mm]	t, [mm]	A_s, [mm^2]	F_{ult}, [KN]	f_y, [MPa]
300000	1150	100	5.81	2.2	126.5

In Equation 5.42 and Table 5.2:

E_s Modulus of elasticity

L Length

t Width

A_s Steel area

F_{ult} Ultimate axial load

f_y Yield stress

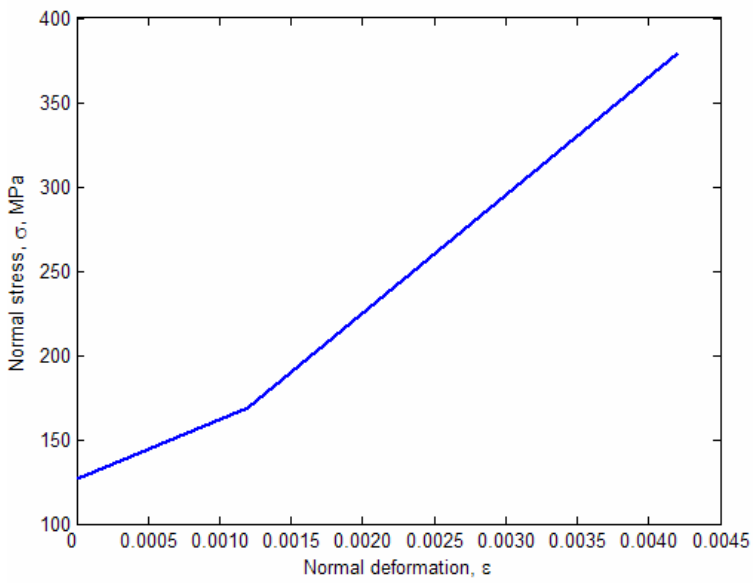

Figure 5.13: Hardening strain vs. normal stress relationship of metallic reinforcement mesh

5.3.2.2 Results

From experimental results detailed in 4.4.2.2, the mean curve of vertical displacement vs. vertical load was used to compare the numerical results, Figure 5.14. It shows a good approximation at the beginning where all curves have similar slope, then the experimental curve becomes different from the two numerical curves. Although the maximum vertical displacement has little variation, both models were able to reach the experimental vertical load. Thus, the relative displacement error for two models does not exceed *E*=11%.

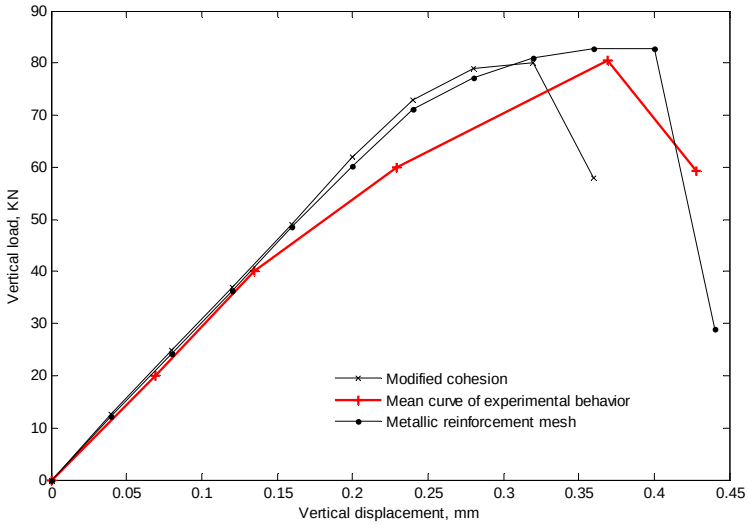

Figure 5.14: Experimental behavior and numeric simulation of reinforced panel

Another advantage of the metallic reinforcement mesh is the reduction of the width and quantity of cracking of the masonry units with respect to those presented in un-reinforced

panels, Figure 5.15. Thus, the width of the cracks drops to half for the metallic reinforcement model and to one quarter for the modified cohesion model.

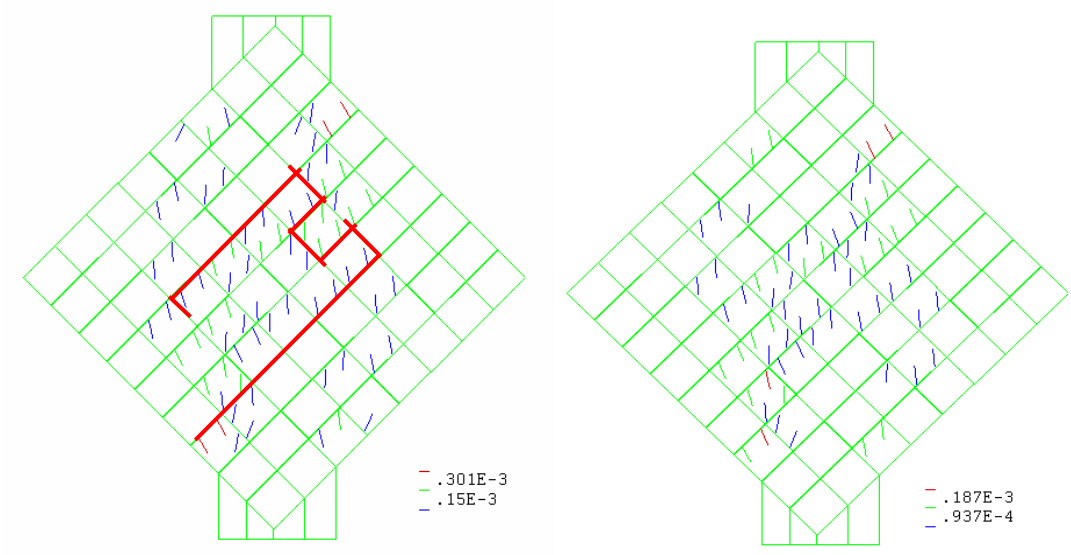

a) b)

Figure 5.15: Width of cracks to maximum vertical displacement, a) Metallic reinforcement model, b) Modified cohesion model

5.4 Micro-model of confined masonry wall

5.4.1 Model of the wall MUR2

5.4.1.1 Description and modeling

Figure 5.16 shows the finite element mesh used to model the confined masonry wall MUR2. The size of the model is 2.5 m X 2.0 m X 0.125 m (Length X Height X Thickness). The masonry units have 0.28 m X 0.06 m X 0.125 m in order to consider the thickness of the joint, each unit have been divided in eight 4-node quadrilateral elements based on linear interpolation and Gauss integration by using 2 X 2 integration. These elements have been drawn in red color. The concrete frame, represented by green quadrilaterals in Figure 5.16, was modeled with the same kind of elements.

An interface 4-node element in two-dimensional configuration zero thickness models the joints and the interface masonry-concrete frame. The local xy axes for the displacements and stress are shown in Figure 5.2.

The longitudinal steel and stirrups in concrete columns are modeled as 1-D elements bonded to adjacent element without possibility of relative displacement and its stiffness is added to stiffness of the quadrilateral elements [102]. It has been considered that only the stirrups placed at the end of the columns has influence on the wall behavior.

5.4.1.2 Mechanical properties

Mechanical properties of the different materials were adopted according to experimental data given of chapter 4 and references. Table 5.3 shows the parameters of joints and interface masonry-concrete frame previously defined in § 5.3.1.2.

Table 5.3 Mechanical properties of mortar joints

k_n, [KN/mm]	k_s, [KN/mm]	f_t, [MPa]	G^I_f, [N/mm]	c_o, [MPa]	$tg(\phi_o)$	$tg(\psi_o)$	$tg(\phi_r)$
86	25	0.30	0.018	0.40	0.70	0.001	0.55
σ_u, [MPa]	δ	f_c, [MPa]	C_s	G_{fc}, [N/mm]	κ_p	G^{II}_f, [N/mm]	
-1.3	5	12	9	0.093	0.093	0.05	

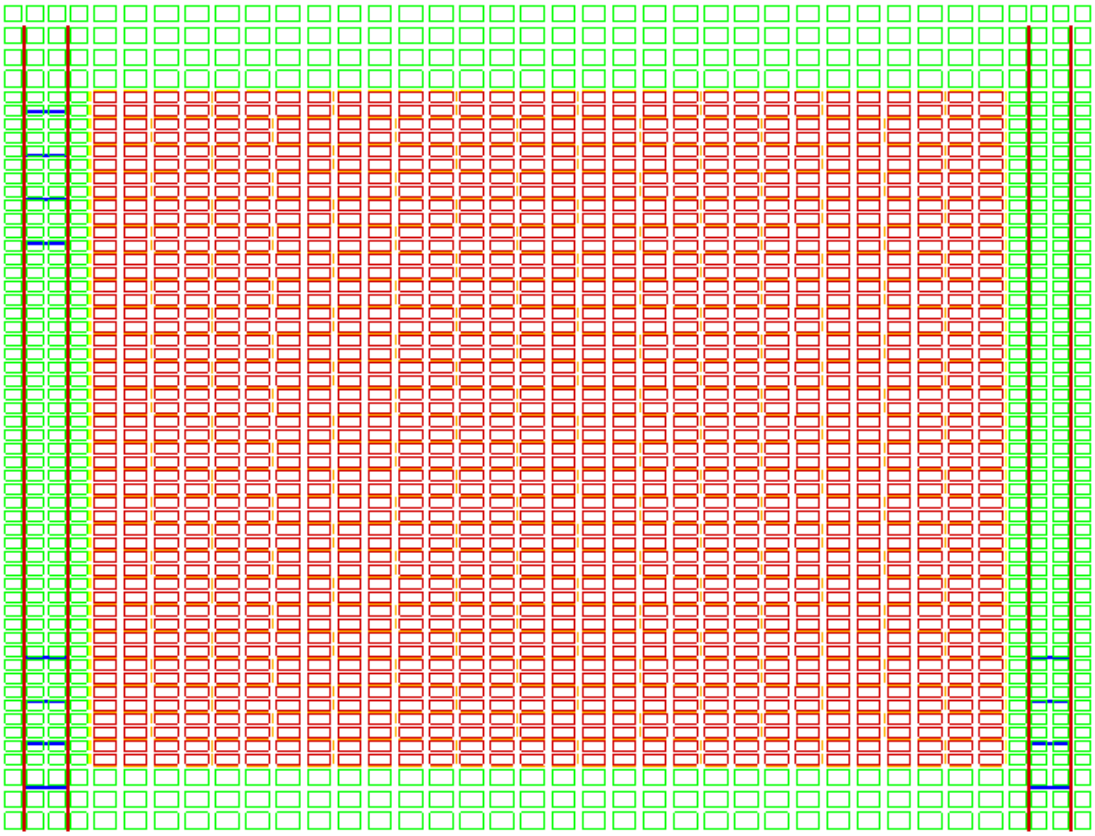

Figure 5.16: Finite element mesh of the confined masonry wall MUR2 (Model M1)

Table 5.4 contains the mechanical properties of the concrete frame, where E_c is the modulus of elasticity, ν is the Poisson's ratio, f'_c is the compressive strength and f_t is the tensile strength supposed equal to 10% of the compressive strength. The first three parameters obtained experimentally were presented in Annex A1 and the values of fracture energy in tension-

compression (G^I_f, G^{II}_f) are taken from references. Table 5.5 shows the mechanical properties of the units, where the modulus of elasticity E_m, the tensile strength f_{tp}, the compressive strength f_p, and the Poisson' ratio υ have been defined in § 4.3.1 and Annex A1. The other parameters have been collected from references. Equation 5.38 computes the crack bandwidth h for both materials.

Table 5.4 Mechanical properties of concrete elements

E_c, [MPa]	ν	f_t, [MPa]	G^I_f, [N/mm]	f'_c, [MPa]	G^{II}_f, [N/mm]	h, [mm]
24506	0.17	2.5	0.06	25.0	5.0	54

Table 5.5 Mechanical properties of masonry units

E_m* [MPa]	ν	f_p [MPa]	G_{fc} [N/mm]	f_{tp}* [MPa]	G^I_f [N/mm]	h [mm]
15000	0.19	6.0	0.06	0.25	0.02	33

* 63% of the experimental value, § 4.3.1 and Annex A1

The Von Mises model is proposed in order to define the behavior of the longitudinal reinforcement. Table 5.6 and Figure 5.17 summarize the mechanical properties and experimental curve presented in Annex A1. Besides, nominal values of the modulus of elasticity and yield stress were proposed for stirrups.

Table 5.6 Mechanical properties of longitudinal reinforcement and stirrups

Longitudinal reinforcement			Stirrups		
E_s [MPa]	f_y [MPa]	A_s [mm^2]	E_s [MPa]	f_y [MPa]	A_s [mm^2]
177548	464	142	200000	253	63

According to preliminary results, it can be seen that the numerical model showed failure by tension effect at the lower mortar joints. In addition, the vertical displacements of the concrete columns were greater than the experimental values. For this reason, it was necessary to put vertical spring elements on top of the wall. The stiffness of this elements was adequately chosen in order to guarantee that the vertical numerical displacement doest not exceed the experimental values. A similar criterion has been proposed by Giambanco, Spallino and Rizo (2001) in order to reproduce the experimental lateral load vs. lateral displacement curve.

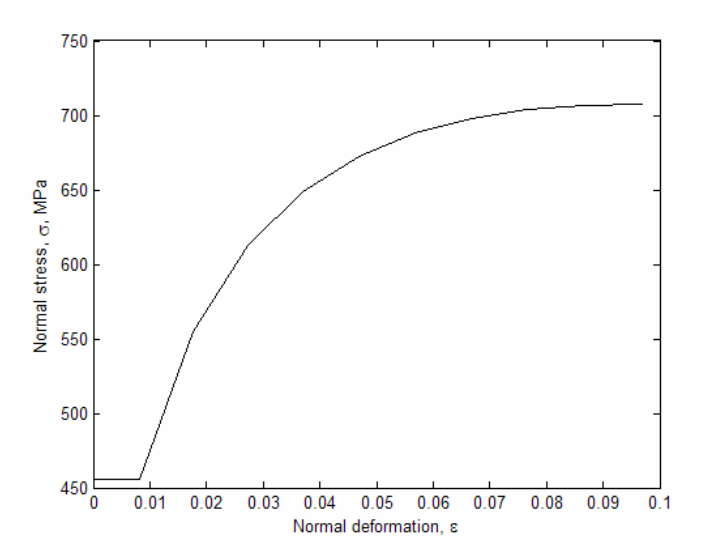

Figure 5.17: Hardening strain vs. normal stress relationship for the longitudinal reinforcement

5.4.1.3 Results

Figure 5.18 shows the horizontal displacement vs. lateral load envelopes of two numerical models and the experimental resistance envelope. The numerical model M1 corresponds to the variables of Tables 5.3 – 5.5 by considering the units behavior defined according to the Rankine model. The numerical model M2 considers the combined Rankine-Von Misses model that defines the behavior of the units with the mechanical properties given in Table 5.5. In addition, the wall resistance was calculated by the means of the failure shear model presented in chapter 6.

In general, the two models are able to asses the experimental results. The slope of the initial branch of both models coincides with the experimental value according to Figure 5.18. Then both models reach the point associated to the first flexural cracks and show afterwards a sudden drop. In the next stage, there is recovering of the structure and the slopes are approximately equal. At the point of maximum resistance, both numerical models recorded close values to the experimental resistance. However, only the model M2 is able to measure the degradation of stiffness and resistance but the last experimental point is not reached.

From Tables 5.7 and 5.8, it can be seen that both models had acceptable results except for the displacement related to the first flexural cracks of the model M1, which has an error equal to 50%. With respect to the load values, the model M2 has the highest error, 17 %, associated to the first flexural cracks. For the maximum load, there is a maximum error of 5.8 %.

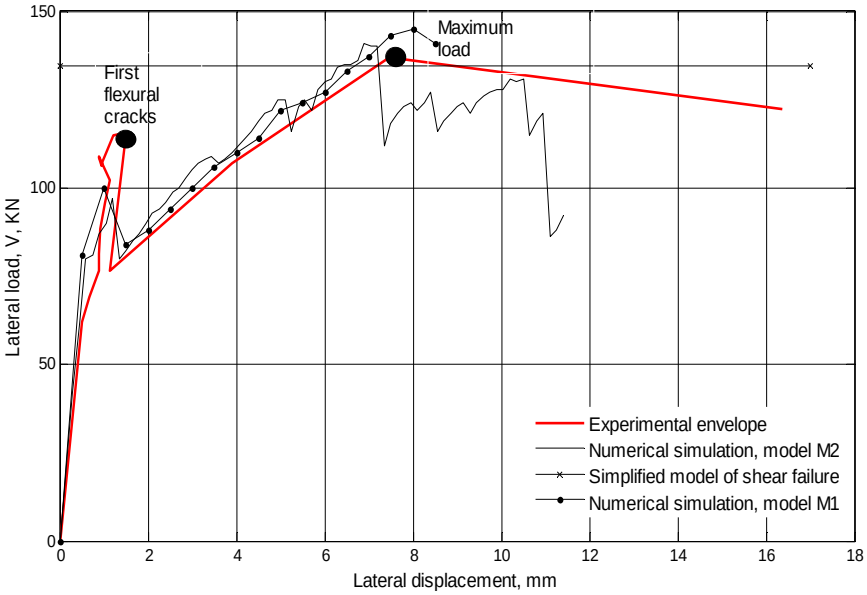

Figure 5.18: Experimental envelope and numerical simulation for the wall MUR2

Table 5.7 Comparison of results for model M1

Results	First flexural cracks				Maximum load			
	Load [KN]	Error %	Displ mm	Error %	Load [KN]	Error %	Displ mm	Error %
Experimental	114	8.7	1.5	50	137.4	5.8	7.7	3.8
Numerical	104		1.0		146.0		8.0	

Table 5.8 Comparison of results for model M2

Results	First flexural cracks				Maximum load			
	Load [KN]	Error %	Displ mm	Error %	Load [KN]	Error %	Displ mm	Error %
Experimental	114	17	1.5	25	137.4	1.8	7.7	6.9
Numerical	97.0		1.2		140		7.2	

Figure 5.19 shows the deformed position of the model M1 to the first flexural cracks related to distortion R = 0.09% that has horizontal displacement at the lower horizontal joints. Figure 5.20 presents the deformed position related to the maximum lateral load. In general, the angle of the damaged diagonal corresponds with respect to the experimental failure pattern. The model is able to simulate the opening of the upper left masonry-columns interface and the failure of some vertical joints. However, the damaged horizontal joints and the opening of the lower right interface do not coincide with the experimental evidence, Figure 5.21.

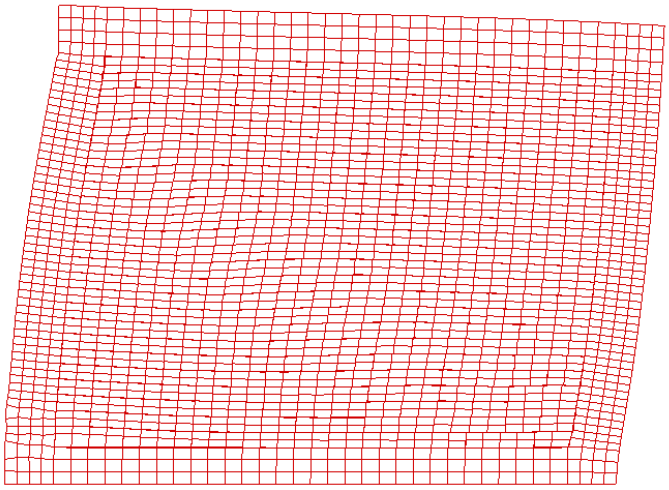

Figure 5.19: Deformed position of the model M1 at first flexural cracks, *R* = 0.09 %, *D* = 1.5 mm

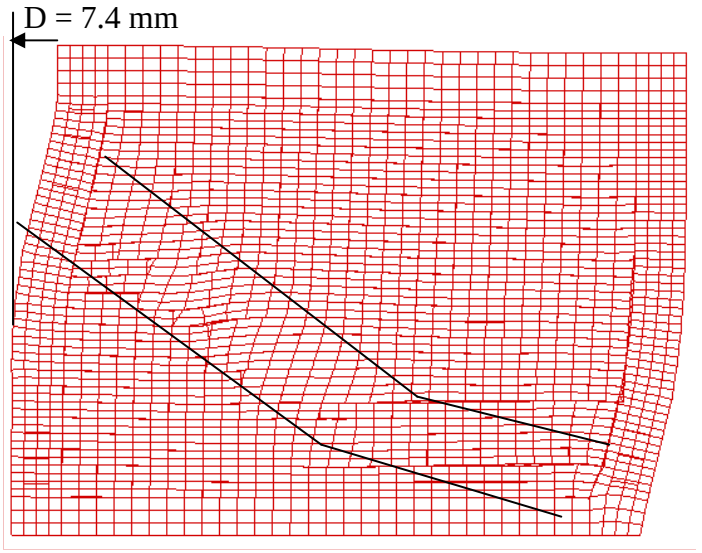

Figure 5.20: Deformed position of the model M1 at maximum load, *R* = 0.45 %, *D*= 7.4 mm

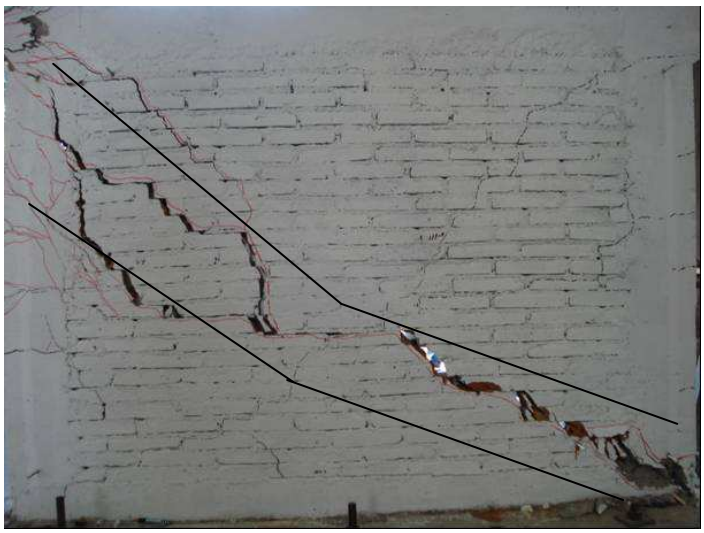

Figure 5.21: Final failure pattern for the wall MUR2

For the masonry units, Figure 5.22 shows the width and the direction of the cracks by tension effect in each integration point that define satisfactory the experimental cracking pattern. The cracking of the units occurs when the tensile stress exceeds the low tensile strength, f_t = 0.25 MPa, 63% of the initial experimental value. However, the failure pattern and the envelope resistance change if this value rises. Besides, the main inclined cracks appear in good agreement with the cracking pattern. The crack width at the bottom right column rises and the stirrups yielded at the end of the test in accordance with the experimental evidence, Figure 5.22 and 5.23b.

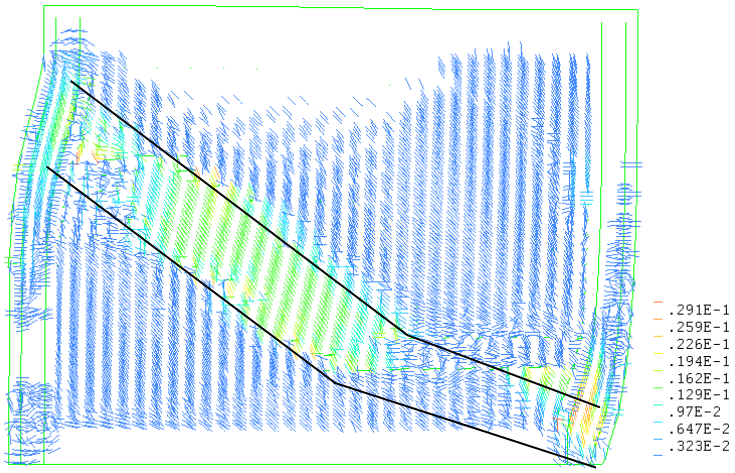

Figure 5.22: Width of cracks of the quadrilateral elements of the model M1 to maximum load and R = 0.45 %

Figure 5.23a presents the numerical and experimental vertical displacement for both columns at the end of the test. It can be seen that the elastic stiffness of the springs elements placed on top of the wall is able to control the deformation by tension effect.

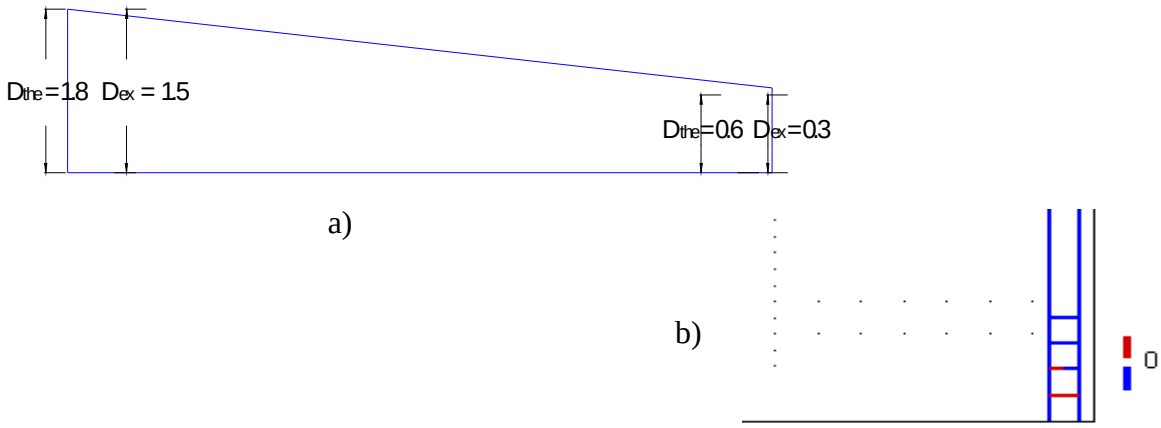

Figure 5.23: Conditions of the model M1 to maximum load, R = 0.45%, a) Numerical and experimental vertical displacements of columns by tension effect, b) Yield of stirrups at the lower left corner

The numerical models presented herein had 3396 elements and their numerical analysis required high computational effort. Then two additional models with less elements were elaborated: one model of four 4-nodes elements for brick and another with four 8-nodes elements for brick (for this case an interface 6-nodes element was used). However, their results were not satisfactory because the first showed excessive deformation at the right interface and the second had problems of convergence.

5.4.2 Model of the wall MUR2 with metallic reinforcement mesh inside the joints

In order to improve the masonry wall behavior, metallic reinforcement mesh referenced in 4.4.2.2 was placed in numerical model M1. Then, three identical straps were placed as is shown in Figure 5.24a. Two straps placed close to the corners and the third placed in the low left area of the wall. However, even if the reinforcement changes the behavior after the first flexural cracks, the masonry wall resistance rises only 6% for the peak load, Figure 5.24b.

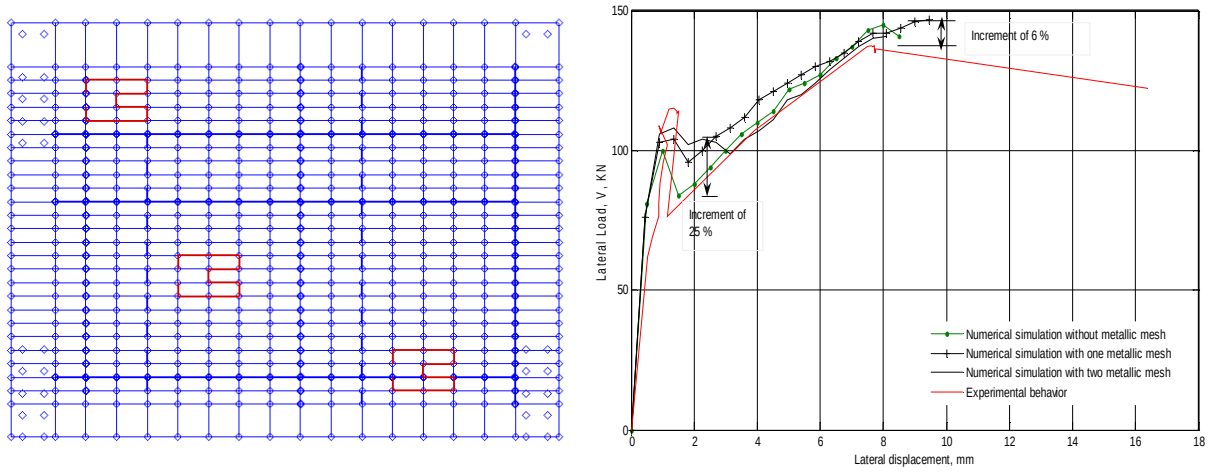

a) b)

Figure 5.24: a) Position of the metallic reinforcement mesh in model M1, b) Influence of metallic reinforcement mesh on masonry wall behavior

As there is no experimental evidence about this item, numerical results are not conclusive. Two main causes may govern this situation: a) the micro-model is not able to simulate the influence of the metallic reinforcement mesh, b) the location and/or the form of the straps is not adequate.

5.5 Masonry modeling by using a macro-model level two

5.5.1 Background

Among the macro-models adopted to evaluate the masonry behavior, a special attention is devoted to those where masonry is modeled as 1-D element subject to compression. For example, Smyrou (2006) and Crisafulli et. al (2000) use this type of model to evaluate the hysteretic behavior of the masonry walls subjected to lateral cyclic load, meanwhile Cruz (2002) proposes a simplified model to compute the masonry walls resistance under lateral load regardless the lateral displacement. A disadvantage of these models is to evaluate the equivalent width of the diagonal element, which has not physical dimension and its evaluation is not clear.

Another alternative is to developed models that suppose the failure surface along the wall diagonal [98]. In this way, the bases of the macro-model developed herein are:

- analysis of the experimental behavior of the confined masonry walls tested under lateral cyclic load [4] [13] [20] [21] [36] [48] [107],
- experimental results of the walls MUR1 and MUR2(chapter 4),
- experimental behavior of the masonry panels subject to diagonal tension(chapter 4), and
- results of the shear simplified model developed to evaluate the masonry walls resistance (chapter 6)

Then, the confined masonry wall under lateral and vertical load, Figure 5.25a, can model according to Figure 5.25b. Herein, k_M is the masonry lateral stiffness and k_C is the column lateral stiffness. This model does not consider the flexural and axial stiffness of both components. Thus, the wall modeled as the parallel system according to Figure 5.25c has only one degree of freedom, i.e. the lateral displacement. The model supposes that both columns fail simultaneously by shear effect.

5.5.1.1 Behavior of masonry

The mechanical properties of the diagonal spring element are computed from results of the diagonal tension on masonry panels, § 4.4.2.3. Two values are currently referenced from these tests, the shear stress τ_{yield} and the modulus of the rigidity. Then Equation 5.43[11] evaluates the shear strain γ_{yield} at the final point of the elastic behavior according to Figure 5.26.

Because there are not sufficient experimental data, the ultimate shear strain γ_{max} has the value obtained in § 4.4.2.3, Equation 5.44. According to experimental results obtained herein and referenced [38], the horizontal shear strain measured on the diagonal tension tests is not significant. Therefore, Equation 5.45[11] computes the vertical deformation δ_v of masonry panel along its vertical length L_v .

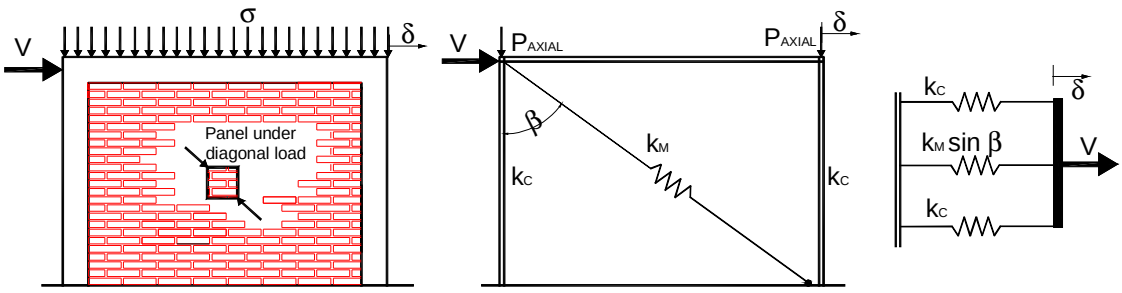

a) b) c)

Figure 5.25: a) Confined masonry wall subject to lateral and vertical load, b) Macro-model, c) Model simplified by considering only shear deformation

$$\gamma_{yield} = \tau_{yield} / G \tag{5.43}$$

$$\gamma_{max} = 0.0015 \tag{5.44}$$

$$\delta_v = L_v \gamma \tag{5.45}$$

The horizontal displacement associated to the masonry yield is the horizontal projection of the diagonal displacement, Equation 5.46, where β is the angle of the wall diagonal with respect to the vertical direction, and L_{dm} is the length of the masonry diagonal. In the same case, Equation 5.47 evaluates the ultimate horizontal displacement proposed as 25% greater than the experimental value.

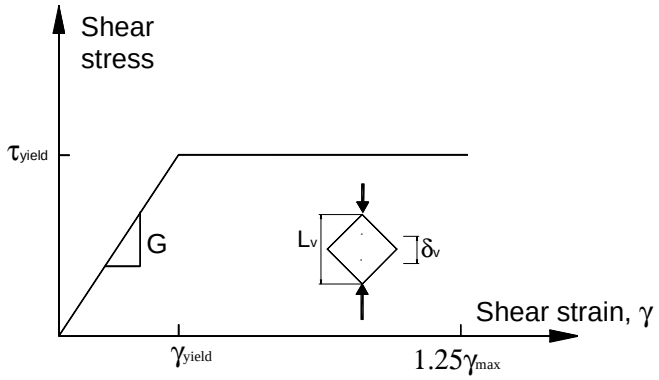

Figure 5.26: Behavior of a masonry panel subject to vertical load

$$\delta_{yield} = \gamma_{yield} L_{dm} \sin(\beta) \quad (5.46)$$

$$\delta_{ult} = 1.25 \gamma_{max} L_{dm} \sin(\beta) \quad (5.47)$$

From the results of the shear failure model developed in § 6.4, Equation 5.48 defines the yield lateral load, V_{yield}. Herein, τ_r is the shear strength stress defined by the lowest value of the Equation 5.49 or Equation 5.50 in function of the modulus of the rigidity.

$$V_{yield} = 0.8 A_{dm} \sin(\beta) \tau_r \quad (5.48)$$

If G > 1000 MPa

$$\tau_r = \begin{cases} \tau_{yield} / (1+2.5CV) \\ 0.8\sqrt{f_m^*} \end{cases} \quad (5.49)$$

If G <= 1000 MPa

$$\tau_r = \tau_{yield} \quad (5.50)$$

Where:

V_{yield}	Lateral load associated to the yield displacement δ_{yield}
A_{dm}	Cross-sectional area of the masonry diagonal
β	Angle of the wall diagonal with respect to the vertical direction, Figure 5.25
τ_r	Shear stress of masonry related with the rigidity modulus
τ_{yield}	Shear strength obtained on the diagonal tension tests, § 4.4.2.3
CV	Coefficient of variation, [42][45]
f^*_m	Design compressive strength of masonry, [42][45]
G	Rigidity modulus of the masonry, § 4.4.2.3

The ultimate lateral load of the masonry, $V_{ult,}$ associated to the ultimate lateral displacement, $\delta_{ult,}$ considers the contribution of the vertical load evaluated by Equation 5.51 according to the results presented in § 6.4.1.2. Herein, f is the percentage of the vertical load supported by the masonry, Equation 5.52. Consequently, the two values of the masonry stiffness defined in Figure 5.27, k_{M1} and k_{M2}, can be evaluated.

$$V_{ult} = A_{dm} \sin(\beta) \left(\tau_r + f \sin(\beta) \cos(\beta) \sigma\right) \quad (5.51)$$

$$f = A_m E_m \Big/ \left(A_m E_m + 2 A_c E_c \right) \tag{5.52}$$

Where:

V_{ult} Lateral load associated to the ultimate displacement δ_{ult}

A_{dm} Cross-sectional area of the masonry diagonal

f Distribution factor of the vertical load, § 6.3

β Angle of the wall diagonal with respect to the vertical direction, Figure 5.25

σ Vertical acting stress

A_m Cross-sectional horizontal area of the masonry

A_c Cross-sectional horizontal area of the columns

E_m Elasticity modulus of the masonry

E_c Elasticity modulus of the columns

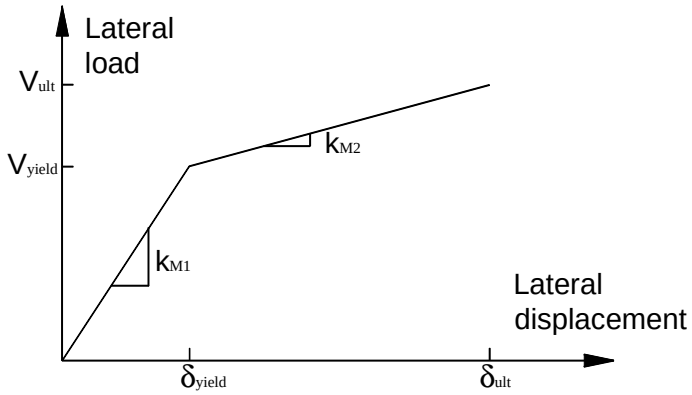

Figure 5.27: Lateral load vs. lateral displacement curve of masonry spring element

5.5.1.2 Behavior of concrete columns

In order to evaluate the elastic stiffness of the masonry walls, Tomazevic (2000) takes into account both shear and flexural deformations of the two components: masonry and concrete frame. Herein, the spring diagonal element defined above gives the stiffness of the masonry. As the vertical displacement is not important for both columns of the wall MUR2, § 4.5.8, it can be supposed that the upper boundary has a fix-ended conditions. Then, Equation 5.53 computes the stiffness of the concrete columns [106], where H is the column length.

$$k_C = 12EI \Big/ H^3 \tag{5.53}$$

The term EI is variable during the load process according to Figure 5.28. In the first phase has a linear behavior until the first cracking. In the non-linear range, however, the stiffness of the concrete columns is defined as the secant stiffness, which follows the displacement on the idealized curve [106].

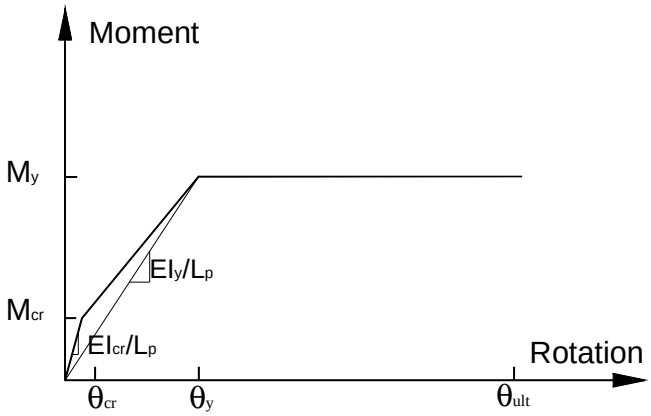

Figure 5.28: Moment vs. rotation relationship of concrete elements

The constitutive relations of the concrete and longitudinal steel are necessary to define the moment-rotation curve, Figure 5.28. In this research work, the modified model of Kent and Park (1971) presented in Annex A3 defines the concrete behavior while the mechanical properties of the reinforcement steel has been defined in Annex A1.

In other way, Equation 5.54 defines the plastic hinge length [89] and Equation 5.55 [89] computes the shear associated to cracking moment M_{cr} or yield moment M_{yield}.

$$L_p = h \tag{5.54}$$

$$V = 2M_i / H \tag{5.55}$$

Where:

L_p	Plastic hinge length
h	Total depth of the concrete columns
V	Load shear related to the moment i-moment
H	Column length

5.6 Analysis procedure and results

The analysis procedure at each stage presented is as follows [89]:

a) According to prior stage is obtained the stiffness matrix of the structure (K_T) from the stiffness of the members (k_C, k_M). At the first stage all members have elastic stiffness,

$$K_T = k_M + 2k_C \tag{5.56}$$

b) A unit horizontal force is applied,

c) The displacement associated to unit force (Δ_{UN}) is evaluated,

$$\Delta_{UN} = 1/K_T \tag{5.57}$$

d) The shear associated to unit force (V_{UN}) is obtained for each element, k_i is the stiffness of the concrete or masonry,

$$V_{UN} = k_i \Delta_{UN} \tag{5.58}$$

e) For each element, the parameter α (ratio shear remaining before reaching the next point of the behavior curve vs. shear associated to unit force) is obtained. The lowest value of α gives the shear increment for this stage, V_S is the next value of shear resistance curve and $V_{AC(i-1)}$ is the cumulated shear at the prior stage,

$$\alpha = \left(V_S - V_{AC(i-1)}\right) / V_{UN} \tag{5.59}$$

f) The shear increment (ΔV_{EL}) for each element and total shear (V_T)are obtained

$$\Delta V_{EL} = \alpha V_{UN} \tag{5.60}$$

$$V_T = \Delta V_{ELi} + V_{AC(i-1)} \tag{5.61}$$

g) The displacement increment (Δ_i) and total displacement(Δ_T) are evaluated, $\Delta_{AC(i-1)}$ is the cumulated displacement at the prior stage

$$\Delta_i = \alpha \Delta_{UN} \tag{5.62}$$

$$\Delta_T = \Delta_i + \Delta_{AC(i-1)} \tag{5.63}$$

h) Return to the first step

i) The process finish when all elements reach their shear capacity

5.6.1 Results of the wall MUR2

Table 5.9 shows the parameters that define Figures 5.27 and 5.28. Chapter 4 and Annex A1 contain the experimental data of the wall MUR2. For the other walls, the experimental data are taken from references [4] [48] [107].

Table 5.9 Data of masonry spring elements and columns

Wall or author	Masonry (KN, m)				Concrete columns (KN/m)	
	V_{yield}	V_{ult}	δ_{yield}	δ_{ult}	EI_{cr}	EI_y
MUR2	101.2	126.4	1.46E-3	3.91 E-3	2243.2	321.1
Aguilar (1997)	77.8	119.5	1.66 E-3	4.13 E-3	499.3	174.3
Hernandez and Urzua (2002)	80.0	113.4	0.89 E-3	4.20 E-3	709.3	217.4
Treviño et. al (2004)	93.0	154.7	0.49 E-3	4.27 E-3	1044.3	207.3

Figure 5.29 shows the numeric envelope curve for the wall MUR2. The process has four increments, the first finishes when the columns reach the cracking shear, the second finishes with the cracking of the masonry, the thirst finishes when the masonry reaches the ultimate shear, and the last ends with the shear yield of the columns.

The model is not able to measure the resistance and stiffness degradation after the maximum load because the two columns reached their resistance simultaneously and the stiffness matrix becomes non-positive. However, the two branches of the experimental and numerical envelopes have similar slopes and both loads are close for the permissible distortion, 0.25 %. In general, it can be seen that the macro-model has adequate concordance until a distortion equal to 0.5 %.

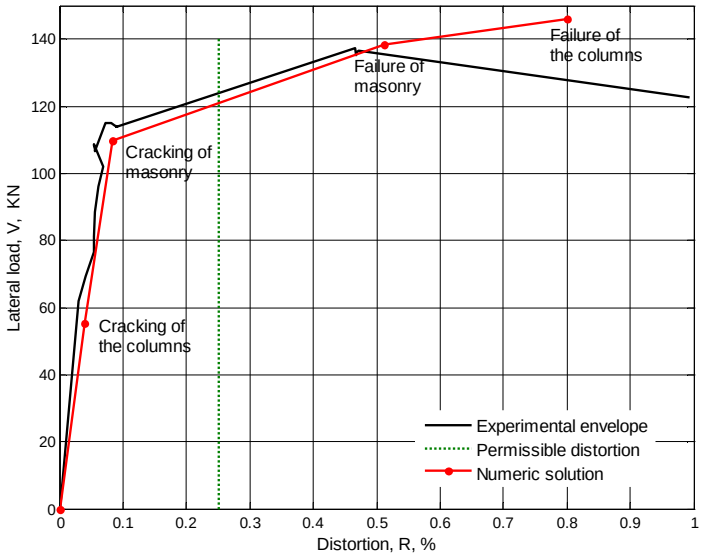

Figure 5.29: Experimental positive envelope and numeric solution of the wall MUR2

Figure 5.30 shows two numerical solutions of the wall MUR2: one obtained by micro-model and the other obtained by macro-model, as well as two experimental envelopes. The first

experimental envelope shows the extreme curves of the hysteretic cycles, the second experimental envelope contains the maximum load and maximum distortion of each cycle.

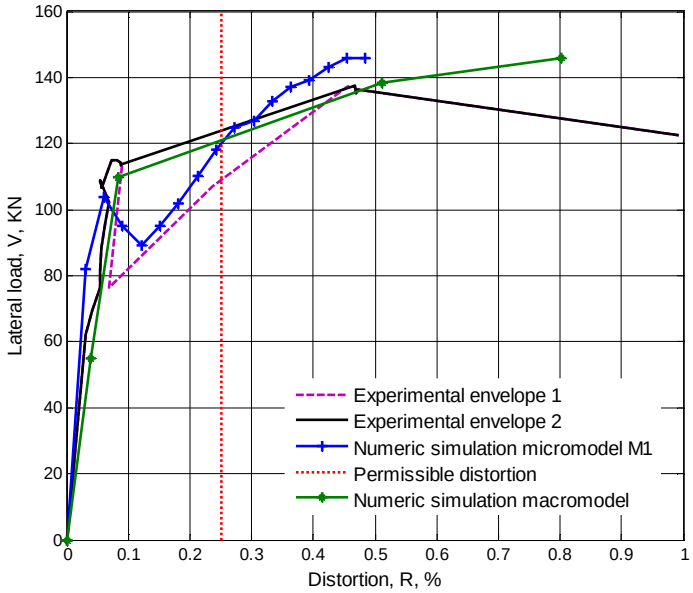

Figure 5.30: Experimental positive envelope and numeric solution of the wall MUR2

Table 5.10 summarizes the ratio (numerical values vs. experimental data) of the two models. The elastic stiffness and the rotation associated to the yield masonry have the highest ratio ranging from 0.64 to 1.35. However, the ratio values of the masonry yield load, load to permissible distortion and maximum load ranges from 0.91 to 1.08. From these results, it can be seen that the macro-model is capable to evaluate the envelope resistance until a distortion equal to 0.5 %. For the three last parameters, it gives close values to those obtained by the micro-model elaborated through the finite element method.

Table 5.10 Ratio experimental value vs. numerical value

Parameter	Experimental	Micro-model	Macro-model	Ratio Micro/Exp	Ratio Macro/Exp
Elastic stiffness (KN /mm)	121	164	78	1.35	0.64
Yield load (KN)	115	104	109	0.91	0.95
Load to 0.25 % distortion (KN)	118	120	120	1.02	1.02
Maximum Load (KN)	136	146	134	1.08	0.99
% Rotation associated to yield load	0.09	0.06	0.08	0.67	0.89

5.6.2 Results for other walls

For assessing the performance of this macro-model, additional referenced walls [4][48][107] were analyzed. Unlike the wall MUR2, the wall tested by Aguilar (1997) has vertical load acting, and then Figure 5.31 shows the masonry contribution, where can be seen a different slope for the second branch. Figures 5.32 and 5.33 present the experimental envelopes and the numeric simulation for other walls. The test information and mechanical properties of the walls are defined in chapter 6. All figures presented the permissible distortion equal to 0.25% according to local code.

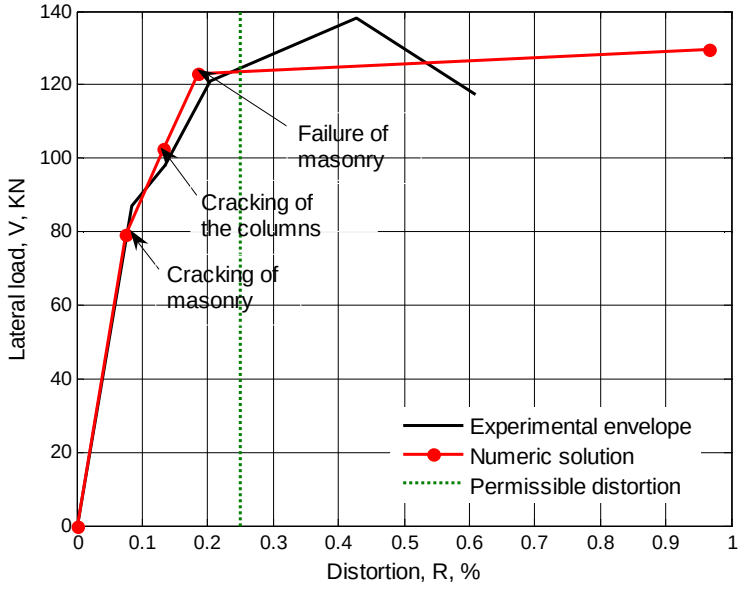

Figure 5.31: Experimental positive envelope by Aguilar (1997) and numeric solution

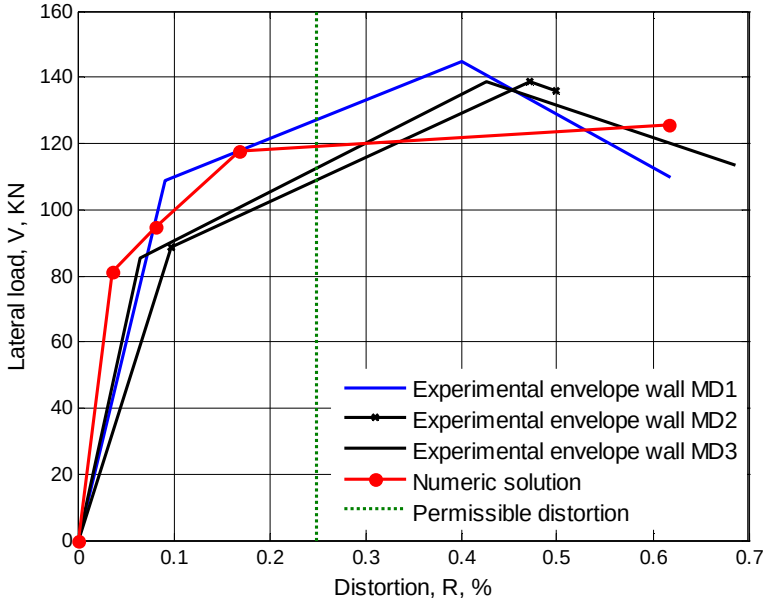

Figure 5.32: Experimental positive envelope by Hernandez and Urzua (2002) and numeric solution

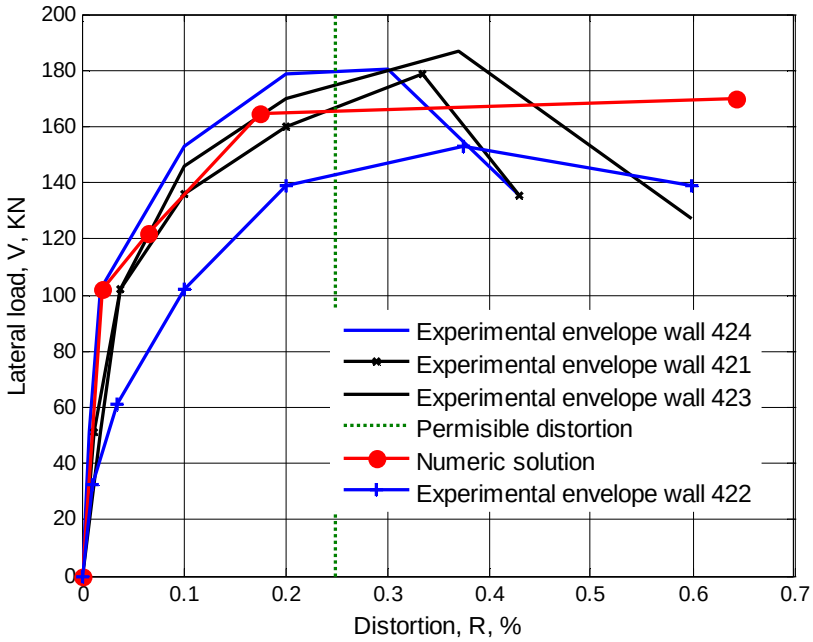

Figure 5.33: Experimental positive envelope by Treviño et. al (2004) and numeric solution

The performance of the macro-model is summarized in Table 5.11 by means of the ratio (numerical values vs. experimental values). For the walls tested by Hernandez and Urzua (2002) and Treviño et. al (2004), the experimental values used to do the comparison are the average obtained from all tests. From these results, it can be seen that only three values have high variation: the elastic stiffness of the walls tested by Hernandez and Urzua (2002) and Treviño et. al (2004) and the distortion to yield load of the walls tested by Hernandez and Urzua (2002). The remaining values range from 0.87 to 1.11.

Table 5.11 Ratio numerical value vs. experimental value

Parameter and Author	Aguilar (1997)	Hernandez and Urzua (2002)	Treviño et. al (2004)
Elastic stiffness	1.03	2.04	1.20
Yield load	0.90	0.87	1.11
Distortion to yield load	0.88	0.42	1.10
Load to distortion 0.25 %	1.00	1.02	0.98
Maximum load	0.91	0.87	0.94

Two additional applications of this macro-model were developed. The first applied to the ground floor of 3-D masonry structure two levels tested under cyclical loads by Sanchez et. al (1996). Two parallel systems of two masonry confined walls for each level, 2.4 m X 2.50 m (Length X Height) and 1.6 m X 2.50 m, and two-slab concrete composed the structure, Figure 5.34. The second application is for a system of two identical walls that the previous test fixed

by means of a slab concrete, it is referenced as wall WWW, Figure 5.36. Both applications show the adequate performance of the macro-model because the numerical envelope is close to the experimental envelope inside the range of the permissible distortion. However, the elastic stiffness of the numerical envelope of the 3-D structure has some variation with respect to the experimental envelope, Figure 5.35. The agreement rises for the second case according to Figure 5.37.

Numerical results of other complex models were used in order to comparer the results of the macro-model developed herein. Then Coral (2004) studied both structures by using the model of the strut diagonal under incremental load, their results have identical estimation of the structural behavior as is shown in Figure 5.38 and Figure 5.39.

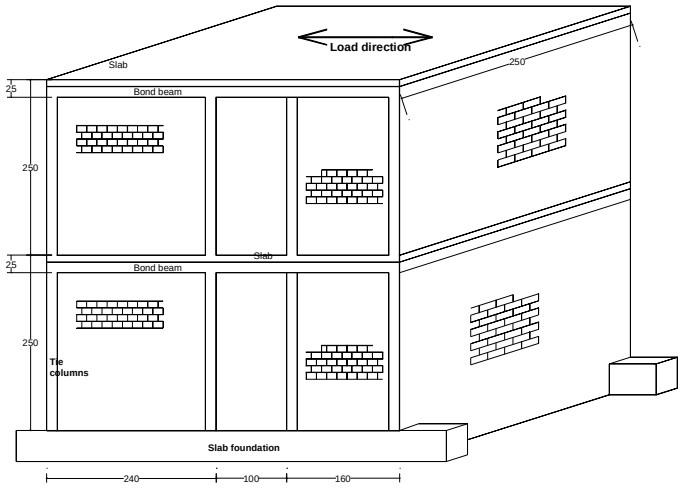

Figure 5.34: 3-D masonry structure tested by Sanchez et. al (2000)

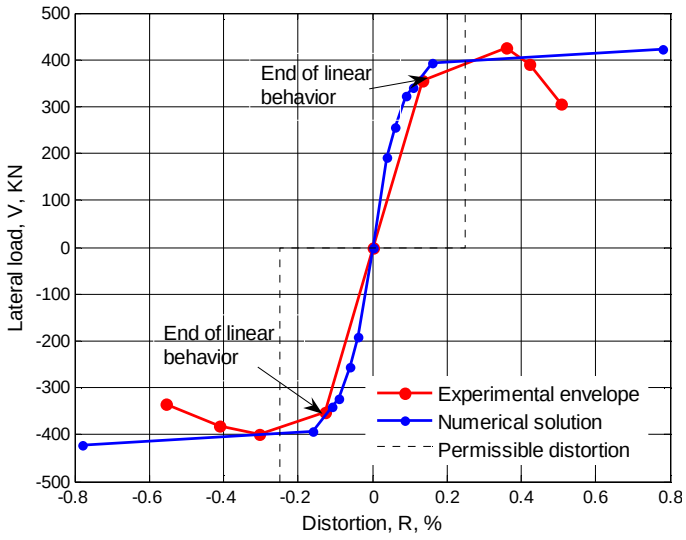

Figure 5.35: Experimental envelope and numeric solution of 3-D masonry structure [96]

Alvarez (2000) analyzed the wall WWW through the 818 finite elements by using the model of the smeared crack. He modeled all materials (masonry, concrete, and reinforcement steel) by considering a rigid interface concrete-masonry. Unlike Alvarez (2000), Ishibashi and Kastumata (1994) modeled the interface concrete-masonry by using spring elements, see incise 3.4.1. Thus, according to Figure 5.38 and Figure 5.39, the macro-model developed herein has equal estimation that other complex models built by means of the finite element method.

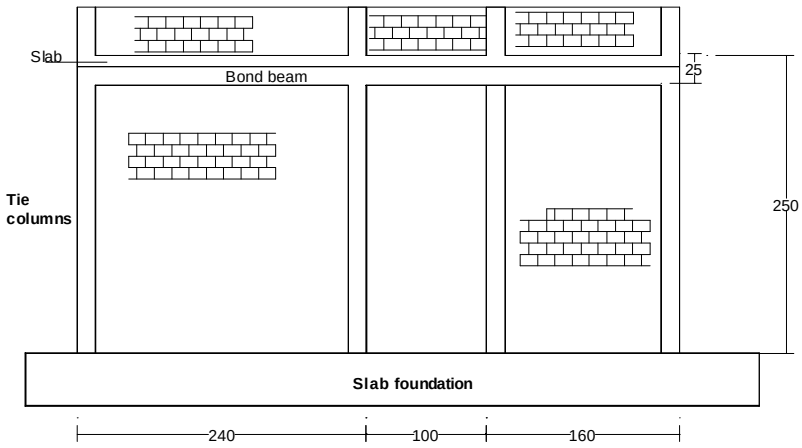

Figure 5.36: Geometrical characteristics of the wall WWW [50]

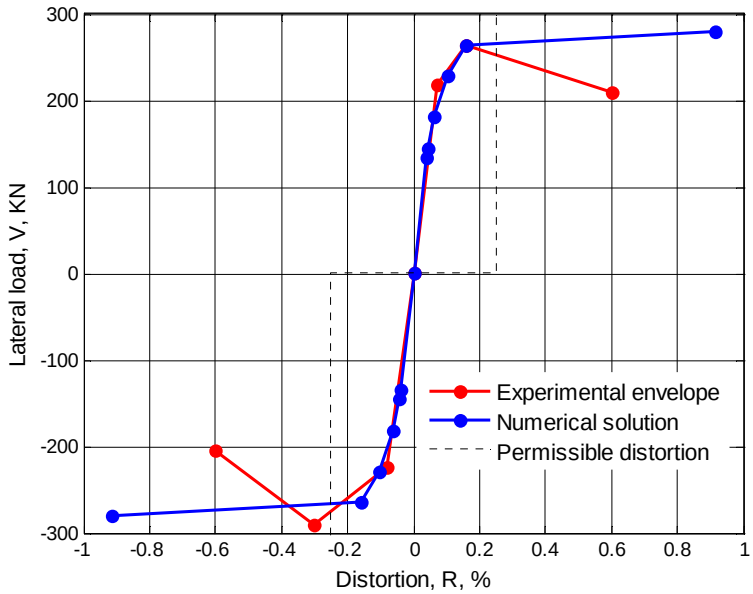

Figure 5.37: Experimental envelope and numeric solution of the wall WWW [50]

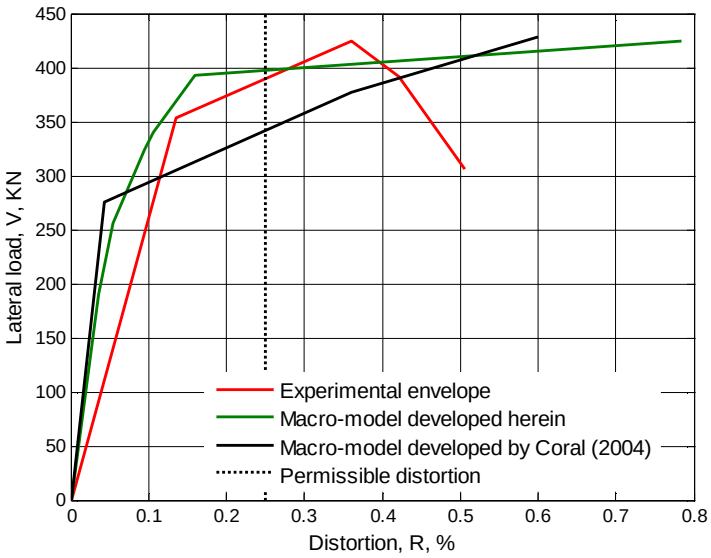

Figure 5.38: Comparison among different models for the 3-D structure

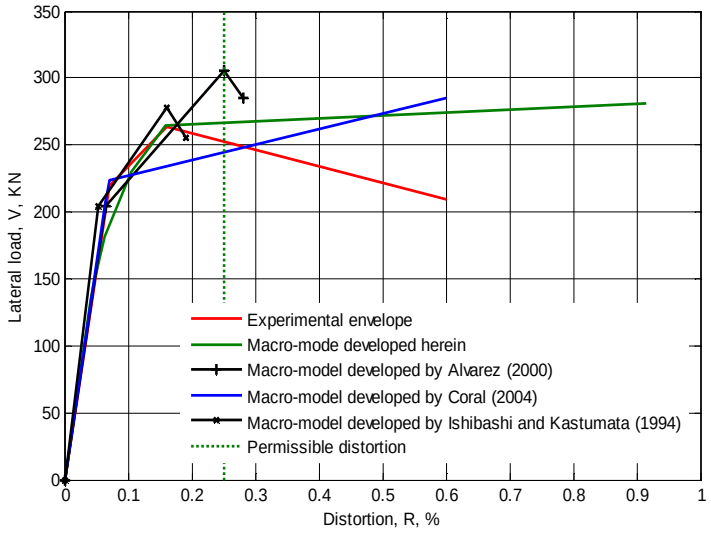

Figure 5.39: Comparison among different numeric models for the wall WWW

5.7 Conclusions

In order to analyze the sensitivity of the proposed mesh, several models of the un-reinforced panel were elaborated. Thus, it can be determined that the units modeled through 4 [4-nodes elements] or 16 [4-nodes elements] have the better estimation of the experimental behavior. Thus, the vertical load vs. vertical displacement numerical curve is similar to the experimental curve as well as the failure mode, cracking of the units and slipping of the joint. In addition, numerical simulations proved that the cohesion has the highest influence on the panel behavior.

With respect to the reinforced panels, both models, one with modified cohesion and other with a 1-D element inside the joint, simulate adequately the experimental behavior. Additional benefits observed were the increment of the resistance and the reduction of the crack's width.

In other way, two models were proposed in order to analyze the wall MUR2. Then the model M1 considers brittle behavior of the units while the model M2 shows a combined behavior tension-compression. Thus, the model M2 can overestimate the unit resistance because the joint model already considers the compression resistance of the system. This situation can be avoided if the compressive strength of the units is artificially increased in order to guarantee only the tension failure of the units.

The model M1 has good agreement until the maximum lateral load. At this point, according to experimental evidence, the cracks extend along the wall diagonal and the units are cracked or there is slipping of the joints: it could be one reason for which the numerical model cannot evaluate the wall behavior after this point. By considering the compressive resistance of the units after of the point of maximum load, the model M2 is able to define the behavior of the descendent branch until 12 mm of horizontal displacement. From these results, it can be concluded that the tension failure mechanism associated to model M1 has brittle behavior while the tension-compression failure mechanism associated to model M2 is more ductile.

For the model M1, the failure numerical pattern related to the maximum lateral load is similar to the failure experimental pattern except for the slipping of the horizontal joints at the lower right corner and the opening of the interface at the right side of the wall. In addition, the cracking of the left concrete column is similar to the experimental mode. This model was able to predict the cracking at the end of the right column and the yield of the lower stirrups.

The control parameters during the test were the horizontal displacement on top of the wall and the vertical displacement of the concrete columns. The last was used to propose the stiffness of the vertical spring elements on top of the wall in order to prevent the tension failure of the joints. In addition, to obtain the failure pattern and the lateral load vs. lateral displacement relationship, the tensile strength and the modulus of elasticity of the units were reduced to 63 % of the experimental values while the dilatancy angle had a value close to zero.

According to experimental evidence, the masonry walls have a symmetrical behavior under lateral load. Then, the two micro-models can assess the envelope of resistance and are useful to evaluate the influence of the mechanical properties of the each material on the global

behavior. However, this model is not able to measure the increment of the masonry resistance caused by the metallic reinforcement mesh are inserted inside the joints.

A main disadvantage of the micro-models proposed herein is the large number of mechanical properties: some have been presented in chapter 4 and Annex A1, others haven been proposed according to references and the others have been evaluated approximately by means of experimental data. In addition, these models show a large number of freedom degrees, which causes high computational effort to develop its analysis.

With respect to the macro-model, their results are adequate by considering its simplicity. For the wall MUR2, the agreement of the results is similar to that obtained by means of micro-model.

The wall tested by Aguilar (1997) had the same type of units that the wall MUR2. Thus, the behavior of both walls was similar and the concordance of the results obtained by means of the macro-model was adequate. However, the walls tested by Hernandez and Urzua(2002) and Treviño et. al (2004) were built with lime-cement blocks and hollow concrete blocks. Then, the masonry behavior on the diagonal tension tests may be different from that proposed as base for this model. In addition, the distribution of the vertical load between frame and masonry is different to that existent in walls built with solid clay bricks. However, this model proposes an adequate envelope of resistance until the permissible distortion that is equal to 0.25%.

Additional results show the sufficient robustness of this macro-model to evaluate the resistance envelope of the structural system of the walls or 3-D structure and its assessment is identical to those of the complex models. Because of its simplicity and performance, the model is useful to evaluate the wall behavior from the mechanical properties of the masonry and concrete elements and can be applied for the masonry buildings design.

CHAPTER 6

Simplified models to asses the lateral masonry walls bearing capacity

6.1 Introduction

This chapter presents two simplified models their goal is to assess the resistance of the confined masonry walls under lateral load regardless the lateral displacement. Both models assume the failure generated by cracking of the wall diagonal, the difference is the cracking nature. The first model, called shear failure [98], assumes that the diagonal cracking occurs when the shear stress along the wall diagonal is greater than the masonry shear strength. This model also supposes the cracking of the columns by shear effect.

The second model, called induced tension failure, assumes that the diagonal cracking occurs when the normal tension stress along the wall diagonal exceeds the tensile strength of masonry [61][62][97]. Both models consider the influence of the vertical load on the resistance of the walls.

6.2 Experimental information

For assessing the performance of the simplified models, experimental results collected from tests on twenty-seven walls developed in American Latin countries were used: a) eight walls built in Venezuela, b) seventeen walls built in Mexico, and c) two walls built in Colombia. Table A4.1 (Annex A4) presents the characteristics of the walls and types of applied loads. Walls 1-8 tested by Marinilli and Castilla (2003) and walls 9-16 tested by Treviño et al. (2004) were built from hollow concrete blocks while walls 17-19 were built from lime-cement blocks by Hernandez and Urzua (2002). Walls 20-27 were built from solid clay bricks and tested in different places, thus, wall 20 was tested by Aguilar (1997), walls 21-23 were tested by Meli and Salgado (1969), walls 24-25 were tested in this project, and walls 26-27 were tested in Colombia [13].

Table A4.2 (Annex A4) shows additional characteristics and Figure 6.1 defines the wall geometry expressed in Table A4.1 and Table A4.2. Finally, Table A4.3 (Annex A4) contains the mechanical properties necessary to apply both models.

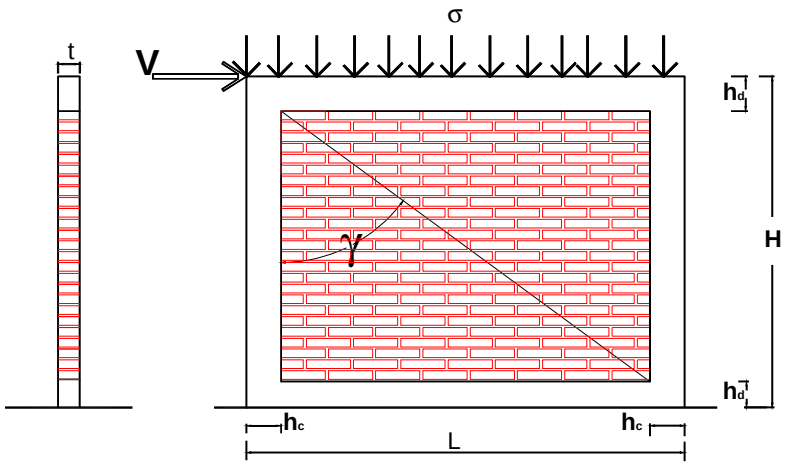

Figure 6.1: Geometrical properties of confined masonry walls

For walls tested in Mexico without information of the modulus of elasticity, we adopted the normative equations [42][44]. For walls 1-8, the shear strength of design τ^*_m was calculated by Equation 6.1 [42] by using the mean shear strength presented by Castilla and Marinilli (2003) with coefficient of variation CV = 0.2, while the modulus of elasticity were evaluated according to Equation 6.2 [68] and Equation 6.3 [42]. With regard to the tensile strength of masonry, the lowest value of the two expressions presented in Equation 6.4 is chosen, one obtained from experimental results defined in Annex A1 and the other based on results obtained by Mebarki et. al (2009).Units of all equations are MPa.

$$\tau^*_m = \tau_m / (1+2.5CV) \tag{6.1}$$

$$E_c = 4729\sqrt{f'c} \tag{6.2}$$

$$E_m = 250 f^*_m \tag{6.3}$$

$$f_t = \min\begin{cases} 0.74\tau_m \\ 0.10 f^*_m \end{cases} \tag{6.4}$$

Herein:

τ^*_m	Design shear strength of masonry
τ_m	Mean of shear strength obtained on diagonal tension test
CV	Coefficient of variation

f_t Tensile strength of masonry

f'_c Compressive strength of concrete

E_c Modulus of elasticity of concrete

E_m Modulus of elasticity of masonry

f^*_m Design compressive strength of masonry

6.3 Vertical load supported by the masonry

According to experimental evidence [4] and in function of its vertical stiffness, the columns and masonry hold on fraction of the vertical acting load on top of the wall. Then the equivalent parallel system of the wall, Figure 6.2, is useful to obtain Equation 6.5 that computes the load distribution factor (*f*) for the masonry by considering the compatibility of the vertical displacement among elements. Herein, A_m, E_m are the area and the elastics modulus of the masonry, A_c and E_c are the area and the elastic modulus of the concrete.

$$f = A_m E_m \Big/ \left(A_m E_m + 2A_c E_c \right) \tag{6.5}$$

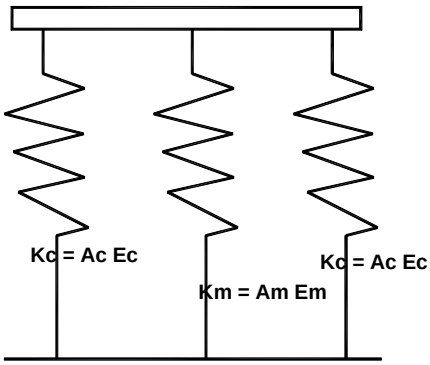

Figure 6.2: Equivalent system masonry-concrete frame

6.4 Shear failure model

The bases of the shear failure model are the behavior of masonry walls referenced herein and the results of the walls MUR1 and MUR2. The model supposes the predominance of the shear deformations with respect to the flexural deformations. In most cases, the failure occurs along the wall diagonal when the acting shear stress exceeds the design shear strength [98]. The wall resistance has a tri-linear envelope according to Flores (1995), Figure 6.3. The first stage ends with the presence of the first diagonal cracking, the second stage ends when masonry and concrete columns are cracked at the peak, finally, yield of the longitudinal steel of

columns defines the last stage. Figure 6.4 shows the damage pattern associated to different levels of distortion.

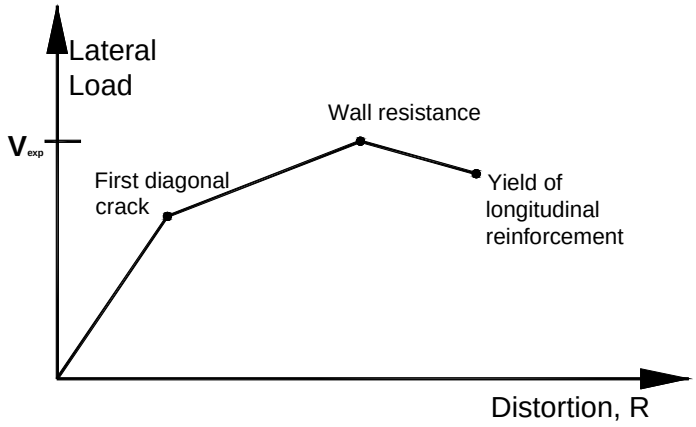

Figure 6.3: Experimental resistance envelope (Flores, 1995)

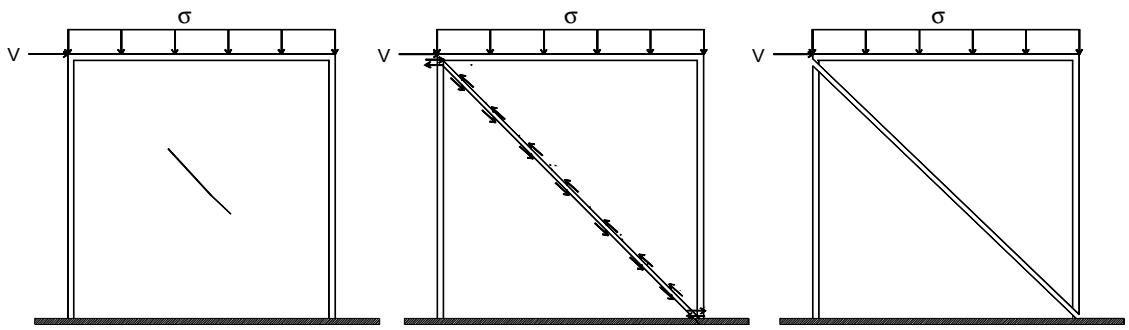

First diagonal crack Intermediate state Wall resistance

Figure 6.4: State of damage for several levels of distortion (Flores, 1995)

The simplified model has the following assumptions:

1. Failure occurs along the wall diagonal, which cracks simultaneously in all length by shear effect.

2. Wall or any of their two parts have behavior as rigid body with respect to its diagonal before and after of failure,

3. Upper beam has infinite flexural stiffness and infinite axial stiffness.

Figure 6.1 shows the forces acting on the masonry wall, where V is the horizontal seismic force, σ is the vertical stress applied, L is the length, H is the height, and γ is the diagonal angle with respect to the vertical direction. Figure 6.5 shows the free body diagram of the upper left node, where the horizontal force V causes tension on the concrete column and compression on the diagonal wall that generates shear stress on masonry.

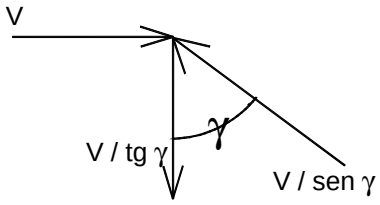

Figure 6.5: Free-body diagram of node B

6.4.1 Masonry wall resistance

Next paragraphs define the wall resistance by considering the masonry resistance, the concrete frame resistance, and the contribution of the vertical load.

6.4.1.1 Masonry resistance

The panel resistance under the diagonal tension test is the maximum load *P* used to evaluate the mean shear strength τ_m according to Equation 6.6[45]. Thus, through an inverse process the value of *P,* which direction coincides with the panel diagonal, is calculated with Equation 6.7. Then by considering the wall of the Figure 6.6a as a set of panels, where the wall diagonal coincides with the diagonals of the *N* panels subjected to diagonal tension (shear), the total resistance P_m is the sum of the resistance P_i of the *N* panels evaluated by Equation 6.8. In this equation, the mean shear strength τ_m is replaced by τ^*_m, which considers the flexion effect and the size effect of the wall. Herein A_d is the diagonal area of the panel and A_{dm} is the diagonal area of the masonry.

$$\tau_m = P / A_d \tag{6.6}$$

$$P = \tau_m A_d \tag{6.7}$$

$$P_m = \sum_{i=1}^{N} \tau^*_m A_{dmi} = \tau^*_m \sum_{i=1}^{N} A_{dmi} = \tau^*_m A_{dm} \tag{6.8}$$

6.4.1.2 Vertical load effect

The vertical force acting on top of the masonry is $f\sigma A_m$, which is in equilibrium on the failure plane by the tangential force F_t and the normal force F_n, the parameter *f* is the ratio of the masonry vertical stiffness with respect to the wall vertical stiffness calculated by Equation 6.5. The parameter A_m is the cross-sectional horizontal area of the masonry and σ is the vertical acting stress. From equilibrium condition applied to the upper wedge of the wall according to Figure 6.6b, Equation 6.9 defines the tangential force F_t

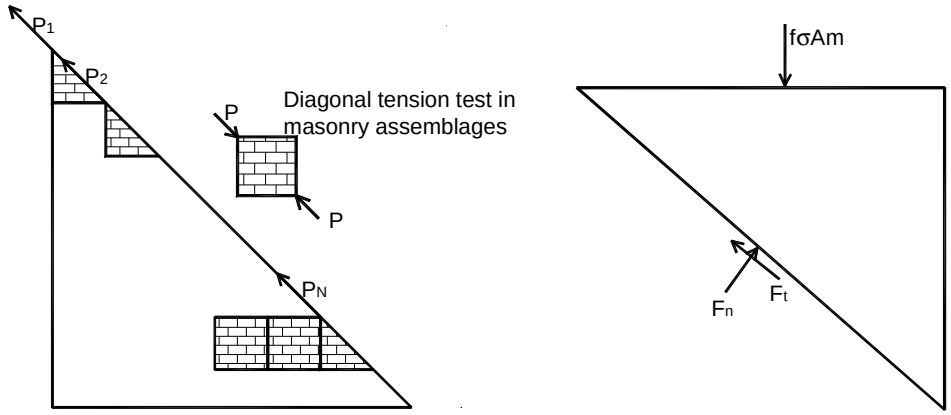

a) b)

Figure 6.6: a) Resistance of masonry, b) Influence of vertical load

$$F_t = f\sigma A_{dm} sen\gamma \cos\gamma \tag{6.9}$$

The sum of the tangential load F_t plus the resistance of masonry P_m, Equation 6.10, gives the resistant load along the diagonal and its horizontal projection provides the resistance of the masonry V_m, Equation 6.11.

$$F_{tt} = A_{dm}(\tau_m^* + f\sigma sen\gamma \cos\gamma) \tag{6.10}$$

$$V_m = A_{dm} sen\gamma(\tau_m^* + f\sigma sen\gamma \cos\gamma) \tag{6.11}$$

6.4.1.3 Columns resistance

Equation 6.12 or Equation 6.13 provide the nominal shear strength of the columns [44], where t and h_c are the dimensions of columns, ρ is the percentage of reinforcement, and f^*_c is the reduced compressive strength. Units of Equations 6.12 and 6.13 are MPa.

If $\rho < 0.015$

$$V_{cr} = 0.31(0.20 + 20\rho) t h_c \sqrt{f_c^*} \tag{6.12}$$

If $\rho >= 0.015$

$$V_{cr} = 0.16 t h_c \sqrt{f_c^*} \tag{6.13}$$

Finally, Equation 6.14 evaluates the resistance of the wall. Equation 6.15 is proposed by the local code to evaluate the resistance at the first diagonal cracking, where A_T is the cross-sectional horizontal area of the wall. Equation 6.16 evaluates the relationship of theoretical resistance vs. experimental resistance.

$$V_{the} = V_m + 2V_{cr} \tag{6.14}$$

$$V_{NTCM} = A_T(0.50v_m^* + 0.30\sigma) \leq 1.5v_m^* A_T \tag{6.15}$$

$$k = V_i / V_{\exp} \tag{6.16}$$

6.4.2 Results

Table 6.1 presents the mean values of the theoretical resistance vs. experimental resistance ratio. It shows that the model predicts a contribution of 81% for the masonry and 12% for the columns. Then the sum of both values gives a mean value μ_k = 0.93 and coefficient of variation CV_k = 0.13. The walls built from solid clay brick registered the extreme values of the *k*, thus, the walls 23 and 29 register a minimum value *k* = 0.73 while the wall 25 has the maximum value, *k* = 1.29. Annex A4 contains the *k* values for whole walls and Figure 6.7 shows the statistical distribution.

Table 6.1 Statistical parameters of *k*

	V_m / V_{exp}	V_{the} / V_{exp}
Mean value, μ	0.81	0.93
C. of variation, *CV*	0.15	0.13

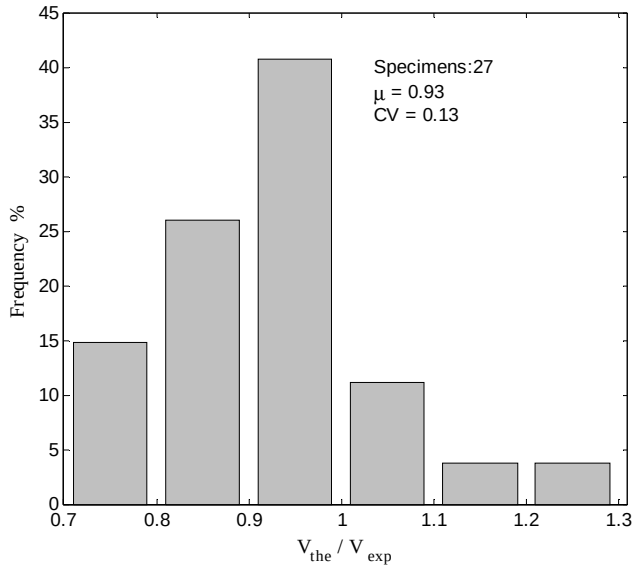

Figure 6.7: Histogram of ratio theoretical resistance vs. experimental resistance

To assess the influence of the heterogeneity of the material, the uncertainty of the mechanical properties and the hypotheses used, it was proposed a normal distribution of error according to Figure 6.8, where can be seen that 89% of the *k* values ranges within the limits $k_{5\%}$ = 0.73

and $k_{95\%}$ = 1.13%. The lognormal and gamma distribution were also used but the results are not satisfactory.

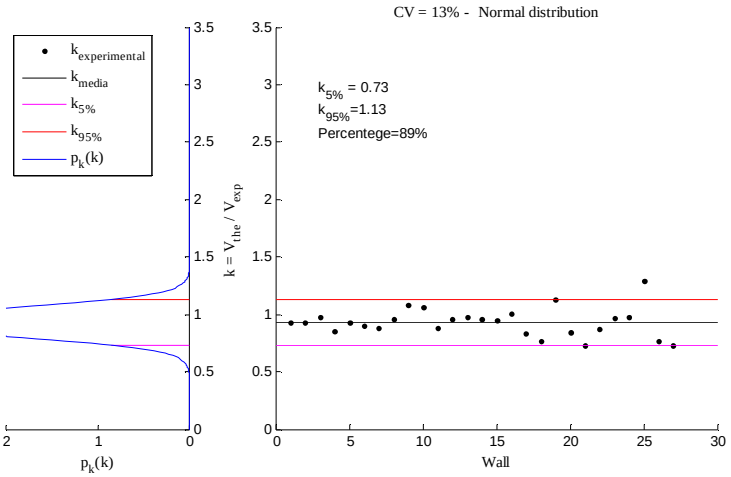

Figure 6.8: Normal distribution of the error model for the ratio *k*

For the walls constructed from hollow concrete blocks, masonry provides 84% of resistance and the columns provide 11% with mean value μ_k = 0.95 and coefficient of variation CV_k = 0.07, Table 6.2. According to Table 6.3, for walls built from lime-cement-blocks, masonry provides 78% of resistance and the concrete columns provide 13% with mean value μ_k = 0.91. Finally, for walls built with solid clay brick, masonry contributes at 80 % and the columns provide 12% to obtain a mean value μ_k = 0.92.

Table 6.2 Statistical parameters of *k* for concrete hollow blocks

Wall	$k = V_m / V_{exp}$	$k = V_{the} / V_{exp}$
Mean value, μ_k	**0.84**	**0.95**
C. of variation, CV_k	0.08	0.07

Table 6.3 Statistical parameters of *k* for cement-lime blocks

Wall	$k = V_m / V_{exp}$	$k = V_{the} / V_{exp}$
Mean value, μ_k	**0.78**	**0.91**

Table 6.4 Statistical parameters of *k* for clay solid bricks

Wall	$k = V_m / V_{exp}$	$k = V_{the} / V_{exp}$
Mean value, μ_k	**0.80**	**0.92**
C. of variation, CV_k	0.06	0.05

In other way, a similar function to normative Equation 6.15 [42][45] can be calculated by using Equations 6.11, 6.17, and 6.18. The resultant Equation 6.19 shows the contribution of vertical load on the total shear strength, where A_m is the cross-sectional horizontal area of the masonry and F_v, which represents the angle of friction of the masonry, is function of the masonry stiffness vs. wall stiffness ratio and the wall geometry. It can be seen that the values of F_v are close to those proposed by the local code [42][45] except for the third type of the units according to Table 6.5.

$$A_m = A_{dm}\, sen\gamma \tag{6.17}$$

$$F_v = f\, sen\gamma cos\gamma \tag{6.18}$$

$$V_m = A_m(v_m^* + F_v\sigma) \tag{6.19}$$

Table 6.5 Coefficient of friction F_v

Walls and kind of units used	F_v in this project	F_v local code
Walls 1 -17, concrete hollow blocks	0.33	0.30
Walls 18-20, cement-lime blocks	0.30	
Walls 21-29, clay solid bricks	0.20	

With respect to the design resistance expressed by Equation 6.15 [45], the mean value for all walls is μ_k = 0.58 as is shown in Table 6.6, it means that the masonry walls have an over-strength equal to 1.72 by considering a factor of strength reduction unit.

Table 6.6 Statistical parameters of *k* according to building local code

Wall	Mean value, μ_k	C. of variation, CV_k
Concrete Hollow Blocks	0.64	0.06
Cement-Lime Blocks	0.58	0.18
Clay Solid bricks	0.52	0.23

6.5 Induced tension failure model

This model assumes the failure pattern caused by induced tension along the wall diagonal, which occurs when the normal stresses caused by the seismic load on the wall diagonal are greater than the tensile strength of masonry according to Figure 6.9a [61][62][97]. This model does not consider the contribution of the columns but it considers the distribution of the vertical load.

The simplified model has the following assumptions:

1. Failure occurs along the wall diagonal, which cracks simultaneously in all length by induced tension effect.

2. Upper beam has infinite flexural stiffness and infinite axial stiffness.

3. Mechanical properties of the columns are similar to those of the masonry.

6.5.1 Masonry wall resistance

The model assumes that the columns and masonry support a fraction of the vertical load in function of the ratio masonry axial stiffness vs. wall axial stiffness according to Equation 6.5. Then the vertical load on the failure surface has two components, one normal component, and other parallel component, Figure 6.9b. The normal force generated by the vertical stress and the force generated by the tensile strength of masonry have the same direction and sense and the sum of these values represent the resistance of the masonry. In other way, the force that cracks the wall is the sum of the tangential force caused by the vertical stress and the component of the seismic load along the wall diagonal. In this way, Equations 6.20 and Equation 6.21 shows the parallel force F_{pd} and the normal force F_{nd} on the failure surface. Applying the equilibrium conditions along the wall diagonal when the resistant forces are equal to the acting forces, one can be evaluated the lateral load V, which generates the diagonal cracking, Equation 6.22.

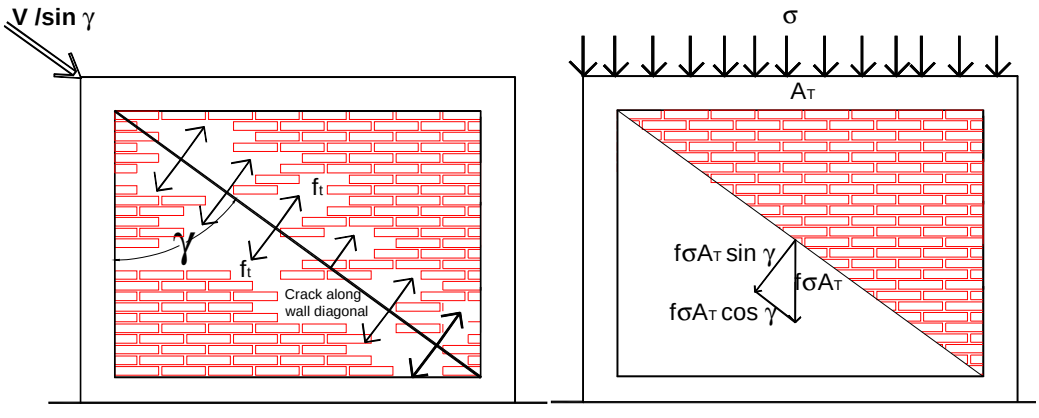

a) b)

Figure 6.9: a) Diagonal cracking by induced tension, b) Influence of the vertical load

$$F_{pd} = V/\sin\gamma + f\,\sigma\,A_T\cos\gamma \tag{6.20}$$

$$F_{nd} = A_d\,f_t + f\,\sigma\,A_T\sin\gamma \tag{6.21}$$

$$V = A_d \left[f_t \sin\gamma + f\sigma \sin^2\gamma \left(\sin\gamma - \cos\gamma \right) \right] \quad (6.22)$$

Where:

F_{pd}	Parallel force to the wall diagonal
F_{nd}	Normal force to the wall diagonal
γ	Diagonal angle with respect to the vertical direction
f	Distribution factor of the vertical load
σ	Vertical stress
A_T	Cross-sectional horizontal area of the wall
A_d	Cross-sectional area of the wall diagonal
f_t	Tensile strength of masonry
V	Lateral resistance of the masonry wall

For walls with ratio $H / L = 1$, the influence of vertical load expressed by the second term of Equation 6.22 becomes equal to zero and it contradicts the experimental evidence. For this reason, it was proposed a fitting function $f(\gamma)=tan(\gamma)$ defined in previous works [61]. Finally, Equation 6.23 evaluates the resistance of the masonry walls.

$$V_{the} = A_d \left[f_t \, f(\gamma) + f\sigma \sin^2\gamma \left(f(\gamma) - \cos\gamma \right) \right] \quad (6.23)$$

6.5.2 Results

The results of the ratio (theoretical resistance vs. experimental resistance), $k = V_{the}/V_{exp}$, are presented in Table A4.7 (Annex A4). It can be seen that the values of k range from 0.75 to 1.95 and the mean value is $\mu_k = 1.17$ and coefficient of variation $CV = 0.23$, Table 6.7. Figure 6.10 shows the histogram of k values of the 27 walls.

To assess the impact of the heterogeneity of the material, the uncertainty of the mechanical properties and the hypotheses used, it was proposed a normal distribution model of error, Figure 6.11, where can be seen that 96% of values of k ranges within $k_{5\%} = 0.73$ and $k_{95\%} = 1.61\%$. In addition, the lognormal and gamma distribution were used but their approximation is not adequate.

Table 6.7 Statistical parameters of *k*

Parameter	$k = V_{the}/ V_{exp}$
Mean value, μ_k	1.17
C. of variation, CV_k	0.23

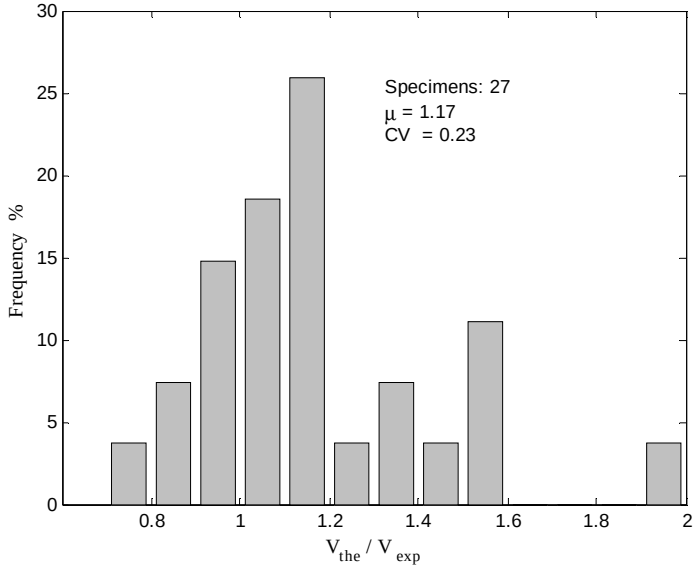

Figure 6.10: Histogram of ratio theoretical resistance vs. experimental resistance

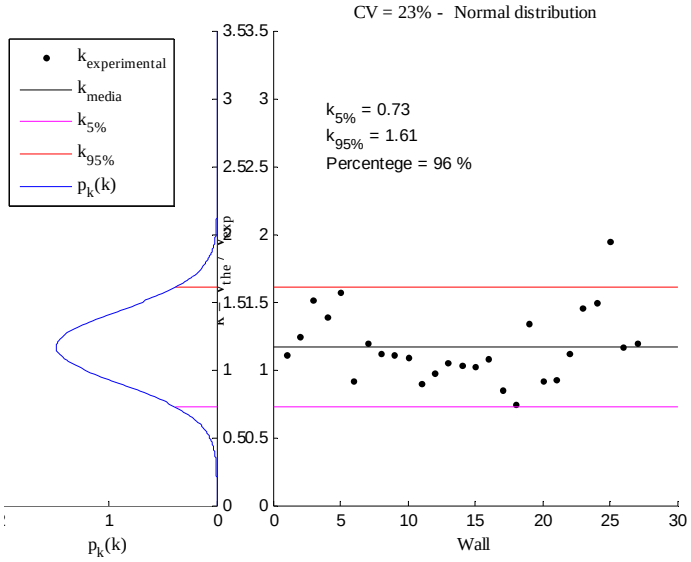

Figure 6.11: Normal distribution of the error model for the ratio *k*

6.6 Comparison of results for both models

Figure 6.12 shows the results of both models. It can be concluded that the shear failure model has better approximation, *CV*= 0.13, whereas the inducted tension failure model has a coefficient of variation *CV* = 0.23. However, both models have similar values of *k* for the

walls 9-18 and both register the maximum value for the wall 25, Figure 6.12. Then, it can be established that the two models are complementary.

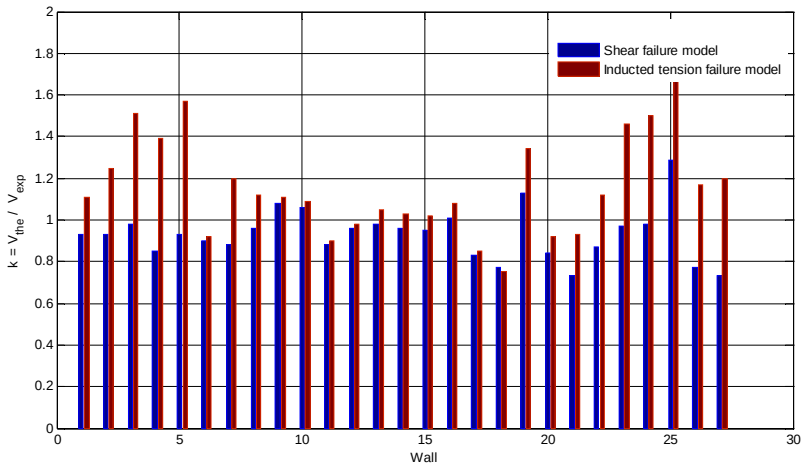

Figure 6.12: Comparison between both models

6.7 Limits of application

An important feature of the proposed models is to limit the value of the masonry resistance expressed by Equation 6.14 and Equation 6.23. Ganz and Thurlimann (1985) and Woodward and Rankin (1985) conducted tests on walls with H / L equal to 1.33, 1.00, 0.67, 0.55, and 0.25. They concluded that the lateral resistance remain constant when σ / f^*_m is greater than 0.25, where f^*_m represents the masonry compressive strength and σ is the acting vertical stress. In this project, the maximum value of v_u / f^*_m = 0.19 corresponds to wall 20 where σ / f^*_m = 0.18 that is less than the experimental limit, Figure 6.12.

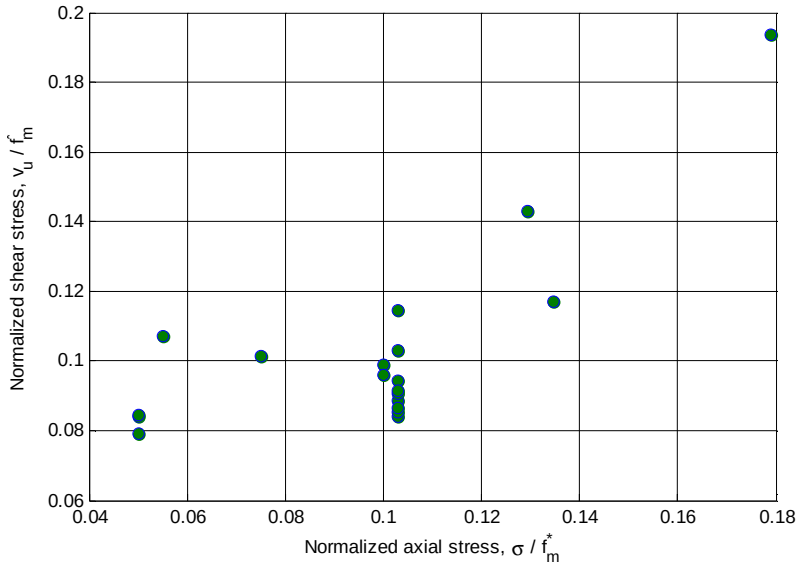

Figure 6.13: Influence of the vertical stress on the shear strength

6.8 Conclusions

The simplified models presented herein were applied to walls with ratio *H/L* ranging from 0.74 to 1.26 with acceptable results, which are independent of the type of load applied and the type of masonry units. The contribution of both masonry and vertical acting load were evaluated in order to assess the resistance of the walls under lateral load, the shear failure model considers also the shear resistance of the columns. The shear strength and the compressive strength of masonry, which are easily obtained by diagonal tension tests of panels and masonry prisms, are the basis for these models.

The shear failure model, based on the assumption that the wall diagonal fails when the shear stress exceeds the diagonal shear strength, is able to assess the wall lateral resistance with good approximation. From the obtained results, it can be seen that the masonry provides 84% of resistances for walls with hollow concrete blocks and 78% for walls with solid clay bricks, whereas the columns provide 11% for both materials. The mean value for whole walls shows that masonry provides 81% of resistance and the columns provide 15%.

The second proposed model assumes that the masonry fails by induced tension along a diagonal (wall diagonal or internal friction angle) when the acting stress are greater than the tensile strength of masonry and it considers the contribution of the vertical load. This model does not assess the shear capacity of columns. One fitting function has been proposed (tan (γ)) with satisfactory results though the coefficient of variation is greater than that of the shear model. The mean value of the ratio theoretical resistance vs. experimental resistance was 1.17

A model of normal distribution error was proposed to consider the variation of mechanical properties, scale factor of specimens, heterogeneity of the materials and simplified assumptions of both models. From the collected results, it can be seen that the shear failure model has better confidence intervals.

Both models avoid the concept of the diagonal compression, which equivalent width is empirical and has no physical meaning. Thus, these models are a useful tool to evaluate the resistance of confined masonry walls. Finally, the author recommends its use for masonry walls where the vertical stress does not exceed 25% of the compressive strength of the masonry in order to avoid the non-linear behavior of the masonry under axial load.

CHAPTER 7

Conclusions and perspectives

This research project is justified by the large use of solid clay bricks in Guerrero State (Mexico) where 70% of the masonry house or masonry buildings are constructed with this material. In this zone, 85% of masonry units are obtained by manual elaboration process that causes up to 40% of variation of its resistance. Furthermore, the design horizontal loads reach 43% of the structures weight.

Besides, most experimental research has been developed in Mexico City, which results have been used to elaborate the Mexico City building code. However, their main parameters have been taken as the basis for other states codes, where the material characteristics, constructive process, and design loads are different. In addition, in the country there are not sufficient structures laboratories to developed full-scale wall tests, which are an excellent tool to evaluate the masonry behavior. Thus, this situation generates uncertainty about the masonry reliability and requires the accurate evaluation of the masonry features.

In order to reduce the seismic vulnerability of masonry structures in Guerrero State, a large experimental program and the use of its results into numerical models to predict the masonry behavior as well as simplified models for assessing the masonry walls resistance have been developed.

Another option to reduce the seismic vulnerability of the masonry structures is to improve the masonry behavior by using different strengthening, which can be placed before or after the earthquake occurrence, or during the construction structure. Then, two types of rehabilitation or retrofit modes have been shown, one placed on the wall surfaces, and the other placed inside the mortar joints. About this last type, there are no available references in Mexico.

With respect to experimental results, the compression strength of masonry units has high coefficient of variation CV =0.43 caused by the manual elaboration process meanwhile the elastic modulus, for which there is no national reference, registers values close to the elastic modulus of the concrete. Then, a mortar denominated type I with compressive strength 75%

greater than the specified strength was used to build all specimens and walls in order to overcome the bad quality of the masonry units. With respect to the mortar joints, their mechanical properties are similar to the referenced values.

The results for the unreinforced panels show the independence of the shear strength with respect to the applied load and level of damage on the perpendicular diagonal. In addition, the failure model associated to the cracking of the units provides the highest resistance. Due to the good quality of the mortar, the rigidity modulus is approximately twice the value referenced and the shear strength is among the highest reported values. For panels with metallic reinforcement within the joints, the shear strength is increased by 20% with respect to resistance of the unreinforced panels and the high adherence between mortar and metallic mesh generates a reduction of the cracking masonry units. Due to the easy constructive process, structural efficiency, and low cost, this material is an adequate alternative to the carbon fibers or fiberglass. In the same way, the masonry prisms registered a modulus of elasticity equal to twice the reported common values.

The test of the wall MUR1 showed an atypical failure pattern with a main quasi-vertical parallel crack close to the left interface masonry-columns while the other direction shows the diagonal cracking until the central area where it drops in vertical direction.

For the wall MUR2, the first load cycles were narrow and short with reduced deformation energy until the first flexural crack, and then two large cycles appears before the maximum load. In this point occurred the cracking at the end of columns with posterior failure of the longitudinal reinforcement. Both diagonals suffered cracking.

The reinforcement of the walls MMR2 and MMR3 fixed the mortar layer and spread the stress over the walls surfaces. Unlike the carbon fibers, this reinforcement has low cost, does not require qualified workmanship, and its structural efficiency is adequate as it can be seen on the repaired wall MMR2, which resistance was similar to that of the wall MUR2. For the wall MMR3 reinforced before the test and with low compressive strength of concrete frame, the failure by compressive effect occurred at the two zones of the load application and prevented the increment of resistance.

For all the walls, the experimental resistance was greater than the theoretical resistance with respect to local code. According to the collected results, the walls had an adequate resistance and the reinforcement guarantees an excellent behavior of the walls under lateral load.

With regard to numerical simulations, the results of the panels' micro-models showed the influence of the finite element mesh. Thus, the modeling with 4 "4-nodes elements" or 16 "4-nodes elements" for each brick provides the best approximation. In addition, the cohesion of the joint is the more important variable on the masonry behavior. Two numerical models of the reinforced panels were able to simulate the experimental behavior while the increase of the resistance and the reduction of the crack width were observed.

A wall similar to those used for the masonry building construction in Guerrero State was analyzed by means of two micro-models. The first considers only a tension behavior of the units while the second considers a combined tension-compression behavior. Although the second model can overestimate the unit resistance because the joint model already supposes the compression behavior of the system, this situation can avoided by using a high compressive strength of the units in order to guarantee its tension failure.

For the first model, the failure numerical pattern related to the maximum lateral load is similar to the failure experimental pattern. However, the slipping of the horizontal joints at the lower left corner and the opening of the masonry-frame interface at the right side of the wall are different for both cases. The model predicts the columns failure and the yield of the lower stirrups. Then, both envelopes are similar until the maximum lateral load. At this point and according to experimental evidence, the units cracking is considerable. Thus, the first model is not able to measure the wall behavior after this point by considering the brittle model proposed for the masonry units. The second model that considers the compression-tension behavior of the masonry units evaluates the behavior of the descendent branch until 12 mm of the horizontal displacement. From the obtained results, it can be concluded that the tension failure associated to the first model has brittle behavior while the second model has ductile behavior.

The spring elements placed on top of the wall allows a coherent resistance envelope and failure pattern even if the tensile strength and the modulus of elasticity of the units were reduced to 63 % of the experimental value and the dilatancy angle was equal to zero.

According to experimental evidence, the masonry walls have quasi-symmetrical behavior under lateral load. Then, the two micro-models assess the resistance envelope and are useful to evaluate the influence of the mechanical properties of each material on the global behavior. However, this type of model is not able to measure the increment of the masonry resistance

caused by the metallic reinforcement mesh placed inside the joints. The two disadvantages of these micro-models are the large number of required parameters and the large quantity of the freedom degrees requiring therefore a large computational effort.

With respect to the macro-model developed herein, the results are adequate by considering its simplicity. Its application to the wall MUR2 is in good agreement with the micro-model. The model applied to other walls built with the same material shows adequate results. Their main advantages with respect to the micro-model are the reduced number of required mechanical parameters for its implementation and the low computational requirements. However, for walls built with lime-cement blocks and hollow concrete blocks, where the masonry behavior and the distribution of the vertical load between frame and masonry may be different, the numerical resistance envelope has some variation with respect to the experimental envelope. For design purposes, where the permissible distortion is 0.25%, the model has adequate results.

The application of the macro-model for a structural system composed by two confined masonry walls and a 3-D structure shows good agreement similar to that obtained with complex models elaborated by the finite element method.

The simplified models applied to walls with ratio Height / Length ranging from 0.74 to 1.26, have acceptable results for all types of the applied load and for all type of masonry units. Its application requires the mechanical properties of the masonry and concrete frame. The results of the shear failure model shows that the masonry provides 81% of resistance and the columns provide 12% with mean ratio (theoretical resistance vs. experimental resistance) equal to 0.93 and coefficient of variation CV = 13%. With respect to ratio of the induced tension model, this mean value is 1.17 and coefficient of variation CV = 23%. A main advantage of both models is to avoid the concept of the diagonal compression, which empirical equivalent width has no “physical meaning”. Finally, the author recommends its use for walls where the vertical stress does not exceed 25% of the compressive strength of the masonry.

The products of this research, which include experimental and numerical results, will be used to evaluate the behavior of confined masonry walls or design masonry building in Guerrero State (Mexico). Thus, it can be concluded that the main objective and goals presented at the beginning of this document have been reached.

The three parts of this research were fundamental and complementary. Then the experimental data (chapter 4) were used to elaborate numerical and simplified models in order to simulate the experimental behavior of the panels or walls (chapter 5 and 6). In addition, the results of the simplified models were useful to check those obtained by means of the numerical models.

Among the principal research activities to be further developed in the near future concerns what follows:

- Evaluate the mechanical properties of the masonry by using other type of mortar
- Carry out tests on masonry walls with metallic reinforcement mesh inside the joints and slender masonry walls under vertical load
- Evaluate the influence of the mechanical properties of the units and the joints on the angle of the failure pattern
- Develop numerical models to analyze the wall behavior reinforced with weld-wire mesh-mortar layer
- Develop numerical models of slender walls
- Extend the application of the simplified models to slender walls

References

[1] ABDOU, L. Modélisation du comportement mécanique des murs en maçonnerie charges dans leur plan. Thèses du Doctorat. Paris: Université de Marne La Vallée, 2005. 173 p.

[2] ABDOU, L., AMI, R., MEFTAH, F. and MEBARKI, A. Experimental investigation of the joint mortar behaviour. *Mechanics Research Communications*, 2006, Vol. 33, p. 370-384

[3] ABDOU, L., AMI, R., MEFTAH, F. and MEBARKI, A. On the sliding behaviour of the brick-mortar interface: An experimental study. *Masonry International Journal*, 2004, Vol. 17 no 3, p. 129-134

[4] AGUILAR, G. Efecto del refuerzo horizontal en el comportamiento de muros de mampostería confinada ante cargas laterales. Tesis de Licenciatura. México: FI-UNAM, 1997. 181 p.

[5] ALCOCER, S. *Personal communication*, 2006

[6] ALCOCER, S., FLORES, L. y SANCHEZ, T. Efecto del empleo de dos tipos de refuerzo horizontal en el comportamiento sísmico de muros de mampostería confinada. En *X Congreso Nacional de Ingeniería Sísmica. Sociedad Mexicana de Ingeniería Sísmica*. México: Editorial SMIS, 1993

[7] ALCOCER, S., MURIA, D. y PEÑA, J. *Comportamiento dinámico de muros de mampostería confinada*. México: II-UNAM, 1999. 119 p.

[8] ALFAIATE, J. and DE ALMEIDA, J. Modelling Discrete Cracking on Masonry Walls. *Masonry International*, 2004, Vol. 17 no 2, p. 83-93

[9] ALVAREZ, J. Estudio analítico sobre el comportamiento no lineal de muros de mampostería confinada con y sin aberturas. Tesis de Maestría. México: FI-UNAM, 2000. 147 p.

[10] ASTM A740-98. Standard Specification for Hardware Cloth (Woven or Welded Galvanized Steel Wire Fabric. ASTM, 2008

[11] ASTM E519-07. Test Method for Diagonal Tension (Shear) in Masonry Assemblages. West Conshohocken: Editorial ASTM, 2007

[12] ANDREAUS, U. Failure Criteria for Masonry Panes under In-Plane Loading. *Journal Structural Engineering*, 1996, Vol. 122, no 1, p. 37-46

[13] ASOCIACION COLOMBIANA DE INGENIERIA SISMICA. *Comportamiento sísmico de muros de mampostería confinada*. Colombia: Universidad de los Andes, Boletín Técnico 45, 1994. 101 p.

[14] ATKINSON, and NOLAND, A proposed failure theory for brick masonry in compression. *In Memory of Third Canadian Masonry Symposium*, 1983, p. 5-1 - 5-17

[15] BARRAGAN, R. Ensaye de una vivienda a escala de dos niveles de mampostería confinada. Tesis de Maestría, México: FI-UNAM, México, 2005. 92 p.

[16] BAZANT, Z. and PLANAS, J. Fracture and size effect in concrete and other quasibrittle material. Edit CRC Press. USA, 1998. 616 p. ISBN 0-8493-8284-X

[17] BLUME, J. and PROULX, J. Shear in grouted brick masonry wall elements. John A. Blume & Associates. California, 1968. 152 p.

[18] BOSILJKOV, V. Micro vs. macro reinforcement of brickwork masonry. *Materials and Structures*, 2006, Vol. 39, p. 235-245.

[19] BRZEV, S. Earthquake-Resistant confined masonry construction [Online]. National Center of Earthquake Engineering. India, 2007. 99 p. ISBN 81-904190-9-9 [Cited 15 april 2009]. Available from World Wide Web: www.nicee.org.

[20] BUSTOS, J. *Estudio del comportamiento sismo-resistente de muros de mampostería encadenada mediante un ensaye en mesa vibratoria* [Online]. Argentina: Universidad Nacional de San Juan. [Cited 8 mars 2009]. Available from World Wide Web:<http://www.ceia.uns.edu.ar/cursos/Sismico/SESION-05-SEMINARIO-modelo-escala.pdf>

[21] CASTILLA, E. y MARINILLI, A. Experiencias recientes en mampostería confinada de bloques de concreto. *Boletín Técnico IMME*, 2003, Vol. 41 no 2-3, p. 28-39

[22] CEN. Methods of tests for masonry –Part 3: Determination of initial shear strength. Brussels, 2002. EN 1052-3

[23] CENTRO NACIONAL DE PREVENCION DE DESASTRES. *Diagnostico de Peligros e Identificación de Riesgos de Desastres en México*. México, 2001, 225 p. ISBN: 970-628-593-8

[24] CHEN ET AL. *Cyclic loading tests of masonry piers –height to width ratio of 1*. California: USA. Report no. UCB/EERC-78/28, 1978. 197 p.

[25] CHOPRA, K. Dynamics of structures. Edit: Prentice-Hall International, New Jersey, Second edition, 2000. 844 p. ISBN 0130869732

[26] COMISION FEDERAL DE ELECTRICIDAD. Manual de diseño de Obras Civiles. Diseño por sismo. CF3-93, 1993.

[27] CONTROLS. Manual de operación del Laboratorio de estructuras de la UAG. México, 2005

[28] CORAL, M. Revisión de algunas de las hipótesis del método simplificado de análisis sísmico para muros de mampostería confinada. Tesis de Maestría, México: FI-UNAM, México, 2004. 92 p.

[29] CRISAFULLI, F., CARR, A., and PARK, R. Analytical modelling of infilled frame structures- A General overview. *Bulletin of the New Zealand for Earthquake Engineering*, 2000, Vol. 33, no 1.

[30] CRISFIELD, M. Non-linear finite element. Analysis of solids and structures. West Sussex, England. Edit: John Wiley & Sons Ltd, 2003. 345 p. ISBN 0471 97059 X

[31] CRUZ, J. Étude des murs de contreventement en maçonnerie d'éléments de terre cuite. Thèse doctorale. Paris : Université de Marné la-Vallée, 2002.

[32] DHANASEKAR, M., PAGE, A. and KLEEMAN, P. The failure of brick masonry under biaxial stress. Proc. Intsn. Of Civ. Engrs. London, England. Part 2, No 79, 1985. p 295-313

[33] DEACERO. Manual Técnico DEACERO. Edit: DEACERO SA DE CV. ISBN 970-9090-00-3.

[34] DEACERO. Malla hexagonal [Online]. [Cited 2 September 2009]. Available from World Wide Web: <http:/www.deacero.com/Web/ Deacero/Esp/Productos/ MallaHexagonal.asp?Op1=1&op2=MallaHexagonal >

[35] DEACERO. Criba grano de plata [Online]. [Cited 17 September 2007]. Available from World Wide Web: http://deacero.com/Web/Deacero/Esp/Productos/CribaGranoDePlata. asp?Op1=1&op2=CribaGranoDePlata

[36] FLORES, L. Estudio analítico de estructuras de mampostería confinada. Tesis de Licenciatura. México, FI-UNAM, 1995. 106 p.

[37] GABOR, A., BENNANI, A., JACQUELIN, E, and LEBON, F. Modelling approaches of the in-plane shear behaviour of unreinforced and FRP strengthened masonry panels. *Composite Structures*, 2006, Vol. 74, p. 277-288.

[38] GABOR, A., FERRIER, E., JACQUELIN, E. and HAMEILN, P. Analysis an modelling of the in-plane shear behaviour of hollow brick masonry panels. *Construction and Building Materials*, 2006, Vol. 20 no 5, p. 308-321

[39] GANZ, H., and THULIRMANN, B. *Tests on masonry wall subjected to axial load and shear*. Institute fur Baustatik and Konstruktion, 1985.

[40] GARCIA, H. and YAMIN, L. A review of masonry construction in Colombia. Masonry in the Americas, *ACI Publication SP-147*, American Concrete Institute, Detroit, 1994. p. 283-305

[41] GIAMBANCO, G., RIZZO, S., and SPALLINO, R. Numerical analysis of masonry structures via interface models. *Computer methods in applied mechanics and engineering*, 2001, Vol. 190, no 49, p. 6493-6511

[42] GOBIERNO DEL DISTRITO FEDERAL. Normas Técnicas Complementarias para Diseño y Construcción de Estructuras de Mampostería. Gaceta Oficial del Distrito Federal, 2004, Vol. Tomo I no 103-BIS, p. 4-53

[43] GOBIERNO DEL DISTRITO FEDERAL. Normas Técnicas Complementarias para Diseño por Sismo. Gaceta Oficial del Distrito Federal, 2004, Vol. Tomo I no 103-BIS.

[44] GOBIERNO DEL DISTRITO FEDERAL. Normas Técnicas Complementarias para Diseño y Construcción de Estructuras de Concreto. Gaceta Oficial del Distrito Federal, 2004, Vol. Tomo I no 103-BIS, p. 88-194

[45] GOBIERNO DEL ESTADO DE GUERRERO. Normas Técnicas Complementarias al Reglamento de Construcciones. Diseño y construcción de estructuras de mampostería. Diario Oficial del Estado de Guerrero, 1989. No 92

[46] GOBIERNO DEL ESTADO DE GUERRERO. Normas Técnicas Complementarias para Diseño por sismos. Diario Oficial del Estado de Guerrero, 1989. No 80

[47] GOBIERNO DEL ESTADO DE GUERRERO. Reglamento de construcción para los municipios del estado de Guerrero. Diario Oficial del Estado de Guerrero, 1994. No 37.

[48] HERNANDEZ, E. y URZUA, D. Pruebas dinámicas de resistencia sísmica de muros de mampostería confinada construidos con materiales pumíticos. *En XIII Congreso Nacional de Ingeniería Estructural*. Sociedad Mexicana de Ingeniería Estructural. Puebla: Editorial SMIE, 2002. p. 337-34

[49] INSTITUTO NACIONAL DE ESTADISTICA Y GEOGRAFIA. *II Conteo Nacional de Población 2005*. México, 2005.

[50] ISHIBASHI, K., and KASTUMATA, H. *A study on nonlinear finite element analysis of confined masonry walls*. México: CENAPRED, CI no 15, 1994. 58 p.

[51] JORGE, A. Estudio del mejoramiento de las propiedades mecánicas del tabique de barro recocido empleado en la mampostería. Tesis de Maestría. Chilpancingo: UAI-UAG, 2005.

[52] KENT, D. and PARK, R. Flexural members with confined concrete. *ASCE Journal*, 1971, Vol. 97, St 7

[53] KOITER, W. Stress-strain relation, uniqueness and variations theorems for elastic-plastic materials with a singular yield surface. *Q. Appl. Mech. 11*, p. 350-354, 1953

[54] KOSTOGLODOV, K. Intersismic deformations in the Guerrero seismic gap. [Online]. [Cited 2 September 2009]. Available from World Wide Web: <http://tlacaelel.igeofcu.unam.mx/~vladimir/>

[55] KUPFER, H. and GERSTLE, D. Behavior of concrete under biaxial stress. *Journal of Engineering Mechanics Division*, 1973, Vol. 99, no EM4, p. 853 – 866.

[56] LOFTI, H. and SHING, B. Interface model applied to fracture of masonry structures. *Journal of Structural Engineering*, 1994, Vol. 120, no 1, p. 63 – 80

[57] LOURENCO, P. Computational strategies for masonry structures. Ph. Doctoral theses. Delft University of Technology, 1996. ISBN 90-407-1221-2. 222 p.

[58] LOURENCO, P. Sensitivity analysis of masonry structures [Online].[Cited 2 Mars 2009]. Available from World Wide Web: <http://www.csarmento. uminho.pt/docs/ncr/de_civil/1998_Lourenco1.pdf, 2008>

[59] LOURENCO, P., and ROTS, J. Multisurface interface model for analysis masonry structures. *Journal of Engineering Mechanics*, 1997, Vol. 123 no. 7, p. 660-668

[60] MADAN, A., REINHORN, M., MANDER, J. and VALLES, R. Modelling of masonry infill panels for structural analysis. *Journal of Structural Engineering*, 1997, Vol. 123, no 10, p. 1295 – 1302

[61] MEBARKI, A., BUI, Q., AMI, R., DELMOTTE, P. and SANCHEZ, S. A simplified mechanical model to asses the bearing capacity of masonry walls: Theory and experimental validation. *Construction and Building Materials*, 2009. ISSN 0950-0618.Vol. 23, no 2, p. 1109 – 1117.

[62] MEBARKI, A., BUI, Q., SANCHEZ, S., AMI, R. and DELMOTTE, P. Comportement mécanique de murs de contreventement en maçonneries: Modèle de traction induite. Chapitre 4. Livre: Risques Naturels et Technologiques. Paris, France. Edit: Presses de l'école nationale des ponts et chaussées, 2008. ISBN 978- 2- 85978-436-2

[63] MELI, R., and ALCOCER, S. Implementation of structural earthquake-disaster mitigation programs in developing countries. *Natural Hazards Review. ASCE*, 2004, Vol. 5, No 1, p. 29-39

[64] MELI, R. y HERNANDEZ, O. *Propiedades de piezas para mampostería producidas en el Distrito Federal*. México: II-UNAM, 1971. 49 p.

[65] MELI, R. y REYES, A. *Propiedades mecánicas de la mampostería*. México: II-UNAM, 1971. 24 p.

[66] MELI, R. y SALGADO, G. *Comportamiento de muros de mampostería sujetos a carga lateral*. México: Editorial II-UNAM, 1969. 102 p.

[67] MERABI, A. and SHING, B. Finite element modeling of masonry-infilled RC frames. *Journal of Structural Engineering*, 1997, Vol. 123, no 5, p. 604 – 613

[68] MINDUR. Norma de Estructura de Concreto Armado para Edificaciones. Análisis y diseño. Covenin-Mindur 1753, 1987.

[69] NAVEZ, A. Estudio teórico-experimental de costos de estructuras de mampostería en zonas sísmicas. Tesis de Maestría. Chilpancingo: UAI- UAG, 2002. 40 p.

[70] ORGANISMO NACIONAL DE NORMALIZACION Y CERTIFICACION DE LA CONSTRUCCION Y EDIFICACION. Industria de la construcción – Concreto hidráulico para uso estructural. NMX C-403-ONNCCE-2004.

[71] ORGANISMO NACIONAL DE NORMALIZACION Y CERTIFICACION DE LA CONSTRUCCION Y EDIFICACION. Industria de la construcción – Bloques, tabiques o ladrillos y tabicones para uso estructural – Especificaciones y métodos de prueba. NMX C-404-ONNCCE-2005.

[72] ORGANISMO NACIONAL DE NORMALIZACION Y CERTIFICACION DE LA CONSTRUCCION Y EDIFICACION. Industria de la construcción – Concreto – Especificaciones. NMX C-155-ONNCCE-2004.

[73] ORGANISMO NACIONAL DE NORMALIZACION Y CERTIFICACION DE LA CONSTRUCCION Y EDIFICACION. Industria de la construcción – Bloques, tabiques o ladrillos y tabicones para uso estructural – Resistencia a la compresión- Método de prueba. NMX C-036-ONNCCE-2004

[74] ORGANISMO NACIONAL DE NORMALIZACION Y CERTIFICACION DE LA CONSTRUCCION Y EDIFICACION. Industria de la construcción – Bloques, ladrillos o tabiques y tabicones – Determinación de la absorción de agua y absorción inicial de agua. NMX C-037-ONNCCE-2005

[75] ORGANISMO NACIONAL DE NORMALIZACION Y CERTIFICACION DE LA CONSTRUCCION Y EDIFICACION. Determinación de la resistencia a compresión diagonal y rigidez a cortante y la resistencia a compresión y modulo de elasticidad de pilas de mampostería de barro y de concreto- Método de prueba. PROYNMX –S/N-ONNCCE-2005

[76] ORGANISMO NACIONAL DE NORMALIZACION Y CERTIFICACION DE LA CONSTRUCCION Y EDIFICACION. Industria de la construcción – Cemento – Determinación de la resistencia a la compresión de cementantes hidráulicos. NMX C-061-ONNCCE-2001

[77] ORGANISMO NACIONAL DE NORMALIZACION Y CERTIFICACION DE LA CONSTRUCCION Y EDIFICACION. Industria de la construcción – Concreto – Resistencia a la tensión por compresión diametral de cilindros de concreto. NMX C-163-ONNCCE-1997

[78] ORGANISMO NACIONAL DE NORMALIZACION Y CERTIFICACION DE LA CONSTRUCCION Y EDIFICACION. Industria de la Construcción – Concreto- Determinación de la resistencia a compresión de cilindros de concreto – Método de prueba. NMX-C-083-ONNCCE-2002

[79] ORGANISMO NACIONAL DE NORMALIZACION Y CERTIFICACION DE LA CONSTRUCCION Y EDIFICACION. Industria de la Construcción – Concreto- Cabeceo de especimenes. NMX-C-109-ONNCCE-2004

[80] ORGANISMO NACIONAL DE NORMALIZACION Y CERTIFICACION DE LA CONSTRUCCION Y EDIFICACION. Industria de la Construcción – Concreto sometido a compresión – Determinación del modulo elástico y relación de Poisson. NMX-C-128-1997-ONNCCE

[81] ORGANISMO NACIONAL DE NORMALIZACION Y CERTIFICACION DE LA CONSTRUCCION Y EDIFICACION. Varillas corrugadas y lisas de acero procedentes de riel, para refuerzo de concreto. NMX-B-018-ONNCCE-1988

[82] ORGANISMO NACIONAL DE NORMALIZACION Y CERTIFICACION DE LA CONSTRUCCION Y EDIFICACION. Varillas corrugadas y lisas de acero procedentes de eje, para refuerzo de concreto. NMX-B-032-ONNCCE-1988

[83] ORGANISMO NACIONAL DE NORMALIZACION Y CERTIFICACION DE LA CONSTRUCCION Y EDIFICACION. Varilla corrugada de acero proveniente de lingote y palanquilla para refuerzo del concreto- Especificaciones y métodos de prueba. NMX-C-407-ONNCCE-2006

[84] PARK, R. and PAULAY, T. Reinforced concrete structures. Edit: John Wiley & Sons, 1989, Second edition. 850 p. ISBN 0471508047.

[85] PAULAY, T., and PRIESTLEY, J. Seismic design of reinforced concrete and masonry buildings. NY, USA: Editorial John Wiley & Sons, 1992. 768 p. ISBN: 97-0-471-54915-4.

[86] PEREZ, J., FLORES, F., y CRUZ, R. Muros de mampostería con bloques multiperforados de concreto. En *XIV Congreso Nacional de Ingeniería Estructural. Sociedad Mexicana de Ingeniería Estructural*. Acapulco: Editorial SME, 2004

[87] PINEDA, J. Comportamiento ante cargas laterales de muros de mampostería confinada reforzados con malla electrosoldada. Tesis de Maestría. México: FI-UNAM, 1996. 172 p.

[88] PUGLISI, M. Modelo del comportamiento de la mampostería confinada basado en la teoría del daño. Tesis Doctoral. Mérida: Universidad de Los Andes, 2007. 133 p.

[89] PURDUE UNIVERSITY. Behavior of reinforced concrete members CE676. School of Civil Engineering, Indiana, USA. 2001

[90] RAIJMAKERS, T. and VERMELTFOORT, A. Deformation controlled meso shear test of masonry piers. Rep. B-92-1156, TNO-BOUW/TU Eindhoven, Build. and Constr. Res. Netherland, 1992.

[91] RAMIREZ, H., y CARREON, H. Reparación y refuerzo por medio de flejes de muros de mampostería para vivienda de bajo costo: Estudio experimental. *Rev. Int. De Desastres Naturales, Accidentes e Infraestructura Civil*, 2003, Vol. 3 no 2, p. 143-156

[92] RODRIGUEZ, M. Confined Masonry Construccion[Online]. [Cited 6 April 2009]. Available from World Wibe Web: <www. world-housing.net>

[93] RUIZ, J. Reparación y refuerzo de una estructura tridimensional de dos niveles a escala natural. Tesis de maestría. México: FI-UNAM, 1995. 251 p.

[94] RUSSO, S. Effect of FRP on the shear strength of masonry. *Masonry International*, 2005, Vol. 18 no 1, p. 1-10

[95] SALGADO, J. Propuesta de reforzamiento de muros de mampostería en zonas sísmicas. Tesis de Licenciatura. Chilpancingo: UAI-UAG, 2000. 127 p.

[96] SANCHEZ, T., ALCOCER, S. y FLORES, L. Estudio experimental sobre una estructura de mampostería confinada tridimensional, construida a escala natural y sujeta a cargas laterales. En *X Congreso Nacional de Ingeniería Estructural*. Sociedad Mexicana de Ingeniería Estructural: Editorial SMIE, 1996, p. 909 - 918

[97] SANCHEZ, S. and MEBARKI, A. A Simplified Model of Shear-Capacity in Confined Masonry Walls. In *Proceedings of the Eighth International Conference on Computational Structures Technology.* Tenerife: Edit H. TOPPING, 2006. ISBN-10 1-905088-07-8 p. 210-218.

[98] SANCHEZ, S. y MEBARKI, A. Método semi-empírico para estimar la resistencia lateral en muros de mampostería confinada. *Revista de la Sociedad Mexicana de Ingeniería Sísmica*, 2009. ISSN – 0185- 092X. Vol. 80, p. 113 - 127

[99] SANCHEZ, S., MEBARKI, A., SOTO, A. y ARROYO, R. Propiedades mecánicas de muretes y pilas con refuerzo metálico. En *XVI Congreso Nacional de Ingeniería Sísmica*. Sociedad Mexicana de Ingeniería Sísmica. Ixtapa-Zihuatanejo: Editorial SMIS, 2007

[100] SCOTT, B., PARK, R., and PRIESTLEY, M. Stress-strain behavior of concrete confined by overlapping hoops at low and high strain rates. ACI Journal, Vol 79, no 1, 1982, p. 13-27

[101] SMYROU, E. Implementation and verification of a masonry panel model for nonlinear dynamic analysis of infilled RC frames. Master Thesis. European School for advanced studies in reduction of seismic risk, Italy, 2006. 108 p.

[102] TNO DIANA. Diana Finite Element Analysis. User's manual Material Library. The Netherlands, 2008. 578 p.

[103] TNO DIANA. Diana Finite Element Analysis. User's manual. Getting Started. The Netherlands, 2008. 144 p.

[104] TNO DIANA. Diana Finite Element Analysis. User's manual. Element Library. The Netherlands, 2008. 666 p.

[105] TODD, D. Let's clean up our language. Editorial: EERI Newsletter, 1994. Vol. 28 (8), p. 3

[106] TOMAZEVIC, M. Earthquake-resistant design of masonry buildings. London, UK: Editorial Imperial College Press, 2000. 268 p. ISBN: 1-86094-066-8.

[107] TREVIÑO, E., ALCOCER, S., FLORES, L., LARRUA, R., ZARATE, J. y GALLEGOS, L. Investigación experimental del comportamiento de muros de mampostería confinada de bloques de concreto sometidos a cargas laterales cíclicas reversibles reforzados con acero de grados 60 y 42. En *XIV Congreso Nacional de Ingeniería Estructural. Sociedad Mexicana de Ingeniería Estructural*. Acapulco: Editorial SME, 2004

[108] UNIDAD ACADEMICA DE INGENIERIA-UAG. Propiedades mecánicas de tabique rojo recocido. Chilpancingo, México 2008.

[109] VAN ZIJL G. Computational modeling of Masonry Creep and Shrinkage. PhD Thesis, Delft University of Technology, 2000. 184 p.

[110] VASCONCELOS, D. y SANCHEZ, T. *Edificaciones de mampostería para vivienda. Capítulo 2. Materiales.* DF, México: Editorial Fundación ICA, 1999. p. 25 -27. ISBN 968-7508 65-5.

[111] VERMELTFOORT, A., RAIJMAKERS, T. and JANSSEN, H. Shear tests on masonry walls. *Proc., 6th North Am. Masonry Conf.*, Philadelphia, Pa. p 1183-1193, 1993.

[112] WOODWARD, K. and RANKIN, F. *Influence of block and mortar strength on shear resistance on concrete block masonry walls.* National Bureau of Standards, Report No NBSIR 85-3143, 1985

[113] YOKEL, F. and FATTAL, J. Failure hypothesis for masonry walls. *Journal of the Structural Division*, 1976, Vol. Division Proc of the ASCE (ST3) no 102, p. 515-532

[114] ZUÑIGA, O. y TERAN, A. Evaluación basada en desplazamientos de edificaciones de mampostería confinada. *Revista de Ingeniería Sísmica*, 2008, Vol. 79, p. 25 -48

[115] ZHU, M. and CHUNG, D. Improving brick-mortar bond strength by the addition of carbon fibers to the mortar. *Cement and Concrete Research*, 1997, Vol. 27, No 12, p. 1829 - 1839

ANNEX A1

Additional tests

This annex contains experimental data used to elaborate the masonry numerical models presented in chapters 5 and 6. In addition, the results of the non-standardized test as tensile strength on metallic reinforcement mesh, tensile strength on masonry circular specimens and tensile strength on circular specimen of the units are presented. This experimental results are useful to propose values of those mechanical properties that have not national references.

A1.1 Compressive strength of concrete

Twenty-three concrete cylinders during the construction of confined masonry walls MUR1 and MUR2/MMR2 were elaborated to control the concrete quality. Concrete cylinders were tested under monotonic load according to specifications [78][79][80]. The mean value of compressive strength was f'_c= 24 MPa with coefficient of variation CV = 0.08, Figure A1.1 and Table A1.1. A set of nine specimens was instrumented to measure the normal stress vs. normal strain relationship, then the mean value of the modulus of elasticity was E_c = 24506 MPa and the Poisson' ratio was ν = 0.17. Experimental data is fitted by means of Equation A1.3 [102] to define the compressive strength associated to normal strain defined by Equation A1.1 and Equation A1.2. Figure A1.2 shows the experimental curves and the proposed equation.

Table A1.1 Mechanical properties of concrete for walls MUR1 and MUR2/MMR2

Statistical experimental values	f'_c, [MPa]	ε_c	E_c, [MPa]	ν
Mean value, μ	24.0	0.0018	24506	0.17
Coefficient of variation, CV	0.08	0.19	0.18	

$$\varepsilon_1 = \frac{f_c^{'}}{3E_c} \qquad \text{(A1.1)}$$

$$\varepsilon_c = \frac{5 f_c^{'}}{3E_c} \tag{A1.2}$$

$$f_c = \begin{cases} f_c^{'} \dfrac{\varepsilon}{3\varepsilon_1} & if\ \varepsilon_1 < \varepsilon \leq 0 \\ f_c^{'} \left[\dfrac{1}{3} + \dfrac{4}{3}\left(\dfrac{\varepsilon - \varepsilon_1}{\varepsilon_c - \varepsilon_1} \right) - \dfrac{2}{3}\left(\dfrac{\varepsilon - \varepsilon_1}{\varepsilon_c - \varepsilon_1} \right)^2 \right] & if\ \varepsilon_c < \varepsilon \leq \varepsilon_1 \end{cases} \tag{A1.3}$$

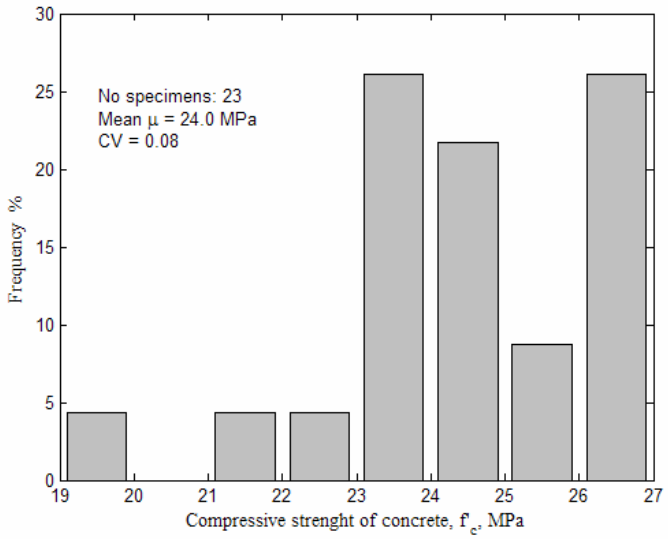

Figure A1.1 Histogram of compressive strength

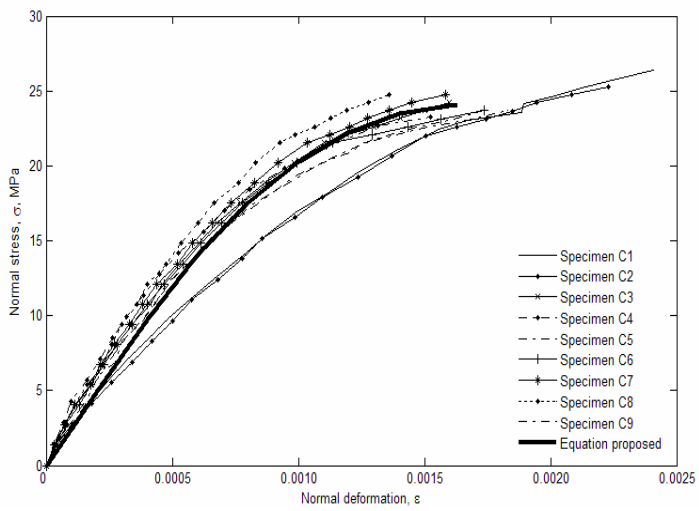

Figure A1.2. Normal strain vs. normal stress relationship of concrete

A1.2 Tensile strength of longitudinal reinforcement

In order to propose a mathematical expression to build the numerical model, tests of tensile strength of longitudinal reinforcement was applied. Three specimens similar to those used in concrete columns of the walls were tested according to local specifications [81][82]. Table

A1.2 shows the mechanical properties while Equations A1.4 - A1.6 [89] were used to obtain the mean curve, Figure A1.3.

Table A1.2 Mechanical properties of longitudinal reinforcement

f_y, [MPa]	f_{su}, [MPa]	ε_y	ε_{su}
464.7	721.5	0.0026	0.0107
ε_{sh}	r	m	E_s, [MPa]
0.1008	0.090	122.17	177548.7

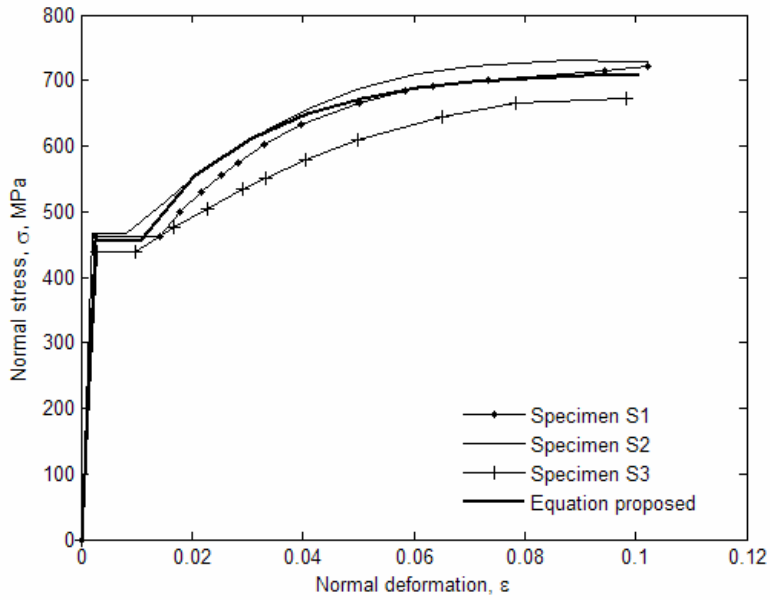

Figure A1.3. Normal strain vs. normal stress relationship of longitudinal reinforcement

$$r=\varepsilon_{su}-\varepsilon_{sh} \tag{A1.4}$$

$$m=\frac{\left(f_{su}/f_y\right)(30r+1)^2-60r-1}{15r^2} \tag{A1.5}$$

$$f_s=\begin{cases} E_s\varepsilon_s & if\ \varepsilon_s\le\varepsilon_y \\ f_y & if\ \ \varepsilon_y\le\varepsilon_s\le\varepsilon_{sh} \\ f_y\left[\dfrac{m\left(\varepsilon_s-\varepsilon_{sh}\right)+2}{60\left(\varepsilon_s-\varepsilon_{sh}\right)+2}+\dfrac{\left(\varepsilon_s-\varepsilon_{sh}\right)(60-m)}{2(30r+1)^2}\right] & if\ \ \varepsilon_{sh}\le\varepsilon_s\le\varepsilon_{su} \end{cases} \tag{A1.6}$$

A1.2 Non-standardized tests

A1.2.1 Tensile strength of metallic reinforcement mesh

A set of nine specimens of metallic reinforcement mesh fabricated according to standard ASTM 740-98[10] was tested to measure its tensile strength as is shown in Figure A1.4. The mean value of the ultimate stress was f_{su} = 379.5 MPa, its coefficient of variation CV = 0.10 and mean axial strain ε_u = 0.005. Figure A1.5 shows the axial stress vs. axial strain relationship of four tests. The maximum force is F_{ult} = 2.20 KN. Table A1.3 summarizes the mechanical properties.

Table A1.3 Mechanical properties of metallic reinforcement mesh

f_y, [MPa]	f_{su}, [MPa]	ε_y	ε_{su}	E_s [MPa]
126.5	379.5	0.0004	0.005	300, 000

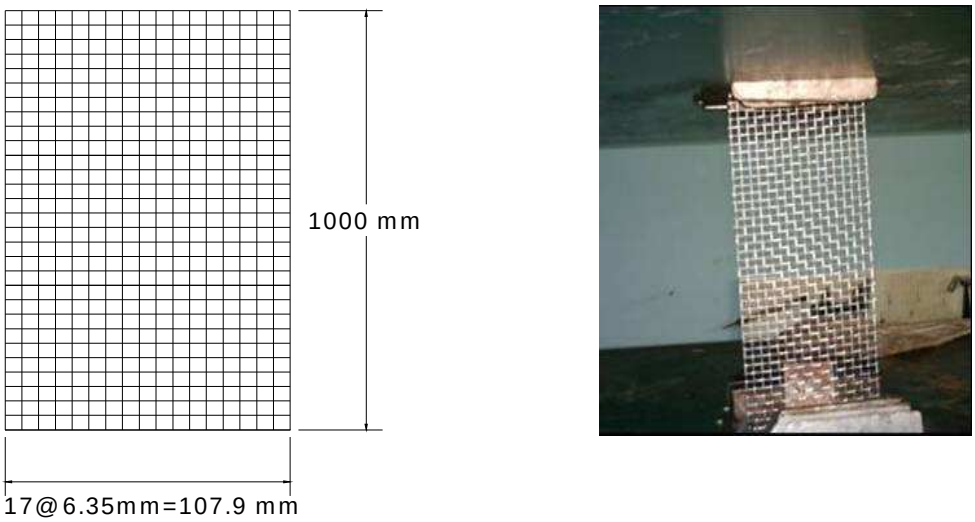

Figure A1.4: Metallic reinforcement specimen and experimental setup on tension test

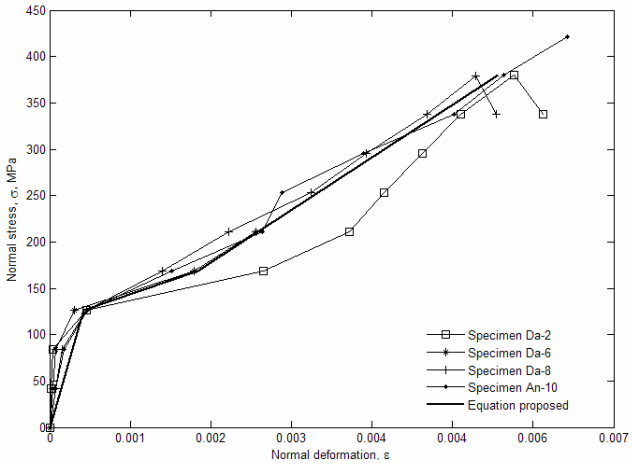

Figure A1.5: Axial stress vs. axial strain relationship of metallic reinforcement mesh

A1.2.2 Tensile strength on masonry circular specimen

In order to evaluate the tensile strength of masonry were tested four circular specimens 0.41 m diameter, the mortar, units and workmanship are similar to those used to build the panels and walls. The load was applied along its vertical diameter and the tensile stress is valued according to Equation A1.7 [77], where l is the length of specimen and d is the diameter. Even if there are not specifications to develop it, the test generates useful information about the masonry behavior. As can seen in Figure A1.6, the specimen CM4 showed sliding of the joint and its tensile strength was less than to that evaluated in the other specimens, the specimen CM3 showed the main cracking along the load axis and generated the failure of masonry units. Table A1.4 shows the results which mean value is f_t = 0.52 MPa without to take account the specimen CM4, the last column describes the failure mode, where TD means failure by diagonal cracking and SJ means failure by sliding joint.

Table A1.4 Tensile strength of masonry on circular specimens

Specimen	f_t, [MPa]	Failure mode
CM1	0.56	TD
CM2	0.51	TD, SJ
CM3	0.50	TD
CM4	0.15	SJ
CM5	0.50	TD

a) b)

Figure A1.6: Failure of circular masonry specimens, a) by diagonal cracking of the masonry units, b) by slipping of the joint

$$f_t = 20P/\pi ld \qquad \text{(A1.7)}$$

It is possible to define the ratio between the shear strength (incise 4.4) and the tensile strength (Table A1.4) by means of Equation A1.8, which is similar to those presented by Yokel and Fattal (1976), Meli and Salgado (1969), and Blume and Proulx (1968).

$$f_t = 0.73\tau \qquad \text{(A1.8)}$$

A1.2.3 Tensile strength on masonry units circular specimen

To evaluate the tensile strength of masonry units were tested thirty circular specimens 70 mm diameter obtained of masonry units, Figure A1.7a. Although the load plane of the test is normal to the true load plane on the wall, Equation A1.7 computes the tensile stress by considering an isotropic behavior of the masonry units. Figure A1.7b shows a typical pattern of splitting after the load application, the mean values was f_{tp} = 0.40 MPa and coefficient of variation CV = 28 %.

a) b)

Figure A1.7: a) Cut of circular specimen brick, b) Splitting failure induced by vertical load application

ANNEX A2

Parameters to define the behavior of masonry walls

Required parameters to assess the walls behavior and load histories applied to the masonry walls, chapter 4, are presented on next paragraphs.

A2.1. Parameters to define the wall behavior

A2.1.1 Distortion

With regard to Figure A2.1 and according to Aguilar (1997), the displacement caused by the lateral load is the sum of the shear displacement D_C and flexion displacement D_B expressed by Equation A2.1 and measured by the LDVT C20 and C21, Figure 4.20. Similarly, Equation A2.2 evaluates the distortion R, where $H_{C20\text{-}C21}$ is the height control. The variable R is the sum of the flexion distortion R_B and shear distortion R_C according to Equation A2.3. In addition, Equation A2.4 evaluates the shear distortion according to mechanics of materials [24], where D_{C24} and D_{C25} are the control lengths of the wall diagonals, δ_{C24} and δ_{C25} are displacements measured for the LDVT C24 and C25(see Figure 4.20), L is the wall length and H is the wall height. Finally, Equation A2.5 expresses the flexion distortion R_B.

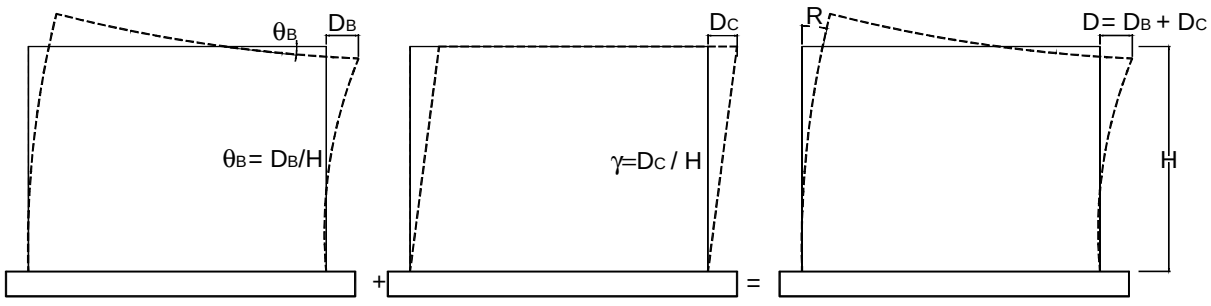

Figure A2.1: Components of displacement and distortion

$$D = D_B + D_C \tag{A2.1}$$

$$R = D / H_{C20-C21} \tag{A2.2}$$

$$R = R_B + R_C \tag{A2.3}$$

$$R_C = \left(\delta_{C24}/D_{C24} + \delta_{C25}/D_{C25}\right)/2LH \tag{A2.4}$$

$$R_B = R - R_C \tag{A2.5}$$

A2.1.2 Stiffness

Another important parameter is the cycle stiffness. This parameter expressed by Equation A2.6 [4] represents the slope between two finals points of a load cycle. Herein K is the stiffness of semi cycle, V^+ is maximum shear load for the positive cycle, V^- is the maximum shear load for the negative semi cycle, R^+ and R^+ are the rotations associated, Figure A2.2a.

$$K = \left(V^+ + \left|V^-\right|\right)/\left(R^+ + \left|R^-\right|\right) \tag{A2.6}$$

A2.1.3 Dissipated energy

Dissipated energy is the sum of the surface of *n*-segments of the load cycle, Figure A2.2b. Equation A2.7 [4] evaluates the energy in each segment, where E_i is the segment energy *i*, V_1, V_2, V_3, V_4, D_2, and D_1 are the values of lateral load and displacement to define the increment *i.*

$$E_i = \left[\left(V_1 + V_2\right) - \left(V_3 + V_4\right)\right]\left(D_2 - D_1\right)/2 \tag{A2.7}$$

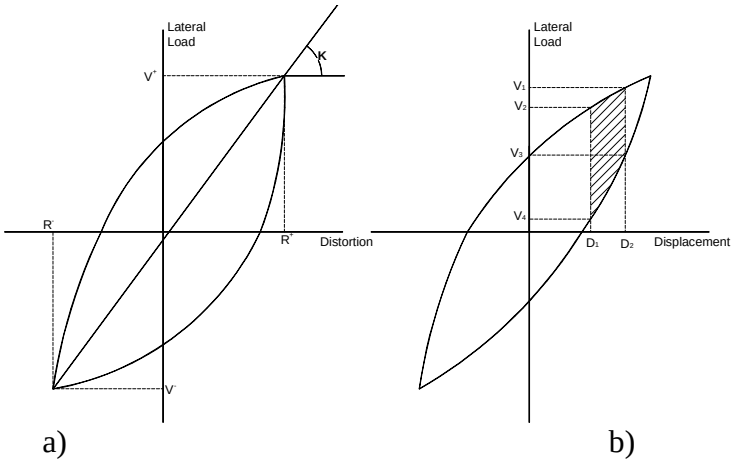

a) b)

Figure A2.2: a) Definition of cycle stiffness, b) Cumulative energy of *i*-segment

A2.1.4 Ductility

According to Park and Paulay (1989), the ductility is the ratio ultimate displacement vs. yield displacement. The authors propose an elastic-plastic perfect model with a plateau defined by a

force equal to 85% of the maximum load, Figure A2.3a. The first point of the plateau is defined by the line that intersects the experimental curve to a value equal to 75% of the maximum load of the proposed model and the intersection of the plateau with the experimental curve defines the ultimate displacement. Equation A2.7 computes the ductility.

$$\mu = R_u / R_y \qquad \text{(A2.7)}$$

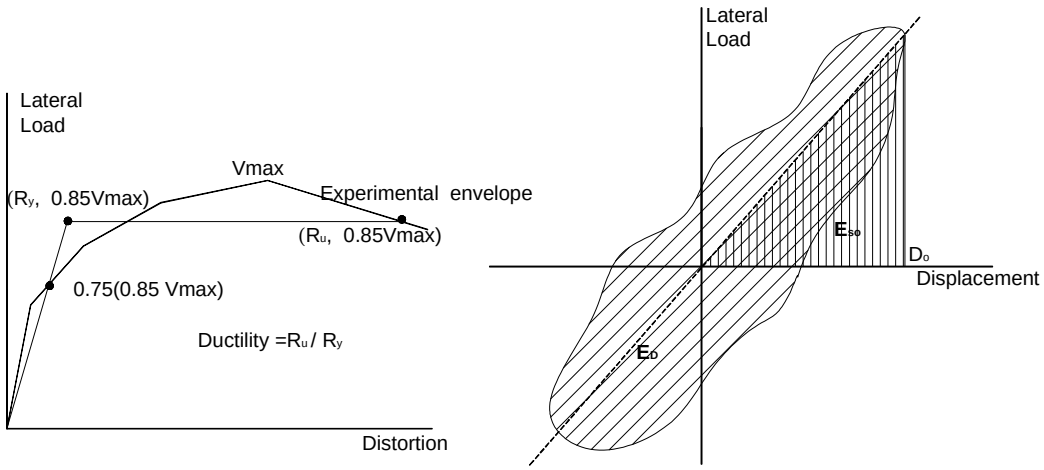

a) b)

Figure A2.3: a) Definition of ductility by Park and Paulay (1989), b) Definition of viscous equivalent damping [25]

A2.1.5 Equivalent viscous damping

Other parameter to define the behavior of masonry walls is the equivalent viscous damping currently used to dynamic analysis. Most common method for defining it is to equate the energy dissipated in a vibration cycle of the actual structure and an equivalent viscous system [25]damping

Other parameter to define the behavior of masonry walls is the equivalent viscous damping currently used to dynamic analysis. Most common method for defining it is to equate the energy dissipated in a vibration cycle of the actual structure and an equivalent viscous system [25]. For the masonry walls, the force-displacement relation obtained from an experiment under cyclic loading with displacement amplitude D_o is determined, Figure A2.3b. The energy dissipated in the wall is given by the area E_D enclosed by the hysteretic loop. Equating this to the energy dissipated in viscous damping leads to Equation A2.8, where the strain energy, $E_{so} = kD_o/2$, is calculated from the stiffness k determined by test.

$$\zeta_{eq} = \frac{1}{4\pi}\frac{E_D}{E_{so}} \qquad \text{(A2.8)}$$

A2.1.6 Load history applied to masonry walls

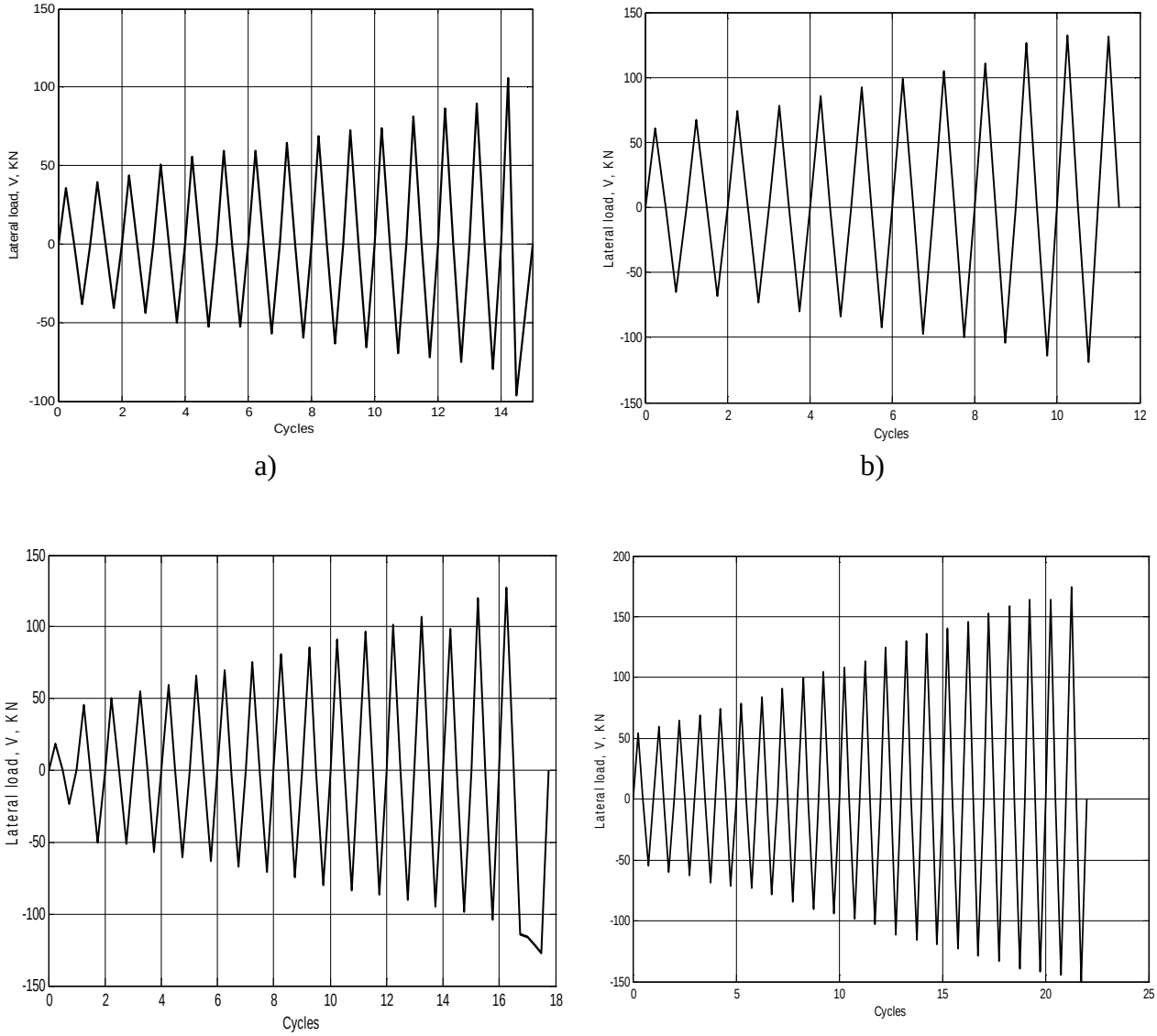

Figure A2.4: Load histories: a) for wall MUR1, b) for wall MUR2, c) for wall MMR2, d) for wall MMR3

ANNEX A3

Concrete behavior under flexural stress

The macro-model presented in chapter 5 requires defining of the concrete behavior. In this research, the model proposed by Kent and Park (1971) and modified by Scott, Park, and Priestley (1982) was used. Figure A3.1 and Equations A3.1- A3.7 define this model.

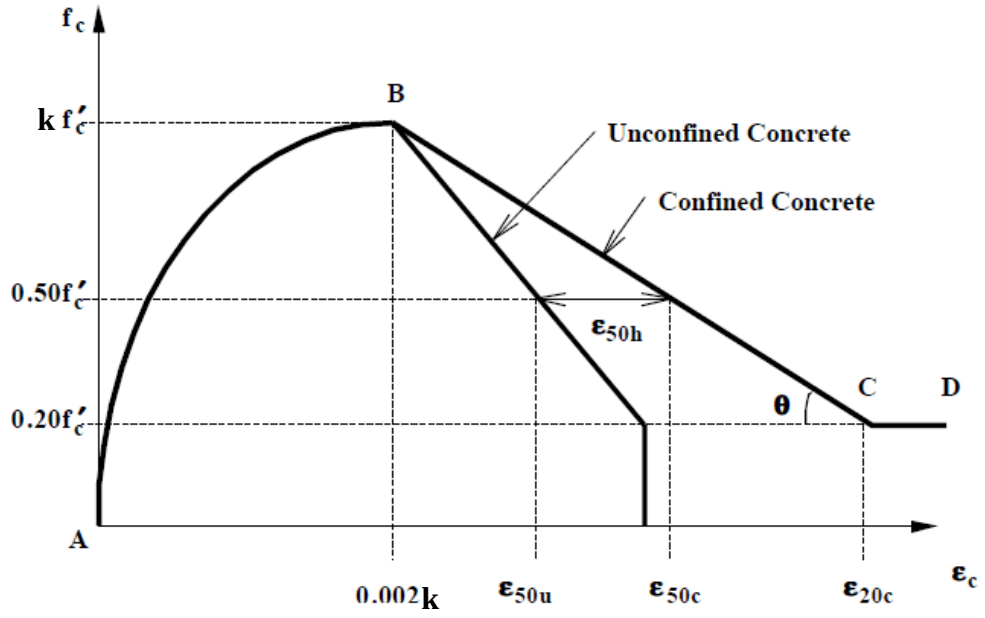

Figure A3.1: Proposed behavioral model of concrete

The parameters are:

If ε_c <= $0.002k$

$$f_c = kf_c^{'}\left[\frac{2\varepsilon_c}{0.002k} - \left(\frac{\varepsilon_c}{0.002k}\right)^2\right] \qquad \text{(A3.1)}$$

If $0.002k < \varepsilon_c <= \varepsilon_{20c}$

$$f_c = kf_c^{'}\left[1 - Z\left(\varepsilon_c - 0.002k\right)\right] \qquad \text{(A3.2)}$$

$$Z=\frac{0.5}{\varepsilon_{50u}+\varepsilon_{50h}-0.002k} \quad \text{(A3.3)}$$

$$k=1+\rho_s f_{yh} \Big/ f_c^{'} \quad \text{(A3.4)}$$

$$\varepsilon_{50h}=0.75\rho_s\sqrt{b/s_h} \quad \text{(A3.5)}$$

$$\varepsilon_{50u}=\frac{3+0.29 f_c^{'}}{145 f_c^{'}-1000} \quad \text{(A3.6)}$$

$$\varepsilon_{20c}=\frac{0.8k}{Z+0.002k} \quad \text{(A3.7)}$$

Herein:

$f_c^{'}$	Compressive strength of concrete
ε_c	Concrete strain
ρ_s	Shear reinforcement ratio
f_{yh}	Yield stress of stirrups
b	Distance between branch of the stirrups
s_h	Distance between stirrups

ANNEX A4

Information about the simplified models

This annex contains the experimental information necessary to asses the performance of the simplified models presented in chapter 6 as well as the values of the parameter *k* for whole walls, were *k* = Theoretical resistance vs. Experimental resistance.

A4.1 Technical information

Table A4.1 Dimension of masonry walls, types of load and units used

Wall	L, [m]	H, [m]	H/L	t, [m]	Load type	Units used
1	2.36	2.30	0.97	0.15	Cyclic	Hollow concrete block
2	2.36	2.30	0.74	0.15	Cyclic	Hollow concrete block
3	2.36	2.30	1.27	0.15	Cyclic	Hollow concrete block
4	3.12	2.30	1.27	0.15	Cyclic	Hollow concrete block
5	3.12	2.30	1.27	0.15	Cyclic	Hollow concrete block
6	1.82	2.30	1.27	0.15	Cyclic	Hollow concrete block
7	1.82	2.30	1.27	0.15	Cyclic	Hollow concrete block
8	1.82	2.30	1.27	0.15	Cyclic	Hollow concrete block
9	2.50	2.45	0.98	0.14	Cyclic	Hollow concrete block
10	2.50	2.45	0.98	0.14	Cyclic	Hollow concrete block
11	2.50	2.45	0.98	0.14	Cyclic	Hollow concrete block
12	2.50	2.45	0.98	0.14	Cyclic	Hollow concrete block
13	2.50	2.45	0.98	0.14	Cyclic	Hollow concrete block
14	2.50	2.45	0.98	0.14	Cyclic	Hollow concrete block
15	2.50	2.45	0.98	0.14	Cyclic	Hollow concrete block
16	2.50	2.45	0.98	0.14	Cyclic	Hollow concrete block
17	2.50	2.50	1.00	0.14	Cyclic	Cement-lime block
18	2.50	2.50	1.00	0.14	Cyclic	Cement-lime block
19	2.50	2.50	1.00	0.14	Cyclic	Cement-lime block
20	2.50	2.50	1.00	0.13	Cyclic	Solid clay brick
21	2.00	2.00	1.00	0.12	Monotonic	Solid clay brick
22	2.00	2.00	1.00	0.12	Monotonic	Solid clay brick
23	2.00	2.00	1.00	0.12	Monotonic	Solid clay brick
24	2.50	1.90	0.76	0.13	Cyclic	Solid clay brick
25	2.50	1.90	0.76	0.13	Cyclic	Solid clay brick
26	3.15	2.15	0.68	0.12	Cyclic	Solid clay brick
27	3.15	2.15	0.68	0.12	Cyclic	Solid clay brick

Table A4.2 Geometrical properties of concrete frame and reinforcement ratio

Wall	Column h_c, [m]	Beam h_d, [m]	p	Wall	Column h_c, [m]	Beam h_d, [m]	p
1	0.15	0.20	0.031	14	0.15	0.15	0.005
2	0.15	0.20	0.031	15	0.15	0.15	0.005
3	0.15	0.20	0.031	16	0.15	0.15	0.005
4	0.15	0.20	0.031	17	0.15	0.10	0.013
5	0.15	0.20	0.031	18	0.15	0.10	0.013
6	0.15	0.20	0.031	19	0.15	0.10	0.013
7	0.15	0.20	0.031	20	0.15	0.10	0.013
8	0.15	0.20	0.031	21	0.20	0.20	0.035
9	0.15	0.15	0.013	22	0.20	0.20	0.035
10	0.15	0.15	0.013	23	0.20	0.20	0.035
11	0.15	0.15	0.013	24	0.20	0.20	0.011
12	0.15	0.15	0.013	25	0.20	0.20	0.011
13	0.15	0.15	0.005	26	0.20	0.20	0.015
				27	0.20	0.20	0.015

Table A4.3 Mechanical properties and experimental resistance

Wall	v^*_m, [MPa]	f_t, [MPa]	σ, [MPa]	f^*_m, [MPa]	f'_c, [MPa]	E_c, [MPa]	E_m, [MPa]	V_{exp}, [KN]
1	0.49	0.53	0.78	7.85	29.43	25,657	6,278	274.7
2	0.49	0.53	0.39	7.85	29.43	25,657	6,278	233.5
3	0.49	0.53	0.00	7.85	29.43	25,657	6,278	182.5
4	0.49	0.53	0.59	7.85	29.43	25,657	6,278	372.8
5	0.49	0.53	0.39	7.85	29.43	25,657	6,278	311.0
6	0.49	0.53	0.78	7.85	29.43	25,657	6,278	206.0
7	0.49	0.53	0.00	7.85	29.43	25,657	6,278	158.0
8	0.49	0.53	0.39	7.85	29.43	25,657	6,278	169.7
9	0.28	0.29	0.54	3.82	23.05	12,031	3,957	154.0
10	0.28	0.29	0.54	3.82	23.05	12,031	3,957	157.0
11	0.28	0.29	0.54	3.82	23.05	12,031	3,957	189.3
12	0.28	0.29	0.54	3.82	23.05	12,031	3,957	173.6
13	0.28	0.29	0.54	3.82	23.05	12,031	3,957	162.9
14	0.28	0.29	0.54	3.82	23.05	12,031	3,957	166.8
15	0.28	0.29	0.54	3.82	23.05	12,031	3,957	167.8
16	0.28	0.29	0.54	3.82	23.05	12,031	3,957	158.9
17	0.20	0.20	0.36	1.47	17.66	10,529	1,905	137.3
18	0.19	0.18	0.36	2.55	17.66	10,529	1,997	141.3
19	0.35	0.34	0.36	2.03	17.66	10,529	2,325	140.3
20	0.26	0.26	0.49	2.65	27.47	10,898	715	138.3
21	0.34	0.35	0.28	10.01	15.60	9,896	1,079	132.4
22	0.34	0.35	0.0	10.01	23.25	12,082	1,079	107.9
23	0.79	0.80	0.0	10.01	32.47	24,987	1,079	191.3
24	0.45	0.43	0.0	4.3	24.9	25,114	2,331	137.0
25	0.45	0.43	0.0	4.3	23.4	22,073	2,331	104.9
26	0.35	0.36	0.26	19.13	28.55	20,639	8,927	225.6
27	0.37	0.38	0.44	22.37	18.84	16,764	8,339	264.9

Herein:

L	Wall length
H	Wall height
t	Wall thickness
ρ	Percentage of reinforcement of the concrete elements all length
h_c	Total depth of columns
h_d	Total depth of beam
v^*_m	design shear strength of masonry according to local code
f_t	Tensile strength of masonry
σ	Vertical stress applied
f'_c	Compressive strength of concrete
E_c	Modulus of elasticity of concrete
E_m	Modulus of elasticity of masonry
f^*_m	Compressive strength of the masonry according to local code
V_{exp}	Experimental resistance

A4.2 Results of the shear failure model

Table A4.4 Ratio *k* of walls built from concrete hollow blocks

Wall	$k = V_m / V_{exp}$	$k = V_{the} / V_{exp}$
1	0.83	0.93
2	0.81	0.93
3	0.83	0.98
4	0.78	0.85
5	0.85	0.93
6	0.77	0.90
7	0.71	0.88
8	0.80	0.96
9	0.95	1.08
10	0.93	1.06
11	0.77	0.88
12	0.84	0.96
13	0.90	0.98
14	0.88	0.96
15	0.87	0.95
16	0.92	1.01

Table A4.5 Ratio *k* of walls built from cement-lime blocks

Wall	$k = V_m / V_{exp}$	$k = V_{the} / V_{exp}$
17	0.69	0.83
18	0.64	0.77
19	1.00	1.13

Table A4.6 Ratio *k* of walls built from clay solid bricks

Wall	$k = V_m / V_{exp}$	$k = V_{the} / V_{exp}$
20	0.69	0.84
21	0.56	0.73
22	0.61	0.87
23	0.8	0.97
24	0.87	0.98
25	1.07	1.29
26	0.71	0.77
27	0.67	0.73

A4.3 Results of the induced tension failure model

Table A4.7 Ratio *k* for whole walls

Wall	$k = V_{the} / V_{exp}$	Wall	$k = V_{the} / V_{exp}$
1	1.11	15	1.02
2	1.25	16	1.08
3	1.51	17	0.85
4	1.39	18	0.75
5	1.57	19	1.34
6	0.92	20	0.92
7	1.20	21	0.93
8	1.12	22	1.12
9	1.11	23	1.46
10	1.09	24	1.50
11	0.90	25	1.95
12	0.98	26	1.17
13	1.05	27	1.20
14	1.03		